

THERMAL AND MASS STRATIFICATION EFFECTS ON MHD FLOW PAST AN ACCELERATED VERTICAL PLATE WITH VARIABLE TEMPERATURE AND EXPONENTIAL MASS DIFFUSION EMBEDDED IN A POROUS MEDIUM

 Digbash Sahu*,  Rudra Kanta Deka

Department of Mathematics, Gauhati University, Guwahati, 781014, Assam, India

**Corresponding Author e-mail: digbashsahu79@gmail.com*

Received March 25, 2024; revised April 12, 2024; accepted April 30, 2024

This study looks at how the impacts of thermal and mass stratification on magnetohydrodynamic (MHD) flow alongside a vertically accelerating plate featuring variable temperature and exponential mass diffusion within a porous medium. The Laplace transform technique is utilized to solve the governing equations related to flow, energy, and mass diffusion. Subsequently, the impact of stratification on the flow field, temperature, and mass diffusion is examined. The study indicates that thermal and mass stratification significantly affects the profiles of velocity, temperature, and mass diffusion. Additionally, it has been discovered that a stable state for the velocity is achieved as both stratification parameters are raised, whereas stable states for the temperature and concentration occur when mass stratification is heightened but thermal stratification is reduced.

Keywords: *MHD flow; Thermal stratification; Mass Stratification; Porous Medium; Accelerated Vertical Plate; Variable Temperature; Laplace Transform*

PACS: 47.55.P-, 44.25.+f, 44.05.+e, 47.11.-j

1. INTRODUCTION

The investigation of heat transfer holds importance across various engineering fields, such as in the cooling of electronic devices, nuclear reactors, and gas turbines. Similarly, a grasp of mass transfer is crucial for several chemical engineering applications, like separation processes, distillation, and absorption. This study aims to explore the combined effects of thermal and mass stratification on the behavior of MHD unsteady flow along an accelerated vertical plate, considering variations in mass diffusion and a variable temperature. The influence of thermal and mass stratifications on the behavior of MHD unsteady flows in fluids is significant, and this research seeks to analyze the interaction of these stratifications.

Early work by [1] and [2] laid the groundwork for understanding transient free convection from vertical flat plates. [3] extended this by investigating unsteady natural convection near doubly infinite vertical plates. Later studies explored diverse aspects of this phenomenon. [4] and [5, 6] investigated transient buoyant flows in stratified fluids, while [7] explored convectively driven flows in stably stratified fluids. Porous media were explored in greater detail. [8] investigated unsteady free convection in a fluid-saturated porous medium, and [9] considered heat and mass diffusion flow by natural convection in a porous medium. The influence of radiation and magnetic fields was also examined. The surveyed literature investigates various aspects of magnetohydrodynamic (MHD) and porous medium flow. [10] analyzed MHD boundary layer flow along vertical plates with ramped temperature. [11] study heat sources in MHD flow past an accelerated plate with variable temperature and mass diffusion. [12] explore thermal diffusion in unsteady MHD convective flow. [13, 14, 15, 16] and [17] examine effects like Hall and ion slip, elastico-viscous fluid behavior, and nanofluid flow dynamics in different MHD contexts, emphasizing the influence of porous mediums and thermal conditions on flow properties and heat transfer. More recent research has delved into the effects of chemical reactions in these flows. [18] and [19, 20] studied unsteady flow past vertical plates with chemical reactions in the presence of thermal stratification. Lastly, [21] extended this to porous media, considering mass diffusion, showcasing the breadth and depth of research in this field.

In this study, we present novel contributions by deriving the exact solution through the Laplace transform technique, achieving this with perfect accuracy, which proves to be an extremely effective strategy for obtaining precise solutions. Prior to this work, there has been no exploration of the combined influences of thermal and mass stratification on the behavior of MHD unsteady flow past a vertically accelerating plate embedded within a porous medium, where both temperature and mass diffusion vary. The aim was to analytically explore the dynamics of MHD unsteady flow past such a plate, taking into account the effects of thermal and mass stratification. Subsequently, we compare the results concerning fluid stratification in both thermal and mass

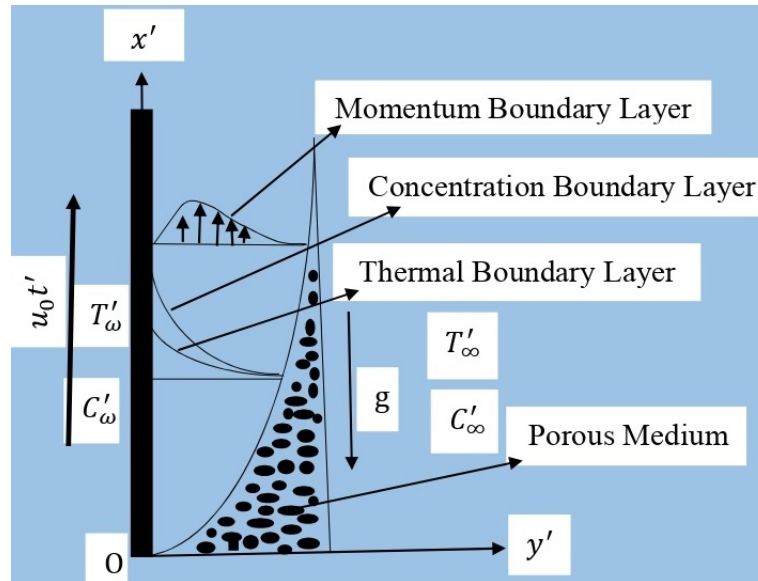


Figure 1. Physical Model and coordinate system

aspects with those of the specific instance lacking any stratification. This study explores and presents the effects of various physical parameters, including γ, ξ, Gr, Gc , the Darcy number (Da), and the Magnetic parameter (M), on the observed profiles through graphical representations. The insights gained from this research hold potential applications across a wide range of industries. For example, the outcomes can be leveraged to enhance thermal system efficiency by minimizing the temperature discrepancy between the walls and the fluid, as well as by accelerating the rate of mass diffusion.

2. MATHEMATICAL ANALYSIS

The governing equations describing the convective movement of an electrically conducting, incompressible, and viscous fluid through a porous medium in presence of a magnetic field, where both mass diffusivity and thermal diffusivity are constant, and incorporating the diffusion-thermo effect, are formulated in vector form as follows:

Momentum Equation

$$\rho \left[\frac{\partial \vec{q}}{\partial t'} + (\vec{q} \cdot \vec{\nabla}) \vec{q} \right] = -\vec{\nabla} p + \vec{J} \times \vec{B} + p\vec{g} + \mu \nabla^2 \vec{q} - \frac{\mu \vec{q}}{k} \quad (1)$$

Energy Equation

$$\rho C_p \left[\frac{\partial T'}{\partial t'} + (\vec{q} \cdot \vec{\nabla}) T' \right] = \alpha \nabla^2 T' \quad (2)$$

Concentration Equation

$$\frac{\partial C'}{\partial t'} + (\vec{q} \cdot \vec{\nabla}) C' = D \nabla^2 C' \quad (3)$$

Consider the MHD unsteady flow of a viscous, incompressible, and stratified fluid over an accelerating vertical plate within a porous medium. The analysis adopts a rectangular Cartesian coordinate system (x', y', t') , where the y' axis is perpendicular to the plate and the x' axis extends vertically upward along the plate. The fluid velocity at any point (x', y', t') is given by $q = (u', 0)$. Initially, at $t' = 0$, the temperature and concentration at the plate are T'_∞ and C'_∞ , respectively. For $t' > 0$, the plate accelerates within its own plane at a velocity of $u_0 t'$ relative to the gravitational force. Additionally, for $t' > 0$, the temperature drops to $T'_\infty + (T'_w - T'_\infty) A t'$, while the concentration increases linearly over time t . Given the plate's infinite dimensions, all flow variables are independent of x' , varying only with y' and t' . Thus, under the standard Boussinesq approximation, specific equations are employed to describe the MHD unsteady flow dynamics. The conversion procedure for equations (1)-(3) has already been addressed by Sarma et al. [22]. Consequently, we obtain the following form.

$$\frac{\partial u'}{\partial t'} = g\beta(T' - T'_\infty) + g\beta^*(C' - C'_\infty) + \nu \frac{\partial^2 u'}{\partial y'^2} - \frac{\sigma B_0^2 u'}{\rho} - \frac{\nu}{k} u' \quad (4)$$

$$\frac{\partial T'}{\partial t'} = \alpha \frac{\partial^2 T'}{\partial y'^2} - \gamma' u' \quad (5)$$

$$\frac{\partial C'}{\partial t'} = D \frac{\partial^2 C'}{\partial y'^2} - \xi' u' \tag{6}$$

with the following initial and boundary Conditions:

$$\begin{aligned} u' = 0 & & T' = T'_\infty & & C' = C'_\infty & & \forall y', t' \leq 0 \\ u' = u_0 t' & & T' = T'_\infty + (T'_w - T'_\infty) A t' & & C' = C'_\infty + (C'_w - C'_\infty) e^{a' t'} & & \text{at } y' = 0, t' > 0 \\ u' = 0 & & T' \rightarrow T'_\infty & & C' \rightarrow C'_\infty & & \text{as } y' \rightarrow \infty, t' > 0 \end{aligned}$$

where a' , α , η , ν , D , and Da are respectively constant, thermal diffusivity, similarity parameter, kinematic viscosity, mass diffusion coefficient, darcy number. The "thermal stratification parameter" and "mass stratification parameter" are termed as $\gamma' = \frac{dT'_\infty}{dx'} + \frac{g}{C_p}$ and $\xi' = \frac{dC'_\infty}{dx'}$ respectively. The term "thermal stratification" refers to the combination of vertical temperature advection $\left(\frac{dT'_\infty}{dx'}\right)$, where the temperature of the surrounding fluid is height-dependent, and work of compression $\left(\frac{g}{C_p}\right)$, the rate at which particles in a fluid do reversible work due to compression. And we provide non-dimensional quantities in the following:

$$\begin{aligned} U = \frac{u'}{(u_0 \nu)^{1/3}}, \quad t = t' \left(\frac{u_0^2}{\nu}\right)^{1/3}, \quad y = y' \left(\frac{u_0}{\nu^2}\right)^{1/3}, \quad \theta = \frac{T' - T'_\infty}{T'_w - T'_\infty}, \quad C = \frac{C' - C'_\infty}{C'_w - C'_\infty}, \\ Gr = \frac{g\beta(T'_w - T'_\infty)}{u_0}, \quad Gc = \frac{g\beta^*(C'_w - C'_\infty)}{u_0}, \quad Pr = \frac{\nu}{\alpha}, \quad Sc = \frac{\nu}{D}, \quad a = a' \left(\frac{\nu}{u_0^2}\right)^{1/3}, \\ M = \frac{\sigma B_0^2 \nu^{1/3}}{\rho u_0^{2/3}}, \quad Da = k' \left(\frac{u_0^2}{\nu^4}\right)^{1/3}, \quad \gamma = \frac{\gamma' \nu^{2/3}}{u_0^{1/3} (T'_w - T'_\infty)}, \quad \xi = \frac{\xi' \nu^{2/3}}{u_0^{1/3} (C'_w - C'_\infty)} \end{aligned}$$

$A = \left(\frac{u_0^2}{\nu}\right)^{1/3}$ is the constant.

$$\frac{\partial U}{\partial t} = Gr\theta + GcC + \frac{\partial^2 U}{\partial y^2} - \left(M + \frac{1}{Da}\right)U \tag{7}$$

$$\frac{\partial \theta}{\partial t} = \frac{1}{Pr} \frac{\partial^2 \theta}{\partial y^2} - \gamma U \tag{8}$$

$$\frac{\partial C}{\partial t} = \frac{1}{Sc} \frac{\partial^2 C}{\partial y^2} - \xi U \tag{9}$$

Non-dimensional forms of initial and boundary Conditions are:

$$\begin{aligned} U = 0 & & \theta = 0 & & C = 0 & & \forall y, t \leq 0 \\ U = t & & \theta = t & & C = e^{at} & & \text{at } y = 0, t > 0 \\ U = 0 & & \theta \rightarrow 0 & & C \rightarrow 0 & & \text{as } y \rightarrow \infty, t > 0 \end{aligned} \tag{10}$$

3. METHOD OF SOLUTION

We discovered that the Laplace transform method produces an equation of non-tractable form for any arbitrary Prandtl or Schmidt number. The non-dimensional governing equations (7)-(9) with boundary conditions (10), are solved for the tractable situation of $Pr = 1, Sc = 1$. Hence, the expressions for velocity, temperature, and concentration profiles can be determined with the help of [23] and [24] are as follows

$$U = \frac{F - Gr}{F - Q} \{g_1(F)\} - \frac{Gc}{F - Q} \{g_2(F) - g_2(Q)\} + \frac{Gr - Q}{F - Q} \{g_1(Q)\} \tag{11}$$

$$\begin{aligned} \theta = \left(t - \frac{t\gamma Gr}{FQ}\right) \left[(1 + 2\eta^2) \operatorname{erfc}(\eta) - \frac{2\eta}{\sqrt{\pi}} e^{-\eta^2} \right] - \frac{\gamma Gc e^{at}}{2FQ} \left[e^{-2\eta\sqrt{at}} \operatorname{erfc}(\eta - \sqrt{at}) + e^{2\eta\sqrt{at}} \operatorname{erfc}(\eta + \sqrt{at}) \right] \\ + \frac{F - Gr}{F - Q} \left\{ \frac{\gamma}{F} g_1(F) \right\} + \frac{Gr - Q}{F - Q} \left\{ \frac{\gamma}{Q} g_1(Q) \right\} - \frac{\gamma Gc}{F - Q} \left\{ \frac{1}{F} g_2(Q) - \frac{1}{Q} g_2(F) \right\} \end{aligned} \tag{12}$$

$$\begin{aligned}
 C = & \frac{t\xi \{2FQ - Gr(F - Q)\}}{FQ(F - Q)} \left[(1 + 2\eta^2) \operatorname{erfc}(\eta) - \frac{2\eta}{\sqrt{\pi}} e^{-\eta^2} \right] - \frac{(FQ - \xi Gc)e^{at}}{2FQ} \\
 & \left[e^{-2\eta\sqrt{at}} \operatorname{erfc}(\eta - \sqrt{at}) + e^{2\eta\sqrt{at}} \operatorname{erfc}(\eta + \sqrt{at}) \right] \\
 & + \frac{\xi(F - Gr)}{F - Q} \left\{ \frac{1}{F} g_1(F) - \frac{1}{Q} g_1(Q) \right\} - \frac{\xi Gc}{F - Q} \left\{ \frac{1}{F} g_2(F) - \frac{1}{Q} g_2(Q) \right\} - \frac{\xi}{Q} \{g_1(Q)\}
 \end{aligned} \tag{13}$$

Where,

$$\eta = \frac{y}{2\sqrt{t}}, \quad F + Q = M + \frac{1}{Da}, \quad F - Q = \sqrt{\left(M + \frac{1}{Da}\right)^2 - 4(\gamma Gr + \xi Gc)}$$

Also, f_i 's are inverse Laplace's transforms given by

$$g_1(p) = L^{-1} \left\{ \frac{e^{-y\sqrt{s+p}}}{s^2} \right\}, \quad g_2(p) = L^{-1} \left\{ \frac{e^{-y\sqrt{s+p}}}{s - a} \right\}$$

We separate the complex arguments of the error function contained in the previous expressions into real and imaginary parts using the formulas provided by [23].

4. CLASSICAL CASE ($\gamma = 0, \xi = 0$)

We derived solutions for the classical case of no thermal and mass stratification ($\gamma = 0, \xi = 0$). We want to compare the results of the fluid with thermal and mass stratification to the case with no stratification. Hence, the solutions for the classical case with boundary conditions (10) by using the Laplace transformation are as follows:

$$\theta_c = t \left\{ (1 + 2\eta^2) \operatorname{erfc}(\eta) - \frac{2\eta}{\sqrt{\pi}} e^{-\eta^2} \right\} \tag{14}$$

$$C_c = \frac{e^{at}}{2} \left[e^{-2\eta\sqrt{at}} \operatorname{erfc}(\eta - \sqrt{at}) + e^{2\eta\sqrt{at}} \operatorname{erfc}(\eta + \sqrt{at}) \right] \tag{15}$$

$$\begin{aligned}
 U_c = & \left(1 - \frac{Gr}{F + Q}\right) g_1(F + Q) - \frac{Gc}{(F + Q)} g_2(F + Q) + \frac{Gc e^{at}}{2(F + Q)} \left\{ e^{-2\eta\sqrt{at}} \operatorname{erfc}(\eta - \sqrt{at}) \right. \\
 & \left. + e^{2\eta\sqrt{at}} \operatorname{erfc}(\eta + \sqrt{at}) \right\} + \frac{tGr}{(F + Q)} \left\{ (1 + 2\eta^2) \operatorname{erfc}(\eta) - \frac{2\eta}{\sqrt{\pi}} e^{-\eta^2} \right\}
 \end{aligned} \tag{16}$$

4.1. Skin-Friction

The non-dimensional Skin-Friction, which is determined as shear stress on the surface, is obtained by

$$\tau = - \left. \frac{dU}{dy} \right|_{y=0}$$

The solution for the Skin-Friction is calculated from the solution of Velocity profile U , represented by (11), as follows:

$$\begin{aligned}
 \tau = & \frac{F - Gr}{F - Q} \left[t\sqrt{F} \operatorname{erf}(\sqrt{Ft}) + e^{-Ft} \sqrt{\frac{t}{\pi}} + \frac{\operatorname{erf}(\sqrt{Ft})}{2\sqrt{F}} \right] - \frac{Gr - Q}{F - Q} \left[t\sqrt{Q} \operatorname{erf}(\sqrt{Qt}) + e^{-Qt} \sqrt{\frac{t}{\pi}} + \frac{\operatorname{erf}(\sqrt{Qt})}{2\sqrt{Q}} \right] \\
 & - \frac{Gc}{F - Q} \left[e^{at} \left\{ \sqrt{a + F} \operatorname{erf}(\sqrt{(a + F)t}) - \sqrt{a + Q} \operatorname{erf}(\sqrt{(a + Q)t}) \right\} + \frac{e^{-Ft} - e^{-Qt}}{\sqrt{\pi t}} \right]
 \end{aligned}$$

The solution for the Skin-Friction for the classical case is given from the expression (16), which is represented by

$$\begin{aligned}
 \tau_c = & \left(1 - \frac{Gr}{F + Q}\right) \left[t\sqrt{F + Q} \operatorname{erf}(\sqrt{(F + Q)t}) + \sqrt{\frac{t}{\pi}} e^{-(F+Q)t} + \frac{\operatorname{erf}(\sqrt{(F + Q)t})}{2\sqrt{(F + Q)t}} \right] + \frac{2Gr}{F + Q} \sqrt{\frac{t}{\pi}} + \\
 & \frac{Gc e^{at}}{(F + Q)} \sqrt{a} \operatorname{erf}(\sqrt{at}) + \frac{Gc}{(F + Q)\sqrt{\pi t}} - \frac{Gc e^{at}}{(F + Q)} \sqrt{a + (F + Q)} \operatorname{erf}(\sqrt{(a + F + Q)t}) - \frac{Gc e^{(F+Q)t}}{(F + Q)\sqrt{\pi t}}
 \end{aligned}$$

4.2. Nusselt Number

The non-dimensional Nusselt number, which is determined as the rate of heat transfer, is obtained by

$$Nu = -\frac{d\theta}{dy}\Big|_{y=0}$$

The solution for the Nusselt number is calculated from the solution of Temperature profile θ , represented by (12), as follows:

$$\begin{aligned} Nu = & 2\sqrt{\frac{t}{\pi}} \left(1 - \frac{\gamma Gr}{FQ}\right) - \frac{\gamma Gc}{FQ} \left[e^{at} \sqrt{a} \operatorname{erf}(\sqrt{at}) + \frac{1}{\sqrt{\pi t}} \right] - \frac{\gamma Gc}{F(F-Q)} \left[e^{at} \sqrt{a+F} \operatorname{erf}(\sqrt{(a+F)t}) + \frac{e^{-Ft}}{\sqrt{\pi t}} \right] \\ & + \frac{\gamma(F-Gr)}{F(F-Q)} \left[t\sqrt{F} \operatorname{erf}(\sqrt{Ft}) + \sqrt{\frac{t}{\pi}} e^{-Ft} + \frac{\operatorname{erf}(\sqrt{Ft})}{2\sqrt{F}} \right] + \frac{\gamma Gc}{Q(F-Q)} \\ & \left[e^{at} \sqrt{a+Q} \operatorname{erf}(\sqrt{(a+Q)t}) + \frac{e^{-Qt}}{\sqrt{\pi t}} \right] + \frac{\gamma(Gr-Q)}{Q(F-Q)} \left[t\sqrt{Q} \operatorname{erf}(\sqrt{Qt}) + \sqrt{\frac{t}{\pi}} e^{-Qt} + \frac{\operatorname{erf}(\sqrt{Qt})}{2\sqrt{Q}} \right] \end{aligned}$$

The solution for the Nusselt number for the classical case is given from the expression (14), which is represented by

$$Nu_c = 2\sqrt{\frac{t}{\pi}}$$

4.3. Sherwood Number

The non-dimensional Sherwood number, which is determined as the rate of mass transfer, is obtained by

$$Sh = -\frac{dC}{dy}\Big|_{y=0}$$

The solution for the Sherwood number is calculated from the solution of Concentration profile C , represented by (13), as follows:

$$\begin{aligned} Sh = & \left(1 + \frac{\xi Gc(Q-F)}{FQ(F-Q)}\right) \left[e^{at} \sqrt{a} \operatorname{erf}(\sqrt{at}) + \frac{1}{\sqrt{\pi t}} \right] - \frac{2\xi(2FQ-Gr(F+Q))}{FQ(F-Q)} \sqrt{\frac{t}{\pi}} - \frac{\xi Gc}{F(F-Q)} \left[e^{at} \sqrt{a+F} \right. \\ & \left. \operatorname{erf}(\sqrt{(a+F)t}) + \frac{e^{-Ft}}{\sqrt{\pi t}} \right] + \frac{\xi(F-Gr)}{F(F-Q)} \left[t\sqrt{F} \operatorname{erf}(\sqrt{Ft}) + \sqrt{\frac{t}{\pi}} e^{-Ft} + \frac{\operatorname{erf}(\sqrt{Ft})}{2\sqrt{F}} \right] + \frac{\xi Gc}{Q(F-Q)} \\ & \left[e^{at} \sqrt{a+Q} \operatorname{erf}(\sqrt{(a+Q)t}) + \frac{e^{-Qt}}{\sqrt{\pi t}} \right] + \frac{\xi(Gr-Q)}{Q(F-Q)} \left[t\sqrt{Q} \operatorname{erf}(\sqrt{Qt}) + \sqrt{\frac{t}{\pi}} e^{-Qt} + \frac{\operatorname{erf}(\sqrt{Qt})}{2\sqrt{Q}} \right] \end{aligned}$$

The solution for the Sherwood number for the classical case is given from the expression (15), which is represented by

$$Sh_c = e^{at} \sqrt{a} \operatorname{erf}(\sqrt{at}) + \frac{1}{\sqrt{\pi t}}$$

5. RESULT AND DISCUSSIONS

We computed numerical values of velocity, temperature, concentration, skin friction, Nusselt number, and Sherwood number from their solutions derived in the preceding sections, for various values of the physical parameters γ, ξ, Gr, Gc, M and Da . This allowed us to get a better understanding of the physical significance of the problem. Moreover, using MATLAB, we plotted them in Figures 2-22.

Figure 2 illustrates the impact of thermal and mass stratification on velocity profiles, showing that both types of stratification lead to reduced velocities. When one form of stratification is held constant, an increase in the other type further decreases velocity. In the same way that [7] shows that fluid velocity drops for thermal stratification $\gamma > 0$, we find that this is also the case for mass stratification $\xi > 0$. Enhancing the parameter of thermal stratification (γ) diminishes the convective potential across the hot plate and the adjacent fluid, reducing the buoyancy force and, subsequently, the flow velocity. Similarly, an increase in the mass stratification (ξ) value leads to a lower concentration gradient between the surface and its environment, diminishing the buoyancy's upward force and thus slowing down the fluid flow. Therefore, the presence of both thermal and mass stratification results in a reduced fluid velocity compared to conditions without stratification.

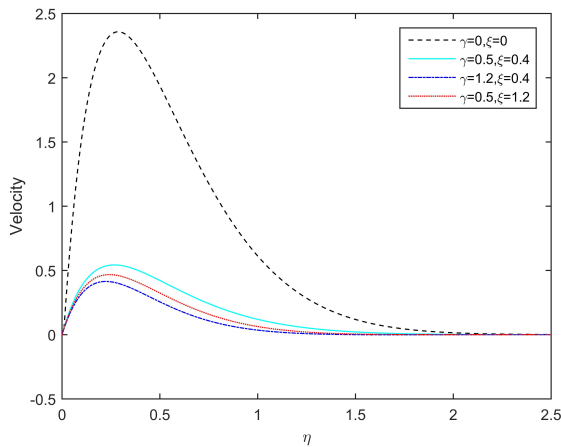


Figure 2. Effects of γ and ξ on Velocity Profile for $Gr = 5, Gc = 5, M = 2, Da = 0.5, t = 1.5, a = 0.2,$

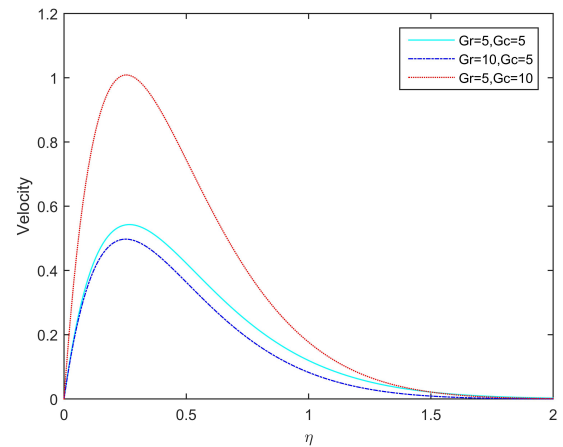


Figure 3. Effects of Gr and Gc on Velocity Profile for $\gamma = 0.5, \xi = 0.4, M = 2, Da = 0.5, t = 1.5, a = 0.2$

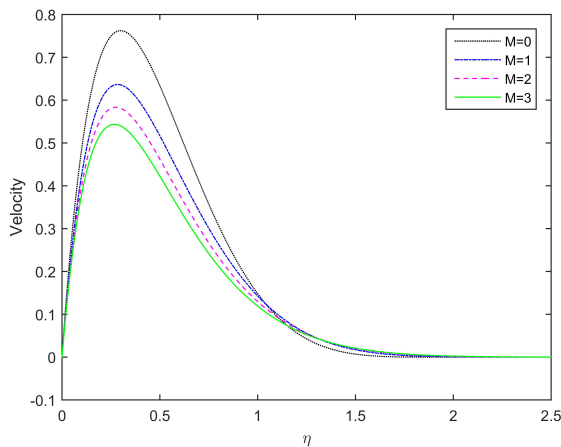


Figure 4. Effects of M on Velocity Profile for $Gr = 5, Gc = 5, \gamma = 0.5, \xi = 0.4, Da = 0.5, t = 1.5, a = 0.2,$

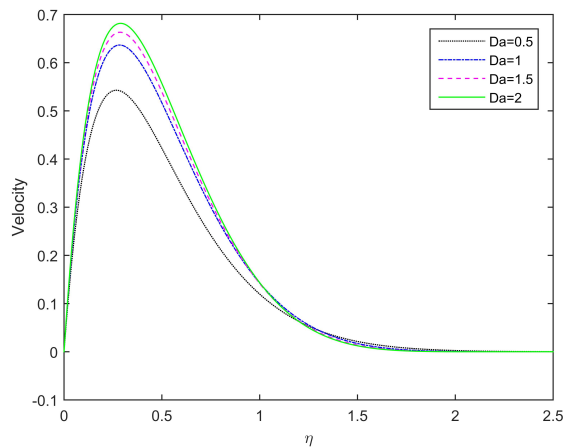


Figure 5. Effects of Da on Velocity Profile for $Gr = 5, Gc = 5, \gamma = 0.5, \xi = 0.4, M = 2, t = 1.5, a = 0.2,$

Hence, both thermal and mass stratification play a crucial role in establishing a stable stratified flow. As seen in Figure 3, Raising the value of Gc leads to a higher velocity, while a rise in Gr causes a decrease in velocity. We can observe from Figure 4 that velocity decreases as (M) grows. Figure 5 shows that as Da and the fluid's porosity increase, there is an elevation in the velocity profile, enabling the fluid particles to move more smoothly.

Figure 6 demonstrates the impact of thermal and mass stratification on the temperature profile. While mass stratification leads to an increase in temperature, an increase in thermal stratification is associated with a reduction in temperature. An increase in thermal stratification (γ) causes the temperature gradient between the vertical plate and the adjacent fluid to diminish. Consequently, this results in a thicker thermal boundary layer and a lower temperature. As shown in Figures 7, and 9, the temperature drops as $Gr, Gc,$ and Da increase and in Figure 8 the temperature increases as M increase. In Figure 10, fluid concentration decreases with increasing mass stratification parameters but increases with increasing thermal stratification. As shown in Figures 11, 12, and 13 the effects of $Gr, Gc, Da,$ and M on concentration are identical to those seen for temperature profiles.

Figures 14, 15, and 16 plot the two stratification's effects on fluid velocity, temperature, and concentration over time. The velocity grows infinitely with time for the Classical case but reaches a steady state when both stratifications are present. The presence of both stratifications influences the temperature profile over time, but an increase in thermal stratification has a more pronounced effect in slowing down the temperature increase compared to an increase in mass stratification. The concentration increases over time, highest with no stratification, and less as thermal or mass stratification values rise.

In Figure 17, skin friction decreases with time in the presence of both stratification compared to no stratification. It decreases over time, with the lowest values occurring for the highest Gc at a constant Gr , as shown in Figure 18. Figures 19, 20, 21 and 22 for both nusselt and sherwood numbers, values rise with time.

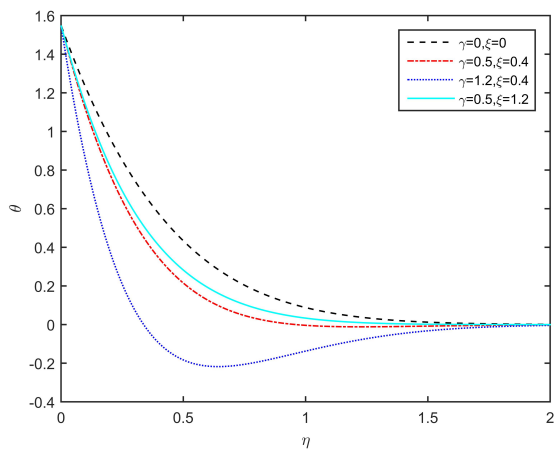


Figure 6. Effects of γ and ξ on Temperature Profile for $Gr = 5, Gc = 5, M = 2, Da = 0.5, t = 1.5, a = 0.2$

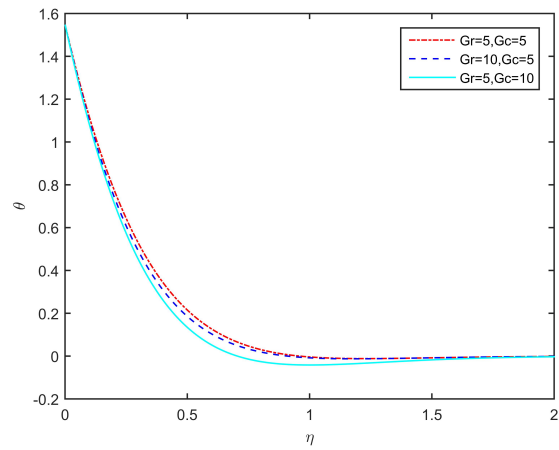


Figure 7. Effects of Gr and Gc on Temperature Profile for $\gamma = 0.5, \xi = 0.4, t = 1.5, M = 2, Da = 0.5, a = 0.2$

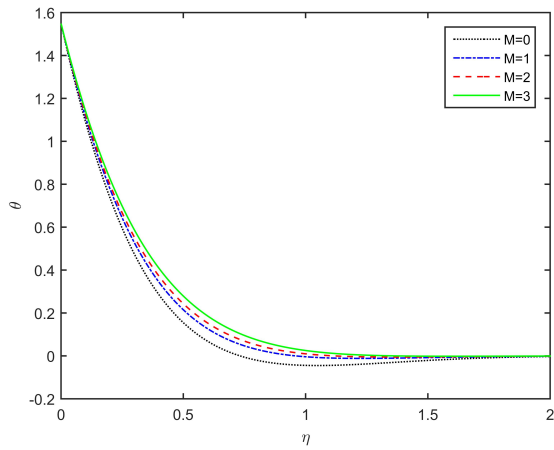


Figure 8. Effects of M on Temperature Profile for $Gr = 5, Gc = 5, \gamma = 0.5, \xi = 0.4, t = 1.5, Da = 0.5, a = 0.2$

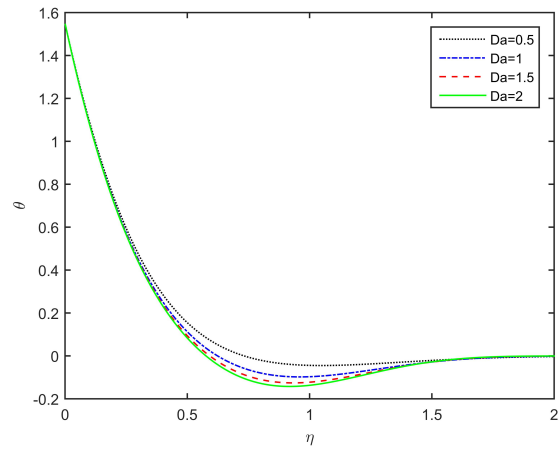


Figure 9. Effects of Da on Temperature Profile for $Gr = 5, Gc = 5, \gamma = 0.5, \xi = 0.4, t = 1.5, M = 2, a = 0.2$

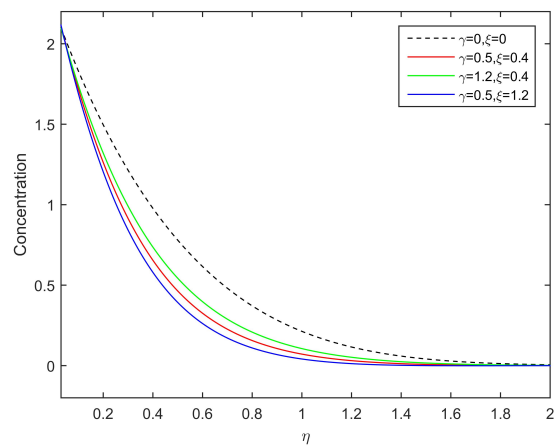


Figure 10. Effects of γ and ξ on Concentration Profile for $Gr = 5, Gc = 5, Da = 0.5, t = 1, M = 2, a = 0.2$

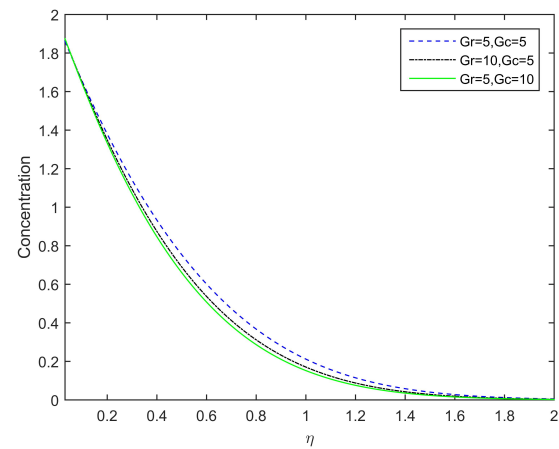


Figure 11. Effects of Gr and Gc on Concentration Profile for $\gamma = 0.5, \xi = 0.4, t = 0.5, M = 2, Da = 0.5, a = 0.2$

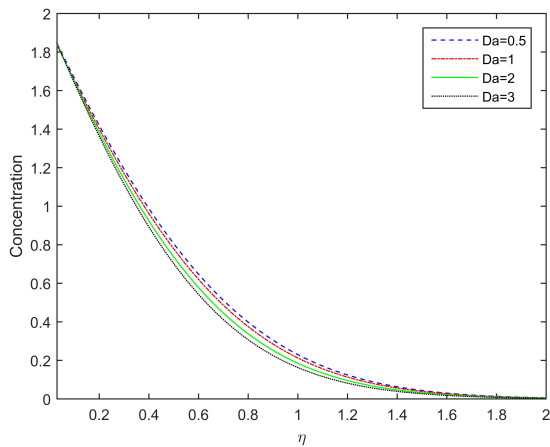


Figure 12. Effects of Da on Concentration Profile for $Gr = 5, Gc = 5, \gamma = 0.5, \xi = 0.4, t = 0.5, M = 2, a = 0.2$

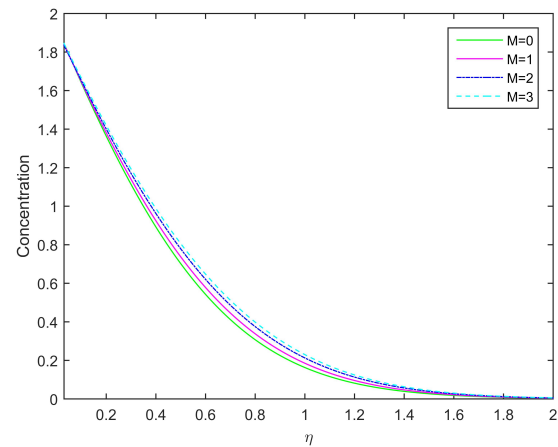


Figure 13. Effects of M on Concentration Profile for $Gr = 5, Gc = 5, \gamma = 0.5, \xi = 0.4, t = 0.5, Da = 0.5, a = 0.2$

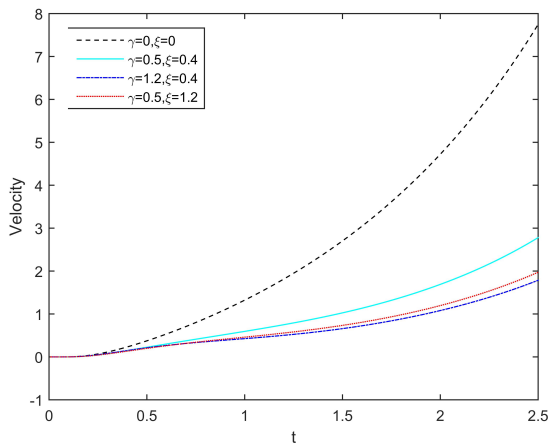


Figure 14. Effects of γ and ξ on Velocity Profile against time for $Gr = 5, Gc = 5, M = 2, Da = 0.5, a = 0.2, y = 1.4$

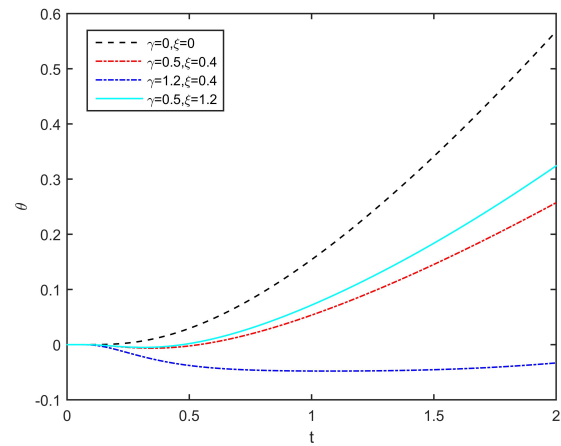


Figure 15. Effects of γ and ξ on Temperature Profile against time for $Gr = 5, Gc = 5, M = 2, Da = 0.5, a = 0.2, y = 1.4$

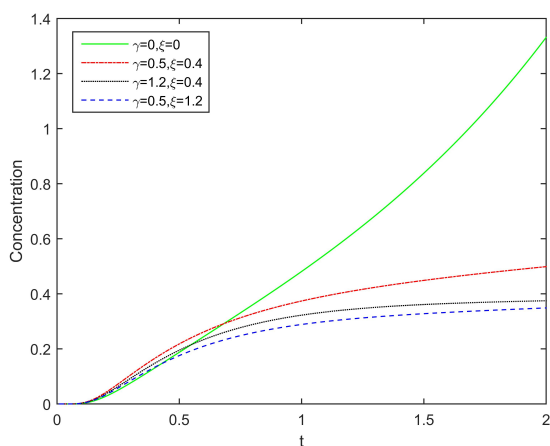


Figure 16. Effects of γ and ξ on Concentration Profile against time for $Gr = 5, Gc = 5, M = 2, Da = 0.5, a = 0.2, y = 1.4$

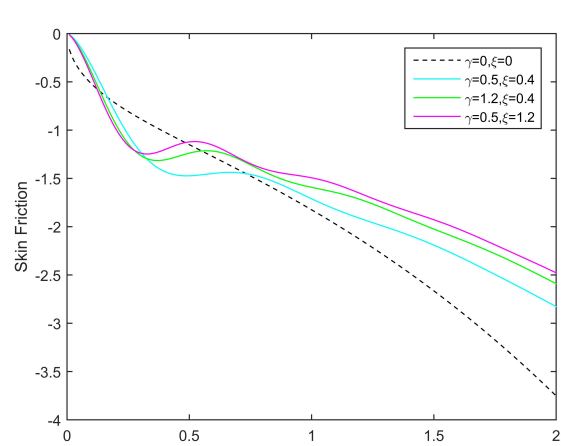


Figure 17. Effects of γ and ξ on Skin friction for $Gr = 5, Gc = 5, M = 2, Da = 0.5, a = 0.2$

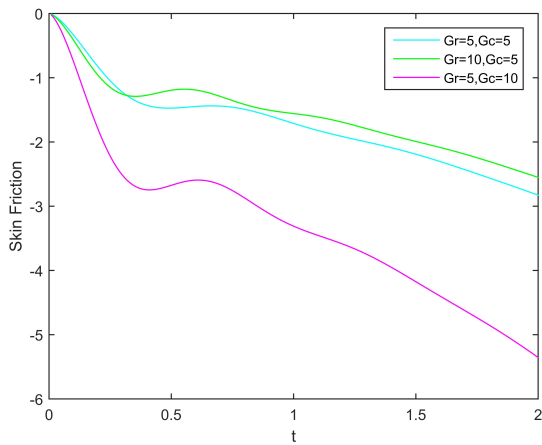


Figure 18. Effects of Gr and Gc on Skin friction for $\gamma = 0.5, \xi = 0.4, M = 2, Da = 0.5, a = 0.2$

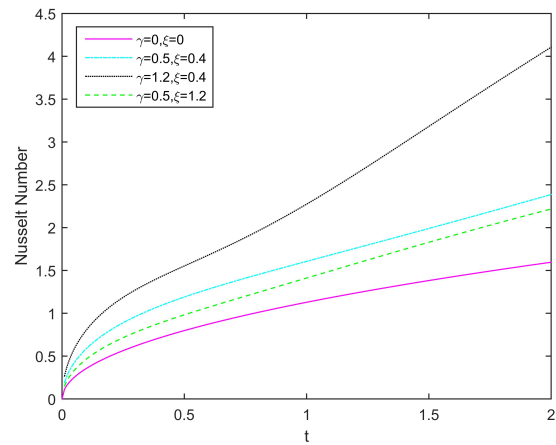


Figure 19. Effects of γ and ξ on Nusselt Number for $Gr = 5, Gc = 5, M = 2, Da = 0.5, a = 0.2$

Higher thermal stratification dampens the increase for nusselt and more so for sherwood, while varying mass stratification shows mixed effects. Higher Gr boosts sherwood's growth at a constant Gc .

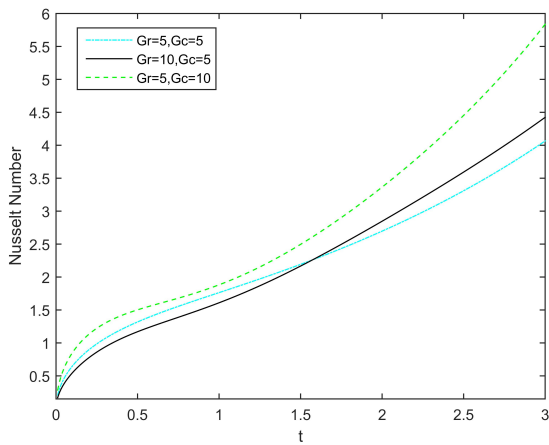


Figure 20. Effects of Gr and Gc on Nusselt Number for $\gamma = 0.5, \xi = 0.4, M = 2, Da = 0.5, a = 0.2$

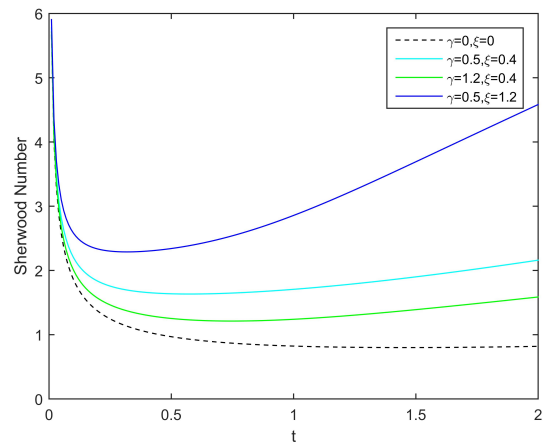


Figure 21. Effects of γ and ξ on Sherwood Number for $Gr = 5, Gc = 5, M = 2, Da = 0.5, a = 0.2$

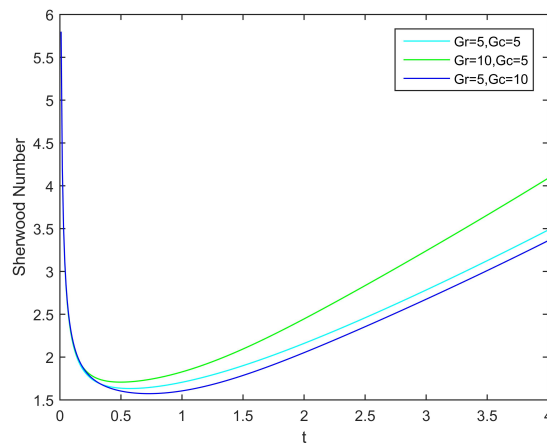


Figure 22. Effects of Gr and Gc on Sherwood Number for $\gamma = 0.5, \xi = 0.4, M = 2, Da = 0.5, a = 0.2$

6. CONCLUSION

The findings from this research indicate that thermal and mass stratification notably diminishes velocity over time, leading the system to achieve equilibrium. For conditions of increased mass stratification and decreased thermal stratification, the system's temperature and concentration levels stabilize. With the concurrent presence of both types of stratification, there is a gradual decrease in skin friction. Additionally, time enhances heat and mass transfer rates, with higher mass stratification and lower thermal stratification increasing both nusselt and sherwood numbers more markedly. These results hold significant implications for the design of porous media systems tailored to manage MHD unsteady flow with stratification features.

ORCID

✉ Digbash Sahu, <https://orcid.org/0009-0005-8925-2048>; ✉ Rudra Kanta Deka, <https://orcid.org/0009-0007-1573-4890>

REFERENCES

- [1] R. Siegel, "Transient free convection from a vertical flat plate," *Transactions of the American Society of Mechanical Engineers*, **80**(2), 347-357 (1958). <https://doi.org/10.1115/1.4012369>.
- [2] E.R. Menold, and K.T. Yang, "Asymptotic solutions for unsteady laminar free convection on a vertical plate," *Trans ASME: J. Appl. Mech.* **29**, 124-126 (1962). <http://doi:10.1115/1.3636443>.
- [3] J.A. Schetz, and R. Eichhorn, "Unsteady natural convection in the vicinity of a doubly infinite vertical plate," *Trans ASME C: J. Heat Transfer*, **84**(4), 334-338 (1962). <https://doi.org/10.1115/1.3684386>
- [4] U.N. Das, R.K. Deka, and V.M. Soundalgekar, "Transient free convection flow past an infinite vertical plate with periodic temperature variation," *J. Heat Transfer*, **121**(4) 1091-1094 (1999). <https://doi.org/10.1115/1.2826063>
- [5] J.S. Park, and J.M. Hyun, "Technical Note Transient behavior of vertical buoyancy layer in a stratified fluid," *International journal of heat and mass transfer*, **41**(24), 4393-4397 (1998). [https://doi.org/10.1016/S0017-9310\(98\)00175-6](https://doi.org/10.1016/S0017-9310(98)00175-6)
- [6] J.S. Park, "Transient buoyant flows of a stratified fluid in a vertical channel," *KSME international journal*, **15**, 656-664 (2001). <http://doi:10.1007/bf03184382>
- [7] A. Shapiro, and E. Fedorovich, "Unsteady convectively driven flow along a vertical plate immersed in a stably stratified fluid," *Journal of Fluid Mechanics*, **498**, 333-352 (2004). <https://doi.org/10.1017/S0022112003006803>
- [8] E. Magyari, I. Pop, and B. Keller, "Unsteady free convection along an infinite vertical flat plate embedded in a stably stratified fluid-saturated porous medium," *Transport in porous media*, **62**, 233-249 (2006). <https://DOI10.1007/s11242-005-1292-6>
- [9] R.C. Chaudhary, and A. Jain, "MHD heat and mass diffusion flow by natural convection past a surface embedded in a porous medium," *Theoretical and Applied Mechanics*, **36**(1), 1-27 (2009). <https://doi.org/10.2298/TAM0901001C>
- [10] Y.D. Reddy, B.S. Goud, and M.A. Kumar, "Radiation and heat absorption effects on an unsteady MHD boundary layer flow along an accelerated infinite vertical plate with ramped plate temperature in the existence of slip condition," *Partial Differential Equations in Applied Mathematics*, **4**, 100166 (2021). <https://doi.org/10.1016/j.padiff.2021.100166>
- [11] A. Selvaraj, and E. Jothi, "Heat source impact on MHD and radiation absorption fluid flow past an exponentially accelerated vertical plate with exponentially variable temperature and mass diffusion through a porous medium," *Materials Today: Proceedings*, **46**, 3490-3494 (2021). <https://doi.org/10.1016/j.matpr.2020.11.919>
- [12] S. Sarma, and A. Nazibuddin, "Thermal diffusion effect on unsteady MHD free convective flow past a semi-infinite exponentially accelerated vertical plate in a porous medium," *Canadian Journal of Physics*, **100**(10), 437-451 (2022). <https://doi.org/10.1139/cjp-2021-0361>
- [13] M.V. Krishna, and A.J. Chamkha, "Hall and ion slip effects on MHD rotating flow of elasto-viscous fluid through porous medium," *International Communications in Heat and Mass Transfer*, **113**, 104494 (2020). <https://doi.org/10.1016/j.icheatmasstransfer.2020.104494>
- [14] M.V. Krishna, K. Jyothi, and A.J. Chamkha, "Heat and mass transfer on MHD flow of second-grade fluid through porous medium over a semi-infinite vertical stretching sheet," *Journal of Porous media*, **23**(8), (2020). <https://doi.org/10.1615/JPorMedia.2020023817>
- [15] M.V. Krishna, N.A. Ahamad, and A.J. Chamkha, "Hall and ion slip effects on unsteady MHD free convective rotating flow through a saturated porous medium over an exponential accelerated plate," *Alexandria Engineering Journal*, **59**(2), 565-577 (2020). <https://doi.org/10.1016/j.aej.2020.01.043>
- [16] M.V. Krishna, and A.J. Chamkha, "Hall and ion slip effects on magnetohydrodynamic convective rotating flow of Jeffreys fluid over an impulsively moving vertical plate embedded in a saturated porous medium with Ramped wall temperature," *Numerical Methods for Partial Differential Equations*, **37**(3), 2150-2177 (2021). <https://doi.org/10.1002/num.22670>

- [17] M.V. Krishna, and A.J. Chamkha, "Hall and ion slip effects on MHD rotating boundary layer flow of nanofluid past an infinite vertical plate embedded in a porous medium," Results in Physics, **15**, 102652 (2019). <https://doi.org/10.1016/j.rinp.2019.102652>
- [18] N. Kalita, R. K. Deka, R. S. Nath, "Unsteady Flow Past an Accelerated Vertical Plate with Variable Temperature in Presence of Thermal Stratification and Chemical Reaction," East European Journal of Physics, (3), 441-450 (2023). <https://doi.org/10.26565/2312-4334-2023-3-49>
- [19] R. S. Nath, R. K. Deka, "The Effects of Thermal Stratification on Flow Past an Infinite Vertical Plate in Presence of Chemical Reaction," East European Journal of Physics, (3), 223-232 (2023). <https://doi.org/10.26565/2312-4334-2023-3-19>
- [20] R.S. Nath, R.K. Deka, and H. Kumar, "The Effect of Thermal Stratification on Unsteady Parabolic Flow Past An Infinite Vertical Plate With Chemical Reaction," East European Journal of Physics, (4), 77-86 (2023). <https://doi.org/10.26565/2312-4334-2023-4-08>
- [21] H. Kumar, and R.K. Deka, "Thermal and Mass Stratification Effects on Unsteady Flow Past an Accelerated Infinite Vertical Plate with Variable Temperature and Exponential Mass Diffusion in Porous Medium," East European Journal of Physics, (4) 87-97 (2023), <https://doi.org/10.26565/2312-4334-2023-4-09>
- [22] S. Sarma, and N. Ahmed, "Dufour effect on unsteady MHD flow past a vertical plate embedded in porous medium with ramped temperature," Scientific Reports, **12**(1), 13343 (2022). <https://doi.org/10.1038/s41598-022-15603-x>.
- [23] M. Abramowitz, I.A. Stegun, and R.H. Romer, "Handbook of mathematical functions with formulas, graphs, and mathematical tables." American Journal of Physics, **56**(10), 958 (1988). <https://doi.org/10.1119/1.15378>
- [24] R.B. Hetnarski, "An algorithm for generating some inverse Laplace transforms of exponential form," Zeitschrift für angewandte Mathematik und Physik ZAMP, **26**, 249-253 (1975). <https://doi.org/10.1007/bf01591514>

**ВПЛИВ ТЕРМІЧНОЇ ТА МАСОВОЇ СТРАТИФІКАЦІЇ НА МГД-ПОТІК ПОВЗ
ПРИСКОРЕНУ ВЕРТИКАЛЬНУ ПЛАСТИНУ ВБУДОВАНУ В ПОРИСТЕ
СЕРЕДОВИЩЕ ЗІ ЗМІННОЮ ТЕМПЕРАТУРОЮ ТА ЕКСПОНЕНЦІАЛЬНОЮ
МАСОВОЮ ДИФУЗИЄЮ**

Дігбаш Саху, Рудра Канга Дека

Факультет математики, Університет Гаухаті, Гувахаті, 781014, Ассам, Індія

У цьому дослідженні розглядається вплив термічної та масової стратифікації на магнітогідродинаміку (МГД) поряд із вертикально прискорюваною пластинною зі змінною температурою та експоненціальною масовою дифузією в пористому середовищі. Техніка перетворення Лапласа використовується для вирішення визначальних рівнянь, пов'язаних із дифузією потоку, енергії та маси. Далі досліджується вплив стратифікації на поле течії, температуру та дифузію маси. Дослідження показує, що теплова та масова стратифікація суттєво впливає на профілі швидкості, температури та дифузії маси. Крім того, було виявлено, що стабільний стан для швидкості досягається, коли обидва параметри стратифікації підвищуються, тоді як стабільні стани для температури та концентрації виникають, коли масова стратифікація підвищується, але термічна стратифікація зменшується.

Ключові слова: МГД потік; термічна стратифікація; масове розшарування; пористе середовище; прискорена вертикальна пластинна; змінна температура; перетворення Лапласа

MODELLING AND SIMULATING THE HEAT TRANSFERENCE IN CASSON EMHD FLUID MOTION EXACERBATED BY A FLAT PLATE WITH RADIANT HEAT AND OHMIC HEATING

 Bamdeb Dey^a,  Dovine Dukru^{a*},  Tusar Kanti Das^b,  Jintu Mani Nath^c

^aDepartment of Mathematics, Assam Don Bosco University, Guwahati-781017, Assam, India

^bDepartment of Mathematics, Dudhnoi College, Dudhnoi-783124, Assam, India

^cDepartment of Mathematics, Mangaldai College, Mangaldai-784125, Assam, India

*Corresponding author email: dovinedukru1@gmail.com

Received March 17, 2024; revised April 18, 2024; accepted April 30, 2024

The current study presents the results of a numerical investigation of thermal radiation's consequences, ohmic heating, and electromagnetic hydrodynamic drag on the Casson fluid flow across a flat surface. By incorporating suitable similarity parameters, the equations that regulate the system are converted into non-linear ordinary differential equations. The MATLAB Bvp4c algorithm is used for computing nonlinear ODEs numerically. To optimize the industrial and ecological processing, it is crucial to study the flow of Casson fluids (including drilling muds, fossilised coatings, different sedimentation, and specific lubricating petroleum products, polyethylene dissolves, and a range of colloids) in the presence of heat transmission. Graphics and tables have been employed to present computational findings for various spans of the tangible variables that dictate the velocity and temperature distributions. The fluid rate decreases when the magnetic and Casson parameters rise, whereas fluid velocity increases as the local electric parameters grow. This exemplifies the intricate relationship between electromagnetic radiation and fluid mechanics. Growing Eckert number, thermal radiation, specific heat, and Biot number boost temperature profiles, whereas growing Casson parameter and local electric parameters diminish them, showing diverse impacts on heat transmission phenomena. Additionally, this inquiry pertains to the coefficient of skin friction and Nusselt values were covered. New experimental studies will benefit from this theoretical work, nevertheless.

Keywords: Heat transfer; Casson fluid; EMHD; Thermal Radiation; Ohmic heating

PACS: 44.05.+e, 44.20.+b, 44.40.+a, 47.50.+d, 47.50.Cd

INTRODUCTION

Research on fluids is based on how they physically behave. Non-Newtonian fluids, a fluid type with many real-world applications, are examined here. Non-Newtonian fluids have grown in significance in recent years owing to their widespread use in many different industries, including engineering, aerodynamics and applications, fabrication, coating, chemical processing, and many more. In the aforementioned fluids, shifts in stress and fluidity have a self-contained connection. The intricacy of unconventional fluids underlying physical properties means that no single model can adequately capture all of their attributes; materials exhibiting this trait include mud, plasma, coatings, and polymeric solutions. A good illustration of an unconventional fluid with viscoelastic, resembling a solid is the Casson fluid. Casson flow has several real-world uses in industries like nanotechnologies, food production, mineral extraction, environmental research, and extractive activities. Accordingly, M. Shuaib et al. [1] evaluate the thermal and thermophysical characteristics of Casson fluid motion as it is induced by a stochastic porous deformable surface. They noticed that as the overall pattern of the thermal source characteristic flourished, the energy conversion rate of the Casson fluid also boosted, and the overall mass movement rate of the medium climbed in tandem. In their study of MHD of Casson fluid circulation via a permeable medium, A.B. Vishalakshi et al. [2] discovered that the main physical utilization is to raise the cooling down process and the Prandtl coefficient sustains the fluid's temperature consistently. A Caputo-Fabrizio applicability to the Casson fluid over an unstable boundary layer has been illustrated by S. Abbas et al. [3]. Heat radiation's impact on the time-varying Casson fluid motion as a function of an enormously propelled slanted surface, energy, and solutal radiative boundary circumstances, and other factors was studied by Endalew and Sarkar [4]. Computing the Casson flow rate across an elevated irregular surface across a Darcy-Forchheimer opaque media under the consequences of viscous dispersion, MHD, radiation, reactants, and Joule combustion was done quantitatively by S. Jaffrullah et al. [5]. S. J. Reddy et al. [6] investigated how evaporation on electrically executing, dense, impermeable, and hybrid Casson and tiny fluids that resemble an adiabatic porous exponentially expanded surface. As the coefficients of the Casson fluid constraints, magnetic attribute, and suction component increase, authors observed that the flow trajectories decline.

The EMHD micropump operates through the use of the Lorenz effect, which arises from interplay between an external field of electric current and magnetic fields. The EMHD micropump offers several benefits over competing models, including an intuitive production process, perpetually flowing power, and the ability to pump in both directions. As M. Buren et al. [7] revealed, it has several potential applications, including fluid thumping, fluidic system flow surveillance, and fluid swirling and blending. Study findings into EMHD micropump applications, such as pivoting EMHD turbines, EMHD flow in perforated surfaces, etc., have long been popular due to the technology's potential to reduce industry-wide fossil fuel use and associated costs. In a recent publication, K. Tian et al. [8] utilized a modified time-fractional Maxwell paradigm to offer predictive and numerical algorithms for EMHD flows. In their study,

A. Ali et al. [9] examined the implications of energy and differential thermal flux on EMHD nanofluid circulation across an extending surface. E. A. Algehyne et al. [10] conducted a simulation focusing on the chemically susceptible EMHD circulation of a tiny fluid via a unidirectional Riga surface, specifically examining the effects of frequency escapes and convective boundary situations. This study by I. Qamar et al. [11] investigated how activation energy was affected of Arrhenius and varying thermal efficiency on EMHD fluid motion through a porous material over an exponentially radiated constricting surface. The inertia within the Carreau composite nanofluid's EMHD Darcy-Forchheimer escape flows via a stretchy layer in an opaque material exhibiting temperature-variant attributes was examined by Mkhathshwa and Khumalo [12]. Their discovery revealed that temperature-variant heat transfer and energy radiation interact together to improve the thermal energy transmission capabilities of the Carreau composite nanofluids. Other researchers have made newer investigations that consider the impact of EMHD available in their works [13–15]. Many industries and areas of technical fields rely on mechanics of fluids which includes heat transmission as one of its core components. The enormous consumption of energy incurred by fluid thermal exchange operations has recently brought them a lot of attention in fields including electronics, aircraft, chemicals, freezing, and advanced engineering. This is closely reminiscent of the study of B. Dey et al. [16], who simulated the heat transfer in viscous fluids over a flat surface at various temperatures and found that fluid dispersion, in addition to changed physical and thermal consequences, significantly impacts various fluid attributes, including heat. The impact of materials on the movement and conduction of heat through a horizontally stretched sheet of microbes and nanoparticles has been investigated by R. Khan et al. [17]. The transmission of heat and circulation modelling for erratic motion in symmetrical pipes with vortex generators were studied by K.S. Rambhad et al. [18]. Using Newton's principle of heating and steady heat transition, P. Jayalakshmi et al. [19] explored the heat transmission characterization of Sisko fluid motion across an elastic sheet in a conductive domain. Hu H. P. [20] addressed fluid motion and heat transmission in a narrow channel exhibiting arranged microgrooves. References [21–23] also provide some recent and similar studies on heat transmission processes.

At the same time, the Ohmic heating repercussions, also known as Joule heating, occur when electromagnetic energy is converted into heat energy because of an electric field's existence and to the electrostatic resistance of the medium. Among the many industrial and manufacturing uses of joule heating are fluorescent lighting, cooking appliances with electric radiators, thermistors, electric fuse panels, and food preservation, among many others. In their discussion of physical processes involving micropolar fluid flows via an elongated surface, B. S. Goud et al. [24] use the RKF-45 and firing techniques to examine the interplay among ohmic radiation and the effects on MHD. M. Hasan et al. [25] examined the results of ohmic heating on unconventional flow rates accompanied by thermal transfer in an asymmetrical permeable conduit. The ohmic dissipative circulation of fluid in an opaque medium along a stretching sheet involving radiant heat underwent investigation by Samuel and Fayemi [26]. The researchers looked at the effects of varying fluidity and chemical reactions. B.J. Gireesha et al. [27] inquired about the ohmic heating's effect on Casson fluid's coupled convection flow in multi-homogeneous gradients (MHD) while taking the cross-diffusion phenomenon into account.

Thermal radiation on the environment has grown significantly important due to its extensive use in technical fields, particularly in the manufacture of parts and machinery, space exploration, power plants, etc. Idowu and Sani [28] examined the effects of heat absorption on the flow's dynamics among stable and undulating surfaces. Their specific focus was on the third-grade circulation of fluid across stagnant surfaces. A study by B. Dey et al. [29] attempted to investigate how radiation affects the laminar surface layer circulation of a mechanically executing, unstable, viscid, intangible liquid moving over an ascending semi-infinite platform that penetrates a permeable channel. M. Prameela et al. [30] looked at how radiant heat worked and the Schmidt coefficient on the MHD motion of a medium around an annulus using the Rosseland model. In their study, M. A. Kumar et al. [31] assessed the implication of thermal energy on laminar adiabatic fluid flow across a spontaneously initiated upright surface in the context of MHD heating. According to what Choudhury and Dey [32] said when an outside magnetic field exists and time-varying extraction acts in an aspect normal to the movement, an inexhaustible conducting visco-elastic fluid flows unsteadily via an opaque medium through a semi-infinite lateral translucent surface.

In light of the aforementioned literature, several investigations on Casson fluid flow are being carried out under different conditions. Nevertheless, there has been scant research on how EMHD affects Casson fluid flow. Hydrothermal warehouses, energy reimbursement, healthcare engineering, thermonuclear plant development, and many more applications are possible with non-Newtonian fluids. So far, no research has demonstrated a scenario where the EMHD Casson fluid is subjected to an amalgamation of thermal radiation, conservative boundary conditions, the ohmic heating impact, and suction through a flat surface. The results of this investigation have several possible applications, such as processes in biological engineering (such as distributing drugs and bloodstream flow), chemical extraction (such as viscoplastic fluids), geophysical mechanics (such as flows of magma and sediment), alimentary processing (including microfluidics), sustainability engineering (such as effluent procedure), and many more fields.

The following unanswered questions are the basis for this examination:

- i) How are the magnetic and local electric field factors influencing the flow of a fluid?
- ii) What effects do ohmic heating parameters and thermal radiation have on heat transfer?
- iii) To what extent do these flow characteristics affect skin friction and the Nusselt number?
- iv) In the context of a convective surface boundary, how does thermal radiation affect the boundary layer?

MATHEMATICAL FORMULATION:

The current model integrates the EMHD effect alongside the ohmic heating over a steady state Casson non-Newtonian fluid flow. The prescribed flow is configured by flat plate with varying temperature across boundary. In addition to it non-linear radiation impact is imparted in the thermal boundary layer equation. Furthermore, the convective boundary condition is presumed at the vicinity of the plate. For a flat plate, the key elements of the flow rate are ‘u’ in a lateral to the separation layer’s outermost edge and ‘v’ in the other axis as demonstrated in Figure 1.

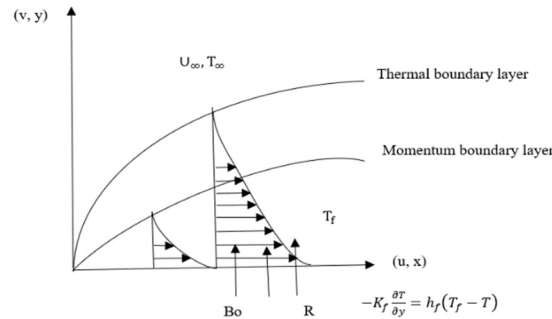


Figure 1. Flow interpretation

The boundary layer mathematical expressions for flow and temperature, based on the assumptions, can be expressed in the following dimensional form:

$$\frac{\partial u}{\partial x} + \frac{\partial v}{\partial y} = 0, \tag{1}$$

$$u \frac{\partial u}{\partial x} + v \frac{\partial u}{\partial y} = \nu_f \left(1 + \frac{1}{\beta} \right) \frac{\partial^2 u}{\partial y^2} - \frac{\sigma_f}{\rho} (B_0^2 u - E_0 B_0), \tag{2}$$

$$u \frac{\partial T}{\partial x} + v \frac{\partial T}{\partial y} = \alpha_b \left[\frac{\partial^2 T}{\partial y^2} - \frac{1}{k_f} \frac{\partial q_r}{\partial y} \right] + \frac{\mu_f}{\rho C_p} \left(1 + \frac{1}{\beta} \right) \left(\frac{\partial u}{\partial y} \right)^2 + \frac{\sigma_f}{\rho C_p} (u B_0 - E_0)^2. \tag{3}$$

With the assumption concerning the x-path thermal heat flow being modest, the number in \$q_r\$ Equation (3) shows the y-path thermal heat flow. The Rosseland diffusion approach may be used to simplify the thermal heat transfer \$q_r\$ about an optically thick fluid, as stated in [35] as:

$$q_r = \frac{4\sigma_f \partial T^4}{3k^* \partial y}. \tag{4}$$

Boundary circumstances refer to:

$$\text{At } y = 0; \quad u = 0, v = 0, -K_f \frac{\partial T}{\partial y} = h_f(T_f - T).$$

$$\text{At } y \rightarrow \infty; \quad u \rightarrow U_\infty, T \rightarrow T_\infty. \tag{5}$$

Similarity transformation:

$$\eta = y \sqrt{\frac{U_\infty}{\nu_f x}}, u = U_\infty f'(\eta), v = \frac{1}{2} \sqrt{\frac{U_\infty \nu_f}{x}} (\eta f'(\eta) - f), \theta = \frac{T - T_\infty}{T_f - T_\infty} \tag{6}$$

$$T_f - T_\infty = Ax^n, P_r = \frac{\nu_f}{\alpha_b} = \frac{\mu C_p}{k}, R = \frac{4\sigma_f (T_f - T_\infty)^3}{k^* K}, C_t = \frac{T_\infty}{T_f - T_\infty}$$

From (2)

$$\left(1 + \frac{1}{\beta} \right) f'''' + \frac{1}{2} f f'' - M f' + M E_1 = 0. \tag{7}$$

Where \$M = \frac{\sigma_f x B_0^2}{\rho U_\infty}\$, \$E_1 = \frac{E_0}{B_0 U_\infty}\$ = local electric parameter

From (3)

$$\left[1 + \frac{4}{3} R [C_t + \theta]^3 \right] \theta'' + 4R [C_t + \theta]^2 \theta'^2 + \frac{1}{2} P_r f \theta' + P_r E_c \left(1 + \frac{1}{\beta} \right) f''^2 + M P_r E_c (f' - E_1)^2 = 0. \tag{8}$$

$$P_r = \frac{\nu_f}{\alpha_b} = \frac{\mu_f}{\rho \alpha_b}, E_c = \frac{U_\infty^2}{(T_f - T_\infty) C_p}$$

Given the aforementioned relevant boundary restrictions:

$$f(0) = 0, f'(0) = 1; \theta'(0) = -Bi(1 - \theta(0)), \tag{9}$$

$$f'(\eta) \rightarrow 0; \theta(\eta) \rightarrow 0 \text{ as } \eta \rightarrow \infty.$$

Skin friction and Nusselt number expression are as follows:

$$\text{Skin friction} = \left(1 + \frac{1}{\beta}\right) f''(0)$$

$$\text{Nusselt Number} = \left(1 + \frac{4}{3}R\right) \theta'(0)$$

METHODOLOGY

This section describes how to solve the non-dimensional regressive momentum and temperature equations numerically. To numerically compute equations 7 and 8, a set of approaches based on the Lobatto 3A formula is utilized, specifically the `bvp4c` algorithm in MATLAB [33-34]. For complex, multivariate formulas, the `bvp4c` solver reliably produces correct solutions because of its mastery of enhanced accuracy threshold valued issues. It improves computing performance and reduces cognitive stress with its adaptable grid refining feature. In this method, initial predictions that are in line with the limiting constraints are necessary for the solution estimation. Afterwards, a different strategy called finite variance is used to adjust and enhance the original approximations via recurrent procedures, using the specified beginning circumstances. Simplifying the issue into a framework of initial ordinary differential equations (ODEs) is necessary for carrying out this process. When it comes to computationally addressing such non-dimensional stochastic conventional differential equations, `bvp4c` is the way to go because its degree of convergence rate is 10^{-6} times faster than other approaches.

RESULTS AND DISCUSSION

In this part, we simulate the motion of a flat plate subjected to Casson fluid and look at how different physical variables, which do not have any dimensions, affect the model. This study looked at how ohmic heating, electromagnetic radiation, and heat transmission factors affect fluid movement. Comprehensive tables and vivid illustrations are part of the content-based evaluation technique. Unless otherwise specified, the values of $M=1.5$, $R=1$, $E_1=0.1$, $Ec=0.05$, $Pr=7$, $Ct=0.2$, $\beta=0.8$, and $Bi=0.2$ are retrieved. The visual representation shows the changing behaviour of velocities $f'(\eta)$ and the temperature $\theta(\eta)$ in the erratic mathematical problem with configurable parameters. Figures 2-4 illustrate the velocity trajectories of the fluid concerning its attributes. The velocity gradients for the M ramifications are shown in Figure 2.

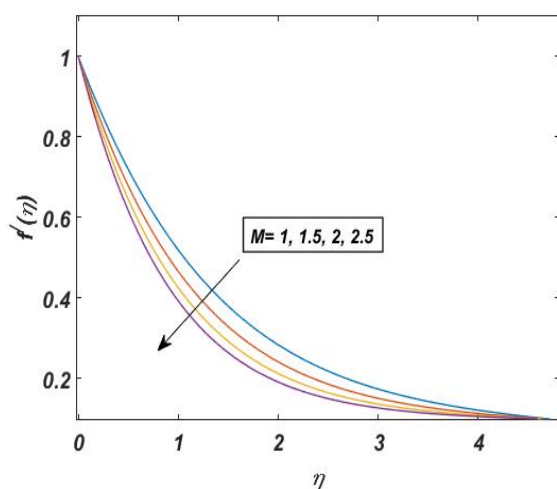


Figure 2. Effects of M on the velocity contour

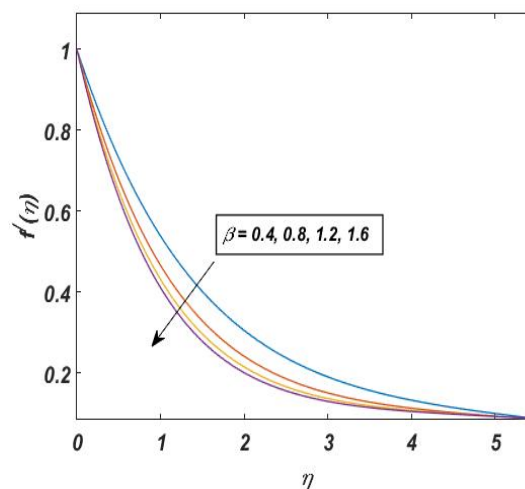


Figure 3. Effects of β on the velocity contour

The graph shows that when the magnetic coefficient M increases, the fluid's rate decreases. The Lorentz impact, which impedes the stream and is executed by the resisting effect, reduces the optimum trajectory and, consequently, the overall uniformity of the notable frontier section. The effect of attraction on a fluid is amplified as its magnetic field increases. Advantages of the Lorentz force phenomenon include pump-less mechanisms, accurate flow monitoring, and control of fluid flows in conductive fluids when subjected to electromagnetic radiation. The rheological behaviour of unconventional fluids, specifically those having stress gradients, like specific pigments, tissues, and sediments, can be described using Casson's paradigm. The fluid's resistance from flowing increases as the Casson parameter β is increased, necessitating more substantial shear forces to get an equivalent mobility. Figure 3 makes this clear that the fluid velocity drops as β rises. The hypothesis underlying this is that when β increases, the viscosity of the fluid thickens, causing it to be harder for the fragments of the medium to pass among themselves.

How the local magnetic characteristics influences E_1 on the velocity deviation is examined in Figure 4. According to this graph, how the distribution of velocity and the frontier layer thicknesses have both grown as the magnitude of E_1 increases indicating that a higher force is exerted regardless of the fluid's transition as a result of the tugging effectiveness. Flow behaviour and thermal stratification are frequently affected by electromagnetic radiation. This change is capable of enhancing the conveyance of heat, which raises the thermal contour because heat is transferred against its origin more effectively, as seen in Figure 5.

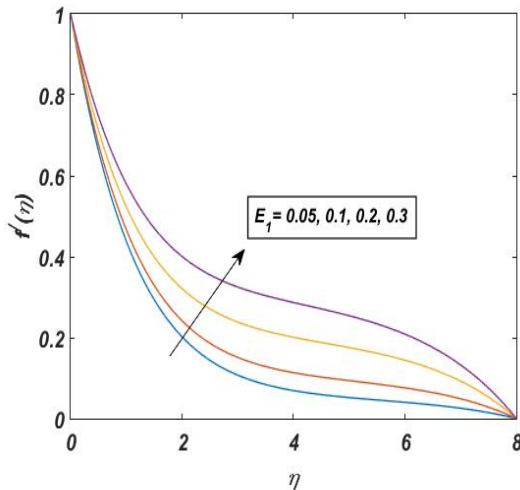


Figure 4. Effects of E_1 on velocity contour

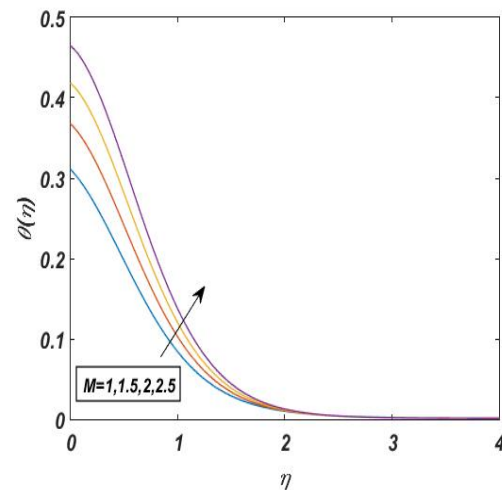


Figure 5. Effects of M on thermal contour

The relationship between transformation of enthalpy and kinetic energy becomes more significant as the Eckert number rises. An enhancement in the Eckert number might result in an upsurge in the temperature gradient as illustrated in Figure 6, since heat transfer through convection is accelerated. This is especially true when examining variations in temperature in circulation hypotheses. It is crucial to comprehend the effects of deviations in the Eckert value in uses in aviation, such as designing of propellers for aircraft and radiation shielding for a spaceship. Scientists and engineers can use this information to create cooling techniques that can handle the extreme conditions that are produced subsequent execution and after landing into the global atmosphere effectively. Casson's model includes specifications for fluidity and yield stress. Increasing Casson's attributes influences the pace of flow of the medium to rise. Figure 7 shows that energy transmission as heat increases due to an elevated viscosity, which in turn causes an enhanced temperature gradient.

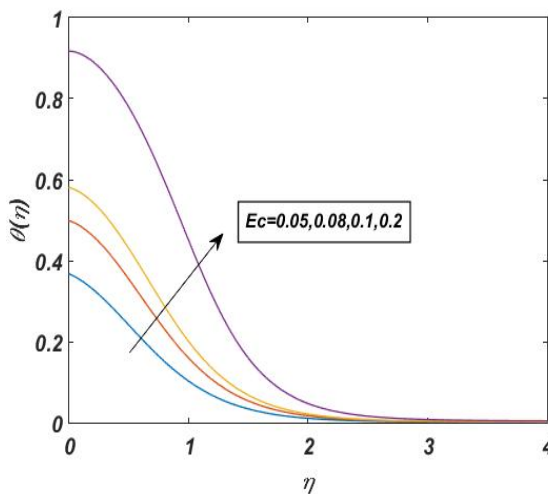


Figure 6. Effects of Ec on thermal contour

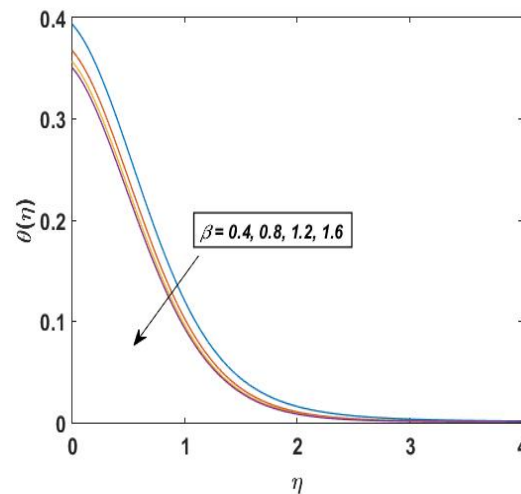


Figure 7. Effects of β on thermal contour

Maximizing efficacy, guaranteeing superior quality, and optimizing workflows all hinge on comprehending the impact of thermal variation on Casson's properties and the fluid's behaviour. In many fields, scientists and mathematicians deal with non-Newtonian fluids; hence, this knowledge aids in decision-making. Figure 8 shows how improved heat transmission and absorption mechanisms can cause temperature distributions in practical applications to rise when thermally radiated parameters like efficiency or absorbance are increased. In thermal solar panels, for example, substances with an elevated absorption rate can soak up brighter light, which in turn increases the thermal output. For manufacturing processes such as furnaces or combustion engines, elevated efficiency allows for better transmission of energy from heated surfaces to the ambient atmosphere, resulting in elevated system heat. Enhanced thermal emission characteristics, including the temperature distribution of a fluid's movement, can be altered by a shift in the local electric parameters, E_1 . The existence of electromagnetic radiation changes the trajectory of heat across the medium, inducing known as electrothermal phenomena. The emission of energy via joule combustion improves as E_1 increases because it places higher forces on energized particles inside the fluid. As apparent in Figure 9, the total thermal distribution of the fluid's motion lowers as a result of this additional energy dissipating as heat. An increasing thermal pattern in a fluid's flow rate is typically associated with an improvement in its specific heat factors, C_t . An increase in C_t indicates that the medium has a greater capacity for preserving thermal energy per mass. An improved temperature contour is the outcome of a greater ability to store heat since more of the energy is dispersed within the medium. Figure 10 shows the uniformity of the fluid's

temperature distribution circulation increases when the specific heat component rises because the fluid can hold and transport more heat. The impact is most noticeable in processes wherein heat transport is crucial, including in power plants, industrial operations, and natural occurrences. In general, the temperature persona grows as the Biot number (Bi) rises in a fluid's motion. The Biot number shows how much of an influence dispersion or transmission has on a material's thermal conductivity relative to how much heat transfer there is at the surface. If the Bi is higher, then convection is more important than conduction. Figure 11 shows that a higher thermal distribution amid the fluid's stream occurs when Bi increases because convection appears more prevalent and the fluid carries additional energy beyond its outermost layer. Hence, because convective radiation is amplified, larger Biot numbers cause fluid circulation mechanisms to have greater thermal gradients.

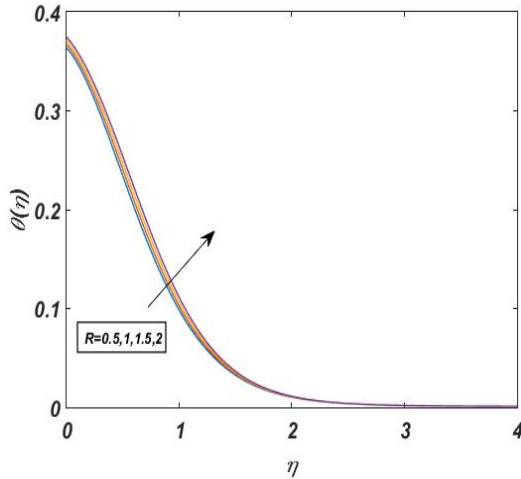


Figure 8. Effects of R on thermal contour

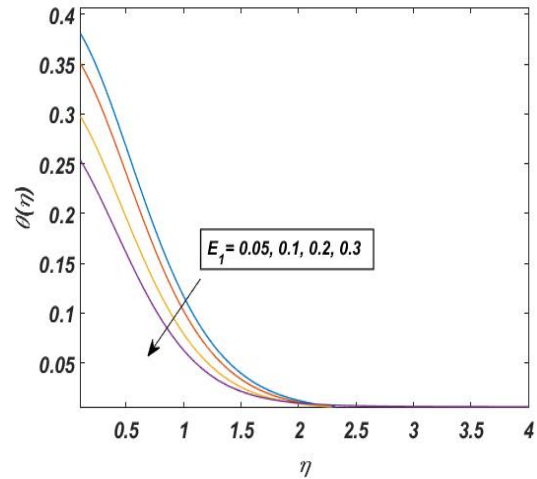


Figure 9. Effects of E_1 on thermal contour

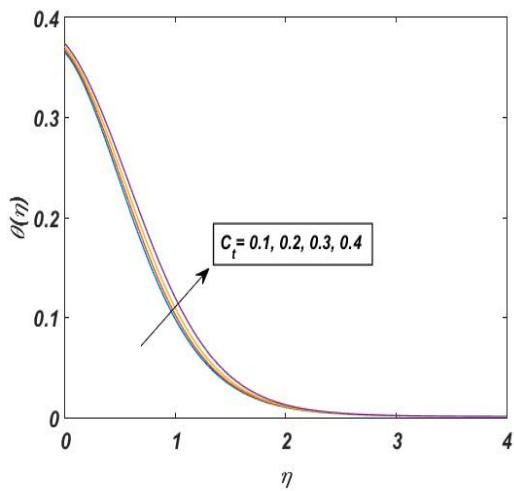


Figure 10. Effects of C_t on thermal contour

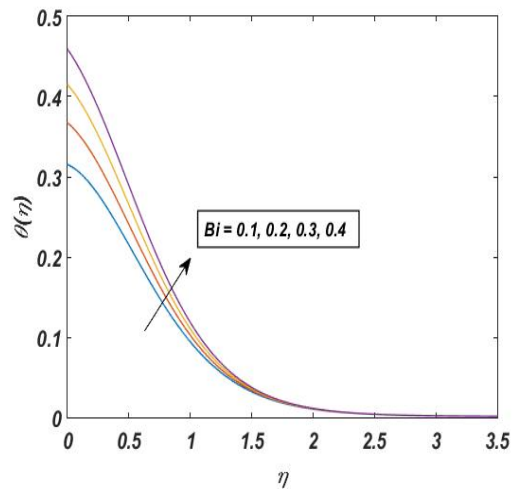


Figure 11. Effects of Bi on thermal contour

The values of skin friction and the Nusselt number are displayed in Tables 1 for different flow characteristics. The concept of skin friction is fundamental to comprehending how fluids behave as they approach substantial materials; it has consequences for many technical and physiological processes, including drag, heat transmission, radiating energy, and flow consistency. For fluid-flow technologies to function well in a variety of contexts, skin friction must be effectively managed. To slow down a moving fluid, Lorentz forces are created when a significant magnetic field induces energy in it. Furthermore, electromagnetism modifies the topology of the surface layer, which leads to less viscous drag and improved flow. Consequently, lessens skin friction by increasing the magnetic specifications, which alter the fluid mechanics via MHD effects. However, when the Casson parameter rises, the resultant stress rises as well, which in turn raises the resistance to flow and shear tension at the fluid-solid interaction, all of which contribute to greater skin friction.

Concerning convective heat transmission, the Nusselt number is fundamental to fluid mechanics. A fluid motion technique's radiative-to-thermal conductivity ratio may be measured using this method. Optimising temperatures in radiators and thermal exchangers are only two examples of the numerous engineering uses that benefit from a comprehension of the Nusselt number. As heat radiation increases, the Nusselt number drops because convection becomes less efficient. Because of the impairment to thermal conduction caused by more substantial layer thickness (shown by higher Casson parameters) and more reluctant thermal dispersion (indicated by higher Biot numbers), the Nusselt number drops. Furthermore, the Nusselt number, which quantifies the strength of heat conduction transport, increases as the

magnetic factors do as a result of magnetoconvection. A higher Eckert number indicates an improved kinetic energy to thermal transference ratio, which improves the efficacy of laminar heat transmission. By fortifying magnetohydrodynamic streams' radiative thermal transfer processes, both elements add to higher Nusselt numbers.

Table 1. Skin friction and Nusselt number

Flow factor		Skin friction	Nusselt number
R	0.5	-1.7512	-0.2121
	1	-1.7512	-0.2953
	1.5	-1.7512	-0.3775
	2	-1.7512	-0.4587
M	1	-1.4715	-0.3217
	1.5	-1.7512	-0.2953
	2	-1.9933	-0.2716
	2.5	-2.2095	-0.2500
Ec	0.05	-1.7512	-0.2953
	0.08	-1.7512	-0.2340
	0.1	-1.7512	-0.1957
	0.2	-1.7512	-0.0385
β	0.4	-2.1871	-0.2831
	0.8	-1.7512	-0.2959
	1.2	-1.5802	-0.3003
	1.6	-1.4875	-0.3031
Bi	0.1	-1.7512	-0.1597
	0.2	-1.7512	-0.2953
	0.3	-1.7512	-0.4095
	0.4	-1.7512	-0.5050

CONCLUSION

Ohmic dissipation is considered in the context of an unconventional Casson fluid flowing steadily across a flat surface. Additionally, an algorithmic strategy for the effect of radiant heat on the creation of thermal frontier layers on a surface with a convective flow limit is covered. Significant tangible constraints are imposed on the indeterminate form of the inconsistent PDEs used in the assessment. Applying the bvp4c method from MATLAB's estimate strategy, numerical solutions to similarity formulations are achieved. In this study, contour graphs and tables are used to investigate the impact that M, beta, E_1 , R, C_1 , Ec, Bi, and Pr have on the velocity and temperature. According to the findings, the outcomes are as follows:

- When the magnetic coefficient M's efficacy causes a decrease in its flow rate, the fluid's motion is transformed into thermal energy, leading to an increase in the surrounding temperature. Increased amounts of elongation indicate a stronger inhibitor for motion, which in turn causes flows to stall dramatically as viscosity grows.
- Raising the Casson parameter makes the media more viscous, which makes it harder for fragments to slip about in it. Particles are less mobile and there is more resistance to flow when the Casson factor is high. This indicates that the fluid's non-Newtonian behaviour is more noticeable, which affects its flow properties and real-world uses.
- For substantial amounts of the Casson parameters, it has been observed that the extent of the boundary layer, which determines momentum, promptly decreases.
- Casson flow velocities are raised when local electric parameters are raised, suggesting possibilities for improved control and manipulation in areas like as microfluidics, medication delivery, and industrial processes. If we can better understand this link, we may optimize processes in the related areas of technology and medicine to make them more efficient and effective.
- The temperature distribution becomes more pronounced as the temperature difference (C_1) grows.
- Heat transfer mechanisms are amplified when the Biot number and thermal emission variable are increased, leading to elevated temperature gradients. This finding is fundamental for improving industrial thermal operations, making sure energy is used efficiently, and boosting efficiency in many technical areas including harvesting solar energy and appliance condensation.

FUTURE SCOPE

Various numerical approaches have also been successful in resolving this issue. Other complicated geometrical structures may be amenable to this method's generalization. This scenario may be supplemented with an assortment of non-Newtonian models. Several crucial physical properties may be used to change the flow fluid's behaviour. So, a lot of potential studies is lying around doing nothing.

Nomenclature

u and v are velocity component along and perpendicular to the plane respectively	B_0 is strength of magnetic field
g is gravitational acceleration	K is thermal efficiency
β Casson parameter	C_p is the specific heat at persistent pressure
q_r is radiative heat flux	K_T is thermal diffusion ration
σ_f is Stefan Boltzmann constant,	η is dimensionless co-ordinate,
k^* is mean absorption	μ is dynamic viscosity
T is temperature of the fluid close to the plate	Pr is Prandtl number
T_f is base plate temperature	θ is non-dimensional temperature
T_∞ is far-field temperature	Ψ is stream function
ρ is fluid density	M is magnetic aspect
h_f heat transfer coefficient	C_t Temperature difference parameter
ν_f is kinematic viscosity	R is thermal radiation parameter
E_1 is local electric parameter	U_∞ is local electric parameter
E_0 is electric field	

ORCID

-  Bamdeb Dey, <https://orcid.org/0000-0002-9002-676X>;
  Tusar Kanti Das, <https://orcid.org/0000-0001-8105-4366>
 Jintu Mani Nath, <https://orcid.org/0000-0002-9596-2936>

REFERENCES

- [1] M. Shuaib, M. Anas, H.U. Rehman, A. Khan, I. Khan, and S.M. Eldin, "Volumetric thermo-convective casson fluid flow over a nonlinear inclined extended surface," *Scientific Reports*, **13**(1), 6324 (2023). <https://doi.org/10.1038/s41598-023-33259-z>
- [2] A.B. Vishalakshi, U.S. Mahabaleswar, M.H. Ahmadi, and M. Sharifpur, "An MHD Casson fluid flow past a porous stretching sheet with threshold non-Fourier heat flux model," *Alexandria Engineering Journal*, **69**, 727-737 (2023). <https://doi.org/10.1016/j.aej.2023.01.037>
- [3] S. Abbas, Z.U. Nisa, M. Nazar, M. Amjad, H. Ali, & A.Z. Jan, "Application of heat and mass transfer to convective flow of casson fluids in a microchannel with Caputo–Fabrizio derivative approach," *Arabian Journal for Science and Engineering*, **49**, 1275–1286 (2024). <https://doi.org/10.1007/s13369-023-08351-1>
- [4] M.F. Endalew, and S. Sarkar, "Modeling and Analysis of Unsteady Casson Fluid Flow due to an Exponentially Accelerating Plate with Thermal and Solutal Convective Boundary Conditions," *Journal of Applied Mathematics*, **2023**, 3065357 (2023). <https://doi.org/10.1155/2023/3065357>
- [5] S. Jaffrullah, W. Sridhar, and G.R. Ganesh, "MHD Radiative Casson Fluid Flow through Forchheimer Permeable Medium with Joule Heating Influence," *CFD Letters*, **15**(8), 179-199 (2023). <https://doi.org/10.37934/cfdl.15.8.179199>
- [6] S.J. Reddy, P. Valsamy, and D.S. Reddy, "Numerical Solutions of Casson-Nano Fluid Flow Past an Isothermal Permeable Stretching Sheet: MHD, Thermal Radiation and Transpiration Effects," *Journal of Nanofluids*, **12**(6), 1503-1511 (2023). <https://doi.org/10.1166/jon.2023.2034>
- [7] M. Buren, Y. Jian, L. Chang, Q. Liu, and G. Zhao, "AC magnetohydrodynamic slip flow in microchannel with sinusoidal roughness," *Microsystem Technologies*, **23**, 3347-3359 (2017). <https://doi.org/10.1007/s00542-016-3125-7>
- [8] K. Tian, S. An, G. Zhao, and Z. Ding, "Two-Dimensional Electromagnetohydrodynamic (EMHD) Flows of Fractional Viscoelastic Fluids with Electrokinetic Effects," *Nanomaterials*, **12**(19), 3335 (2022). <https://doi.org/10.3390/nano12193335>
- [9] A. Ali, H.S. Khan, S. Saleem, and M. Hussan, "EMHD nanofluid flow with radiation and variable heat flux effects along a slandering stretching sheet," *Nanomaterials*, **12**(21), 3872 (2022). <https://doi.org/10.3390/nano12213872>
- [10] E.A. Algehyne, A.F. Alharbi, A. Saeed, A. Dawar, P. Kumam, and A.M. Galal, "Numerical analysis of the chemically reactive EMHD flow of a nanofluid past a bi-directional Riga plate influenced by velocity slips and convective boundary conditions," *Scientific Reports*, **12**(1), 15849 (2022). <https://doi.org/10.1038/s41598-022-20256-x>
- [11] I. Qamar, M.A. Farooq, M. Irfan, and A. Mushtaq, "Insight into the dynamics of electro-magneto-hydrodynamic fluid flow past a sheet using the Galerkin finite element method: Effects of variable magnetic and electric fields," *Frontiers in Physics*, **10**, 1002462 (2022). <https://doi.org/10.3389/fphy.2022.1002462>
- [12] M.P. Mkhathshwa, and M. Khumalo, "Irreversibility scrutinization on EMHD Darcy–Forchheimer slip flow of Carreau hybrid nanofluid through a stretchable surface in porous medium with temperature-variant properties," *Heat Transfer*, **52**(1), 395-429 (2023). <https://doi.org/10.1002/htj.22700>
- [13] M. Irfan, M.A. Farooq, and T. Iqra, "A new computational technique design for EMHD nanofluid flow over a variable thickness surface with variable liquid characteristics," *Frontiers in Physics*, **8**, 66 (2020). <https://doi.org/10.3389/fphy.2020.00066>
- [14] S.M. Atif, M. Abbas, U. Rashid, and H. Emadifar, "Stagnation point flow of EMHD micropolar nanofluid with mixed convection and slip boundary," *Complexity*, **2021**, 3754922 (2021). <https://doi.org/10.1155/2021/3754922>
- [15] S. Khatun, M.M. Islam, M.T. Mollah, S. Poddar, and M.M. Alam, "EMHD radiating fluid flow along a vertical Riga plate with suction in a rotating system," *SN Applied Sciences*, **3**, 452 (2021). <https://doi.org/10.1007/s42452-021-04444-4>
- [16] B. Dey, J.M. Nath, T.K. Das, and D. Kalita, "Simulation of transmission of heat on viscous fluid flow with varying temperatures over a flat plate," *JP Journal of Heat and Mass Transfer*, **30**, 1-18 (2022). <http://dx.doi.org/10.17654/0973576322052>
- [17] R. Khan, A. Ahmad, M. Afraz, and Y. Khan, "Flow and heat transfer analysis of polymeric fluid in the presence of nanoparticles and microorganisms," *Journal of Central South University*, **30**(4), 1246-1261 (2023). <https://doi.org/10.1007/s11771-023-5300-1>
- [18] K.S. Rambhad, V.P. Kalbande, M.A. Kumbhalkar, V.W. Khond, and R.A. Jibhakate, "Heat transfer and fluid flow analysis for turbulent flow in circular pipe with vortex generator," *SN Applied Sciences*, **3**(7), 709 (2021). <https://doi.org/10.1007/s42452-021-04664-8>

- [19] P. Jayalakshmi, M. Obulesu, C.K. Ganteda, M.C. Raju, S.V. Varma, and G. Lorenzini, "Heat Transfer Analysis of Sisko Fluid Flow over a Stretching Sheet in a Conducting Field with Newtonian Heating and Constant Heat Flux," *Energies*, **16**(7), 3183 (2023). <https://doi.org/10.3390/en16073183>
- [20] H.P. Hu, "Theoretical Study of Convection Heat Transfer and Fluid Dynamics in Microchannels with Arrayed Microgrooves," *Mathematical Problems in Engineering*, **2021**, 3601509 (2021). <https://doi.org/10.1155/2021/3601509>
- [21] B. Dey, and R. Choudhury, "Slip Effects on Heat and Mass Transfer in MHD Visco-Elastic Fluid Flow Through a Porous Channel," in: *Emerging Technologies in Data Mining and Information Security: Proceedings of IEMIS 2018*, Vol.1 (Springer, Singapore, 2018), pp. 553-564.
- [22] R. Choudhury, B. Dey, and B. Das, "Hydromagnetic oscillatory slip flow of a visco-elastic fluid through a porous channel," *Chemical Engineering*, **71**, 961-966 (2018). <https://doi.org/10.3303/CET1871161>
- [23] A.H. Mirza, B. Dey, and R. Choudhury, "The detrimental effect of thermal exposure and thermophoresis on MHD flow with combined mass and heat transmission employing permeability," *International Journal of Applied Mechanics and Engineering*, **29**(1), 90-104 (2024). <https://doi.org/10.59441/ijame/181556>
- [24] B.S. Goud, and M.M. Nandeppanavar, "Ohmic heating and chemical reaction effect on MHD flow of micropolar fluid past a stretching surface," *Partial Differential Equations in Applied Mathematics*, **4**, 100104 (2021). <https://doi.org/10.1016/j.padiff.2021.100104>
- [25] M.M. Hasan, M.A. Samad, and M.M. Hossain, "Effects of Hall Current and Ohmic Heating on Non-Newtonian Fluid Flow in a Channel due to Peristaltic Wave," *Applied Mathematics*, **11**(04), 292 (2020). <https://doi.org/10.4236/am.2020.114022>
- [26] D.J. Samuel, and I.A. Fayemi, "Impacts of variable viscosity and chemical reaction on Ohmic dissipative fluid flow in a porous medium over a stretching sheet with thermal radiation," *Heat Transfer*, **52**(7), 5022-5040 (2023). <https://doi.org/10.1002/htj.22915>
- [27] B.J. Gireesha, K.G. Kumar, M.R. Krishnamurthy, S. Manjunatha, and N.G. Rudraswamy, "Impact of ohmic heating on MHD mixed convection flow of Casson fluid by considering cross diffusion effect," *Nonlinear Engineering*, **8**(1), 380-388 (2019). <https://doi.org/10.1515/nleng-2017-0144>
- [28] A.S. Idowu, and U. Sani, "Thermal radiation and chemical reaction effects on unsteady magnetohydrodynamic third grade fluid flow between stationary and oscillating plates," *International Journal of Applied Mechanics and Engineering*, **24**(2), 269-293 (2019). <https://doi.org/10.2478/ijame-2019-0018>
- [29] B. Dey, B. Kalita, and R. Choudhury, "Radiation and chemical reaction effects on unsteady viscoelastic fluid flow through porous medium," *Frontiers in Heat and Mass Transfer (FHMT)*, **18**, 1-8 (2022). <https://doi.org/10.5098/hmt.18.32>
- [30] M. Prameela, D.V. Lakshmi, and J.R. Gurejala, "Influence of thermal radiation on mhd fluid flow over a sphere," *Biointerface Res. Appl. Chem.* **5**(12), 6978-6990 (2021). <https://doi.org/10.33263/BRIAC125.69786990>
- [31] M.A. Kumar, Y.D. Reddy, V.S. Rao, and B.S. Goud, "Thermal radiation impact on MHD heat transfer natural convective nano fluid flow over an impulsively started vertical plate," *Case studies in thermal engineering*, **24**, 100826 (2021). <https://doi.org/10.1016/j.csite.2020.100826>
- [32] R. Choudhury, and B. Dey, "Unsteady thermal radiation effects on MHD convective slip flow of visco-elastic fluid past a porous plate embedded in porous medium," *International Journal of Applied Mathematics and Statistics*, **57**(2), 215-226 (2018).
- [33] A. Paul, J.M. Nath, and T.K. Das, "Thermally stratified Cu-Al₂O₃/water hybrid nanofluid flow with the impact of an inclined magnetic field, viscous dissipation and heat source/sink across a vertically stretching cylinder," *ZAMM-Journal of Applied Mathematics and Mechanics/Zeitschrift für Angewandte Mathematik und Mechanik*, **104**(2), e202300084 (2023). <https://doi.org/10.1002/zamm.202300084>
- [34] A. Paul, J.M. Nath, and T.K. Das, "An investigation of the MHD Cu-Al₂O₃/H₂O hybrid- nanofluid in a porous medium across a vertically stretching cylinder incorporating thermal stratification impact," *Journal of Thermal Engineering*, **9**(3), 799-810 (2023). <https://doi.org/10.18186/thermal.1300847>
- [35] B.K. Jha, B.Y. Isah, and I.J. Uwanta, "Combined effect of suction/injection on MHD free-convection flow in a vertical channel with thermal radiation," *Ain Shams Engineering Journal*, **9**(4), 1069-1088 (2018). <https://doi.org/10.1016/j.asej.2016.06.001>

МОДЕЛЮВАННЯ ТА ІМІТАЦІЯ ВПЛИВУ ТЕПЛООБМІНУ НА ЕМНД ПОТІК CASSON РІДИНИ, ПОСИЛЕНИЙ ПЛОСКОЮ ПЛАСТИНОЮ З ПРОМЕНЕВИМ ТА ОМІЧНИМ НАГРІВОМ

Бамдеб Дей^а, Довін Дукру^а, Тусар Канті Дас^б, Джінту Мані Нат^с

^аФакультет математики, Університет Дона Боско в Ассамі, Гувахаті-781017, Ассам, Індія

^бДепартамент математики, Дудхой коледж, Дудхой, Ассам, Індія

^сДепартамент математики, коледж Мангалдай, Мангалдай-784125, Ассам, Індія

Поточне дослідження представляє результати чисельного дослідження впливу теплового випромінювання, омічного нагріву та електромагнітного гідродинамічного опору на потік рідини Кассона через плоску поверхню. Використовуючи відповідні параметри подібності, рівняння, які регулюють систему, перетворюються на нелінійні звичайні диференціальні рівняння. Алгоритм MATLAB Ввр4с використовується для чисельного обчислення нелінійних ODE. Для оптимізації промислової та екологічної обробки вкрай важливо вивчити потік рідини Кассона (включаючи бурові розчини, скам'янілі покриття, різні відкладення та специфічні мастильні нафтопродукти, поліетилен, що розчиняється, і ряд колоїдів) за наявності теплопередачі. Графіки та таблиці були використані для представлення обчислювальних результатів для різних діапазонів відчутних змінних, які визначають розподіл швидкості та температури. Швидкість рідини зменшується, коли магнітні параметри та параметри Кассона зростають, тоді як швидкість рідини збільшується зі зростанням локальних електричних параметрів. Це є прикладом складного зв'язку між електромагнітним випромінюванням і механікою рідини. Зростає число Еккерта, теплове випромінювання, питома теплоємність і число Біо підвищують профілі температури, тоді як зростання параметра Кассона та локальних електричних параметрів зменшує їх, демонструючи різні впливи на явища теплопередачі. Крім того, цей запит стосується коефіцієнта шкірного тертя та значень Нуссельта. Проте нові експериментальні дослідження виграють від цієї теоретичної роботи.

Ключові слова: теплообмін; рідина Кассона; EMHD; теплове випромінювання; омічний нагрів

THERMAL AND MASS STRATIFICATION EFFECTS ON UNSTEADY MHD PARABOLIC FLOW PAST AN INFINITE VERTICAL PLATE WITH VARIABLE TEMPERATURE AND MASS DIFFUSION THROUGH POROUS MEDIUM

 Pappu Das*,  Rudra Kanta Deka

Department of Mathematics, Gauhati University, Guwahati-781014, Assam, India

**Corresponding Author e-mail: pappudas751@gmail.com*

Received March 03, 2024; revised April 15, 2024; accepted April 22, 2024

This study examines how thermal and mass stratification affect unsteady MHD parabolic flow past an infinite vertical plate through porous medium with variable heat and mass diffusion. Analytical solutions are derived for unitary Prandtl and Schmidt numbers using Laplace transform technique to simulate the the flow's physical process. The investigation takes into account how the flow field is impacted by thermal and mass stratification. Following that, the outcomes of the stratification case are then compared with the scenario in which the flow field has no stratification. The finding of this study can help us comprehend more about the unsteady MHD parabolic flow and provide insightful information for stratified systems.

Keywords: *MHD flow; Vertical plate; Parabolic flow; Electrically conducting fluid; Unsteady flow; Stratified fluid; Porous medium*

PACS: 44.05.+e, 47.11.-j, 47.55.P-, 47.56.+r, 47.65.-d

1. INTRODUCTION

The most evident effect of thermal stratification is felt by anyone who has gone for a summer swim and felt the chilly water a few feet under the warm surface. The process by which density causes a body of fluid to develop comparatively stable and distinct layers is known as stratification of fluid which takes place mostly at higher temperatures. It happens mostly due to change in temperature, concentration, or the presence of various fluids with differing densities. Many natural systems, including lakes and oceans, exhibit the phenomenon of thermal stratification. Stratification obstructs the vertical fluid mixing that influences the exchange of nutrients, carbon, oxygen, and heat.

The study of parabolic flow problem plays an important role because it lessens viscous interactions between adjacent fluid layers and the pipe wall, which helps to minimize energy losses in flowing fluids. The parabolic motion has several uses, including solar cookers, solar concentrators, and parabolic trough solar collectors.

Using an infinite vertical plate in mass and heat transfer process is one of the applications for parabolic flow. Due to their significance in engineering and industrial processes such as the cooling of electronic equipment, sun collectors, solar cookers, solar concentrators, etc.—these difficulties are being studied in great detail. [1], [2], [3] and [4] came up with analytical solutions of different problems of thermal stratification or stratified fluid with various conditions. Numerous authors have been studied MHD flow past vertical plates and cylinders with stratification effects. [5], [6] and [7] studied MHD flow problems past vertical plate with stratification effects. [8] investigated the heat and mass diffusion flow along a surface in porous medium. [9] studied the effects of both thermal and mass stratification past an accelerated infinite vertical plate in porous medium. [10], conducted an investigation on parabolic flow problem past vertical plate, while [11] and [12] investigated MHD parabolic flow problems past vertical plates with several conditions.

In this article, we investigate the combined effects of thermal and mass stratification on unsteady MHD parabolic flow past an infinite vertical plate embedded in a porous medium with variable temperature and mass diffusion. For the unitary Prandtl and Schmidt numbers the solutions are then obtained. The investigation on velocity, temperature and concentration profiles are made under the impacts of variables and displayed on graphs. These variables include the thermal Grashof number Gr , mass Grashof number Gc , magnetic parameter M , time t , Darcy number Da and stratification parameters γ and ξ . On other physical phenomena including the rate of heat and mass transfer and skin friction, the effects of M , Gr , Gc , γ , ξ and t are also studied. For classical case when γ and ξ are absent, the solutions are then obtained and are compared to the original case that is when stratification is present. The conclusion of this study have numerous applications in engineering and several industries.

2. MATHEMATICAL ANALYSIS

In this work, we investigate an unstable MHD parabolic flow in two dimensions across an infinite vertical plate of a viscous, incompressible, and electrically conducting fluid embedded in a porous medium with variable temperature and mass diffusion. In order to examine the flow scenario, we utilize a coordinate system where the x' axis is selected vertically upward along the plate and the y' axis is perpendicular to the plate. The fluid and plate have the same initial fluid concentration C'_∞ and starting temperature T'_∞ . The plate is moving with the velocity $U_R t'^2$ in its own plane at time $t' > 0$ relative to the gravitational field. Also the plate temperature and concentration level are raised to T'_w and C'_w respectively at time $t' > 0$. Due to the infinite length of the plate, all the flow variables are independent of x' and only impacted by y' and t' . The equations for motion, energy, and concentration are then represented by the Boussinesq's approximation as follows:

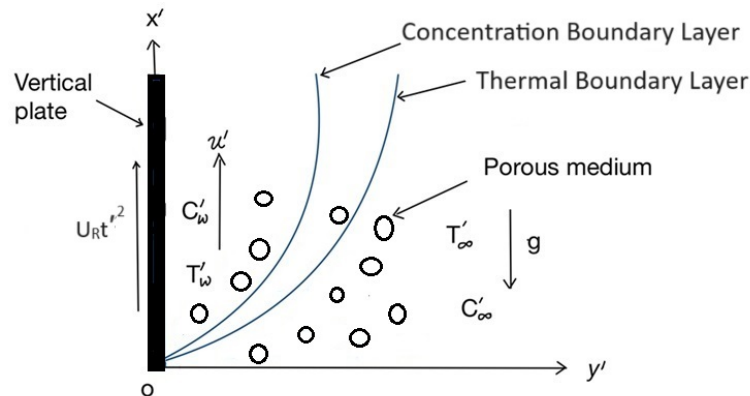


Figure 1. Physical model of the problem

$$\frac{\partial u'}{\partial t'} = \nu \frac{\partial^2 u'}{\partial y'^2} + [g\beta(T' - T'_\infty) + g\beta_c(C' - C'_\infty)] - \frac{\sigma B_0^2 u'}{\rho} - \frac{\nu u'}{k'} \quad (1)$$

$$\frac{\partial T'}{\partial t'} = \frac{k}{\rho C_p} \frac{\partial^2 T'}{\partial y'^2} - \gamma' u' \quad (2)$$

$$\frac{\partial C'}{\partial t'} = D \frac{\partial^2 C'}{\partial y'^2} - \xi' u' \quad (3)$$

Considering the initial and boundary conditions as:

$$u' = 0, \quad T' = T'_\infty, \quad C' = C'_\infty \quad \forall y', t' \leq 0$$

$$u' = U_R t'^2, \quad T' = T'_\infty + (T'_w - T'_\infty) A t',$$

$$C' = C'_\infty + (C'_w - C'_\infty) A t' \quad \text{at } y' = 0, \quad t' > 0 \quad (4)$$

$$u' \rightarrow 0, \quad T' \rightarrow T'_\infty, \quad C' \rightarrow C'_\infty \quad \text{as } y' \rightarrow \infty, \quad t' > 0$$

where, $\gamma' = \frac{dT'_\infty}{dx'} + \frac{g}{C_p}$ denotes the thermal stratification parameter and $\frac{dT'_\infty}{dx'}$ denotes the vertical temperature convection known as thermal stratification. In addition, $\frac{g}{C_p}$ represents the rate of reversible work done on fluid particles by compression, often known as work of compression. The variable (γ') denotes the thermal stratification parameter in our study as the compression work is relatively minimal. Regarding testing of computational methods, compression work is kept as an additive to thermal stratification.

Now, we introduce the following non-dimensional quantities:

$$\begin{aligned}
 y &= \frac{y'}{L_R}, \quad t = \frac{t'}{t_R}, \quad u = \frac{u'}{U_R}, \quad Da = \frac{U_R^2 k'}{\nu^2}, \quad , \quad Pr = \frac{\mu C_p}{k} \\
 M &= \frac{\sigma B_0^2 \nu}{\rho U_R^2}, \quad Sc = \frac{\nu}{D}, \quad \theta = \frac{T' - T'_\infty}{T'_w - T'_\infty}, \quad C = \frac{C' - C'_\infty}{C'_w - C'_\infty}, \quad \Delta T = T'_w - T'_\infty \tag{5} \\
 Gc &= \frac{\nu g \beta_c (C'_w - C'_\infty)}{U_R^3}, \quad U_R = (\nu g \beta \Delta T)^{1/3}, \quad L_R = \left(\frac{g \beta \Delta T}{\nu^2} \right)^{-1/3}, \quad A = \frac{1}{t_R}, \\
 t_R &= (g \beta \Delta T)^{-2/3} \nu^{1/3}, \quad Gr = \frac{\nu g \beta (T'_w - T'_\infty)}{U_R^3}, \quad \gamma = \frac{\gamma' L_R}{\Delta T}, \quad \xi = \frac{\xi' L_R}{C' - C'_\infty}
 \end{aligned}$$

When the non-dimensional quantities defined in (5) above are employed, equations (1), (2), and (3) take on the following forms:

$$\frac{\partial u}{\partial t} = \frac{\partial^2 u}{\partial y^2} + Gr\theta + GcC - \left(M + \frac{1}{Da} \right) u \tag{6}$$

$$\frac{\partial \theta}{\partial t} = \frac{1}{Pr} \frac{\partial^2 \theta}{\partial y^2} - \gamma u \tag{7}$$

$$\frac{\partial C}{\partial t} = \frac{1}{Sc} \frac{\partial^2 C}{\partial y^2} - \xi u \tag{8}$$

And the corresponding initial and boundary conditions (4) then reduce to,

$$u = 0, \quad \theta = 0, \quad C = 0 \quad \forall y, t \leq 0$$

$$u = t^2, \quad \theta = t, \quad C = t \quad \text{at } y = 0, t > 0 \tag{9}$$

$$u \rightarrow 0, \quad \theta \rightarrow 0, \quad C \rightarrow 0 \quad \text{as } y \rightarrow \infty, t > 0$$

2.1. Method of Solution

Solving the non-dimensional governing equations (6), (7) and (8) with respect to the boundary conditions (9) for the unitary Prandtl and Schmidt numbers, we obtain the velocity, temperature and concentration profiles with the help of [13] and [14] as:

$$u = C_1 f(A_1) - C_2 [h(A_1) - h(B_1)] - C_3 f(B_1) \tag{10}$$

$$\theta = t D_1 \left[\left(1 + \frac{y^2}{2t} \right) \operatorname{erfc} \left(\frac{y}{2\sqrt{t}} \right) - \frac{y e^{-\frac{y^2}{4t}}}{\sqrt{\pi t}} \right] + D_2 [f(A_1) - f(B_1)] + D_3 h(B_1) - D_4 h(A_1) \tag{11}$$

$$C = t E_1 \left[\left(1 + \frac{y^2}{2t} \right) \operatorname{erfc} \left(\frac{y}{2\sqrt{t}} \right) - \frac{y e^{-\frac{y^2}{4t}}}{\sqrt{\pi t}} \right] + E_2 [f(A_1) - f(B_1)] + E_3 h(B_1) - E_4 h(A_1) \tag{12}$$

For the sake of succinctness, our study refers to the situation where pressure work is omitted and the environment is isothermal ($\gamma = 0, \xi = 0$) as the classical scenario. The velocity (u^*), temperature (θ^*) and concentration (C^*) profiles for classical case are obtained as,

$$u^* = f(N) - F_1 h(N) + F_1 \left[\left(1 + \frac{y^2}{2t} \right) \operatorname{erfc} \left(\frac{y}{2\sqrt{t}} \right) - \frac{ye^{-\frac{y^2}{4t}}}{\sqrt{\pi t}} \right] \tag{13}$$

$$\theta^* = t \left[\left(1 + \frac{y^2}{2t} \right) \operatorname{erfc} \left(\frac{y}{2\sqrt{t}} \right) - \frac{ye^{-\frac{y^2}{4t}}}{\sqrt{\pi t}} \right] \tag{14}$$

$$C^* = t \left[\left(1 + \frac{y^2}{2t} \right) \operatorname{erfc} \left(\frac{y}{2\sqrt{t}} \right) - \frac{ye^{-\frac{y^2}{4t}}}{\sqrt{\pi t}} \right] \tag{15}$$

where

$$N = M + \frac{1}{Da}, \quad A_1 = \frac{N + \sqrt{N^2 - 4\gamma Gr - 4\xi Gc}}{2}, \quad B_1 = \frac{N - \sqrt{N^2 - 4\gamma Gr - 4\xi Gc}}{2}, \quad C_1 = \frac{A_1}{A_1 - B_1},$$

$$C_2 = \frac{Gr + Gc}{A_1 - B_1}, \quad C_3 = \frac{B_1}{A_1 - B_1}, \quad D_1 = 1 - \frac{\gamma(Gr + Gc)}{A_1 B_1}, \quad D_2 = \frac{\gamma}{A_1 - B_1}, \quad D_3 = \frac{\gamma(Gr + Gc)}{B_1(A_1 - B_1)},$$

$$D_4 = \frac{\gamma(Gr + Gc)}{A_1(A_1 - B_1)}, \quad E_1 = 1 - \frac{\xi(Gr + Gc)}{A_1 B_1}, \quad E_2 = \frac{\xi}{A_1 - B_1}, \quad E_3 = \frac{\xi(Gr + Gc)}{B_1(A_1 - B_1)}, \quad E_4 = \frac{\xi(Gr + Gc)}{A_1(A_1 - B_1)}, \quad F_1 = \frac{Gr + Gc}{N}.$$

And f and h are inverse Laplace transforms and are given by

$$f(A_1) = L^{-1} \left\{ \frac{e^{-y\sqrt{s+A_1}}}{s^3} \right\} \text{ and } h(A_1) = L^{-1} \left\{ \frac{e^{-y\sqrt{s+A_1}}}{s^2} \right\}$$

Using the formulas given by [14], we separate the complex arguments of the error function that were present in the preceding expressions into real and imaginary components.

2.2. Skin-Friction

The non-dimensional computation of skin-friction of the plate is given by:

$$\tau = - \left. \frac{du}{dy} \right|_{y=0} \tag{16}$$

Now from equation (10) we get the expression for skin-friction as,

$$\tau = \frac{C_1}{2} \left[t^2 \sqrt{A} \operatorname{erf}(\sqrt{At}) + \sqrt{\frac{t}{\pi}} t e^{-At} - \frac{\operatorname{erf}(\sqrt{At})}{4A^{\frac{3}{2}}} + \frac{\operatorname{terf}(\sqrt{At})}{\sqrt{A}} + \frac{\sqrt{t} e^{-At}}{2A\sqrt{\pi}} \right] - \frac{C_3}{2} \left[t^2 \sqrt{B} \operatorname{erf}(\sqrt{Bt}) + \sqrt{\frac{t}{\pi}} t e^{-Bt} \right.$$

$$- \frac{\operatorname{erf}(\sqrt{Bt})}{4B^{\frac{3}{2}}} + \frac{\operatorname{terf}(\sqrt{Bt})}{\sqrt{B}} + \frac{\sqrt{t} e^{-Bt}}{2B\sqrt{\pi}} \left. \right] - C_2 \left[t \sqrt{A} \operatorname{erf}(\sqrt{At}) + \sqrt{\frac{t}{\pi}} e^{-At} + \frac{\operatorname{erf}(\sqrt{At})}{2\sqrt{A}} - t \sqrt{B} \operatorname{erf}(\sqrt{Bt}) + \sqrt{\frac{t}{\pi}} e^{-Bt} \right.$$

$$\left. \left. + \frac{\operatorname{erf}(\sqrt{Bt})}{2\sqrt{B}} \right] \tag{17}$$

Skin-friction in classical scenario is obtained as,

$$\tau^* = \frac{1}{2} \left[t^2 \sqrt{N} \operatorname{erf}(\sqrt{Nt}) + \sqrt{\frac{t}{\pi}} t e^{-Nt} - \left(\frac{1}{4N} - t \right) \frac{\operatorname{erf}(\sqrt{Nt})}{\sqrt{N}} + \sqrt{\frac{t}{\pi}} \frac{e^{-Nt}}{2N} \right] - \frac{Gr + Gc}{N} \left[t \sqrt{N} \operatorname{erf}(\sqrt{Nt}) + \sqrt{\frac{t}{\pi}} (2 + e^{-Nt}) + \frac{\operatorname{erf}(\sqrt{Nt})}{\sqrt{N}} \right] \tag{18}$$

2.3. Plate Heat Flux (Nusselt Number)

The non-dimensional form of rate of heat transfer (Nusselt Number) is given by,

$$Nu = -\frac{d\theta}{dy}\Big|_{y=0} \tag{19}$$

Now from equation (11) we get the expression for Nusselt number as,

$$Nu = 2D_1\sqrt{\frac{t}{\pi}} + \frac{D_2}{2} \left[t^2\sqrt{A}erf(\sqrt{At}) + \sqrt{\frac{t}{\pi}}te^{-At} - \frac{erf(\sqrt{At})}{4A^{\frac{3}{2}}} + \frac{terf(\sqrt{At})}{\sqrt{A}} + \frac{\sqrt{t}e^{-At}}{2A\sqrt{\pi}} - t^2\sqrt{B}erf(\sqrt{Bt}) - \sqrt{\frac{t}{\pi}}te^{-Bt} + \frac{erf(\sqrt{Bt})}{4B^{\frac{3}{2}}} - \frac{terf(\sqrt{Bt})}{\sqrt{B}} - \frac{\sqrt{t}e^{-Bt}}{2B\sqrt{\pi}} \right] - D_4 \left[t\sqrt{A}erf(\sqrt{At}) + \sqrt{\frac{t}{\pi}}e^{-At} + \frac{erf(\sqrt{At})}{2\sqrt{A}} \right] + D_3 \left[t\sqrt{B}erf(\sqrt{Bt}) + \sqrt{\frac{t}{\pi}}e^{-Bt} + \frac{erf(\sqrt{Bt})}{2\sqrt{B}} \right] \tag{20}$$

For classical case, Nusselt number is derived as,

$$Nu^* = 2\sqrt{\frac{t}{\pi}} \tag{21}$$

2.4. Sherwood Number

The non-dimensional form of rate of mass transfer (Sherwood Number) is given by,

$$Sh = -\frac{dC}{dy}\Big|_{y=0} \tag{22}$$

Now from equation (12) we get the expression for Sherwood number as,

$$Sh = 2E_1\sqrt{\frac{t}{\pi}} + \frac{E_2}{2} \left[t^2\sqrt{A}erf(\sqrt{At}) + \sqrt{\frac{t}{\pi}}te^{-At} - \frac{erf(\sqrt{At})}{4A^{\frac{3}{2}}} + \frac{terf(\sqrt{At})}{\sqrt{A}} + \frac{\sqrt{t}e^{-At}}{2A\sqrt{\pi}} - t^2\sqrt{B}erf(\sqrt{Bt}) - \sqrt{\frac{t}{\pi}}te^{-Bt} + \frac{erf(\sqrt{Bt})}{4B^{\frac{3}{2}}} - \frac{terf(\sqrt{Bt})}{\sqrt{B}} - \frac{\sqrt{t}e^{-Bt}}{2B\sqrt{\pi}} \right] - E_4 \left[t\sqrt{A}erf(\sqrt{At}) + \sqrt{\frac{t}{\pi}}e^{-At} + \frac{erf(\sqrt{At})}{2\sqrt{A}} \right] + E_3 \left[t\sqrt{B}erf(\sqrt{Bt}) + \sqrt{\frac{t}{\pi}}e^{-Bt} + \frac{erf(\sqrt{Bt})}{2\sqrt{B}} \right] \tag{23}$$

For classical case, Sherwood number is obtained as,

$$Sh^* = 2\sqrt{\frac{t}{\pi}} \tag{24}$$

3. RESULTS AND DISCUSSIONS

The solutions obtained from the previous section’s numerical computations are displayed in Figures from 2 to 25 and discuss the effects of various physical parameters on temperature, velocity, concentration fields, skin friction, Nusselt number, and Sherwood number, which provides us with better insight of the problem in terms of physical significance. It has been found that a stratified fluid moves slower in compare to unstratified fluid because of density varying property a resistive type of force (Lorentz force) occurs which lowers the flow velocity. The velocity profiles are shown in figures from 2 to 7 for different values of magnetic parameter M ,

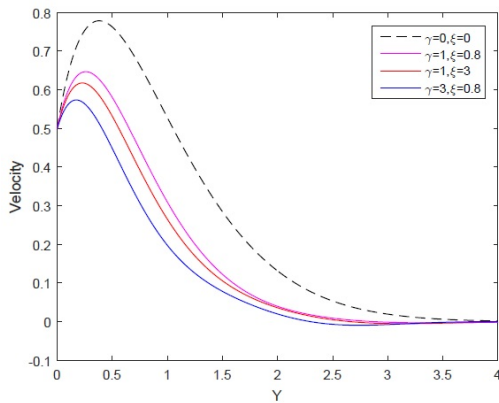


Figure 2. Effects of γ and ξ on Velocity Profile for $Gr = 5, Gc = 5, t = 1, M = 1, Da = 0.5$

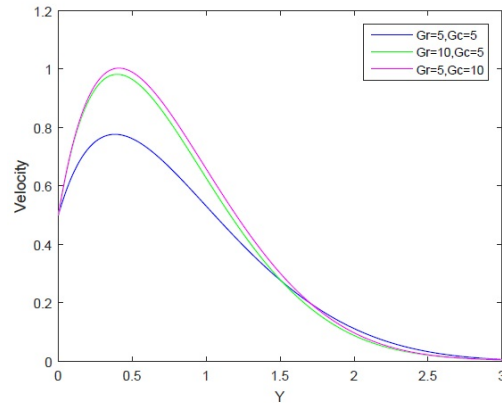


Figure 3. Effects of Gr and Gc on Velocity Profile for $\gamma = 1, \xi = 0.8, t = 1, M = 1, Da = 0.5$

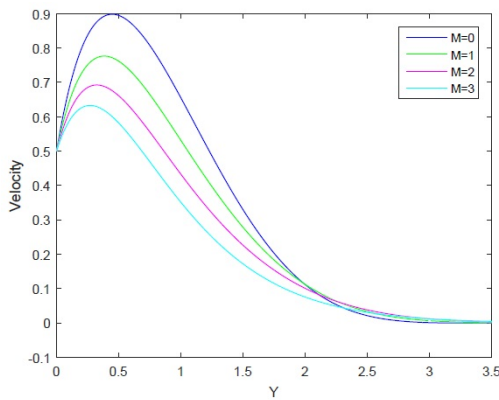


Figure 4. Effects of M on Velocity Profile for $\gamma = 1, \xi = 0.8, Gr = 5, Gc = 5, t = 1, Da = 0.5$

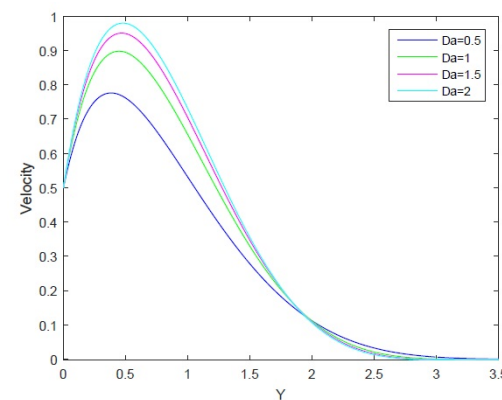


Figure 5. Effects of Da on Velocity Profile for $\gamma = 1, \xi = 0.8, Gr = 5, Gc = 5, M = 1, t = 1$

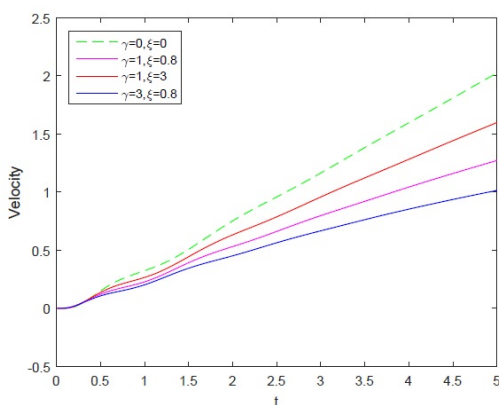


Figure 6. Effects of γ and ξ on Velocity Profile against time for $y = 1, Gr = 5, Gc = 5, M = 1, Da = 0.5$

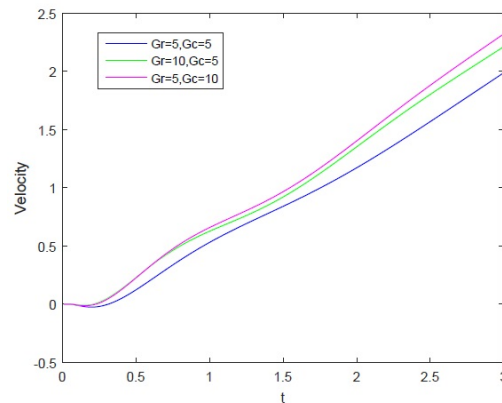


Figure 7. Effects of Gr and Gc on Velocity Profile against time for $y = 1, \gamma = 1, \xi = 0.8, M = 1, Da = 0.5$

Darcy number Da , thermal Grashof number Gr , mass Grashof number Gc , thermal stratification parameter γ , mass stratification parameter ξ and time t . As the values of γ and ξ , which stand for thermal and mass stratification, rise, the velocity decreases. It has been observed that when the magnetic parameter M increases, the velocity profile falls because the flow velocity is lowered due to a resistive type of force known as the Lorentz force occurs. When thermal Grashof number Gr , mass Grashof number Gc , and Darcy number Da increase, velocity profile and velocity profile against time increase as well in both classical and non-classical cases. The velocity profile against time increases in classical ($\gamma = 0$ and $\xi = 0$) case in compare to the stratified case.

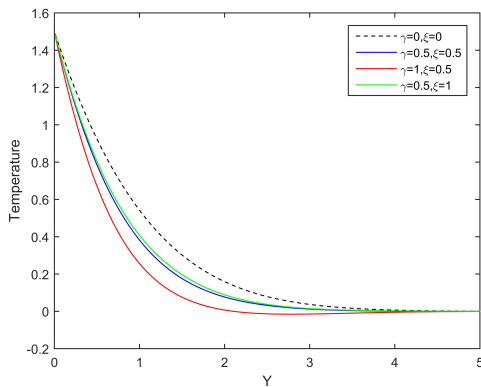


Figure 8. Effects of γ and ξ on Temperature Profile for $Gr = 5, Gc = 5, t = 1.5, M = 1, Da = 0.5$

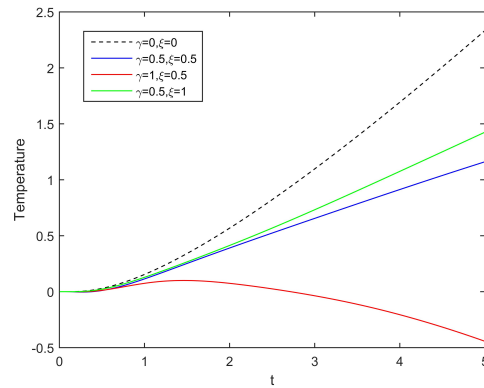


Figure 9. Effects of γ and ξ on Temperature Profile against time for $y = 1.5, Gr = 5, Gc = 5, M = 1, Da = 0.5$

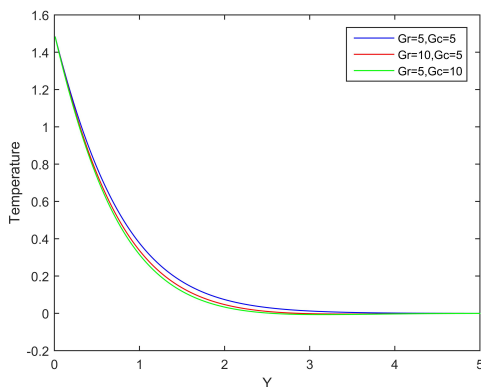


Figure 10. Effects of Gr and Gc on Temperature Profile for $\gamma = 1, \xi = 0.8, t = 1.5, M = 1, Da = 0.5$

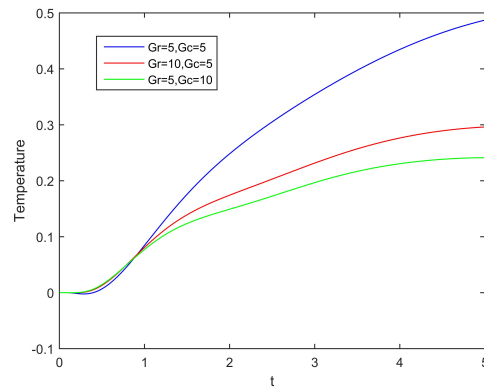


Figure 11. Effects of Gr and Gc on Temperature Profile against time for $y = 1.5, \gamma = 1, \xi = 0.8, M = 1, Da = 0.5$

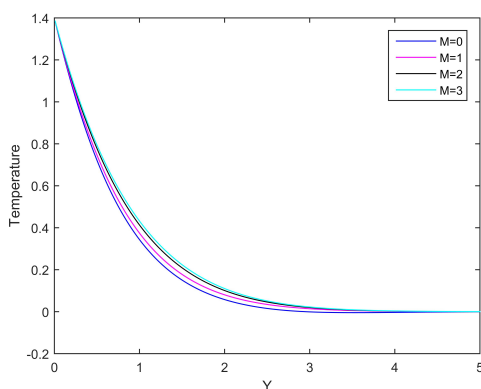


Figure 12. Effects of M on Temperature Profile for $\gamma = 1, \xi = 0.8, Gr = 5, Gc = 5, t = 1.5, Da = 0.5$

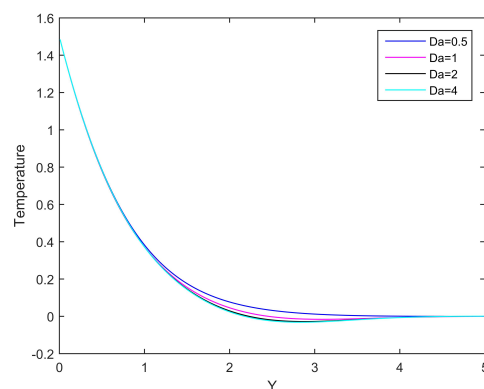


Figure 13. Effects of Da on Temperature Profile for $\gamma = 1, \xi = 0.8, Gr = 5, Gc = 5, t = 1.5, M = 1$

The temperature and concentration profiles with and without stratification for various values of $\gamma, \xi, M, Gr, Gc, Da$ and t are shown graphically in figures 8 to 19. From figures 8 and 9 it is seen that temperature is more in classical case as compared to the non-classical case. Likewise figures 14 and 15 depict that concentration is less in stratified fluid in compare to the unstratified fluid. Figures 12 and 18 depict the effect of magnetic parameter M on temperature and concentration profile. Temperature and concentration increase as M increases. From figures 13 and 19 it is seen that as Darcy number (Da) grows, temperature and concentration fall down.

It is clear from figures 10 and 11 and 16 and 17 that temperature and concentration decrease when the thermal and mass Grashof numbers (Gr and Gc) increase.

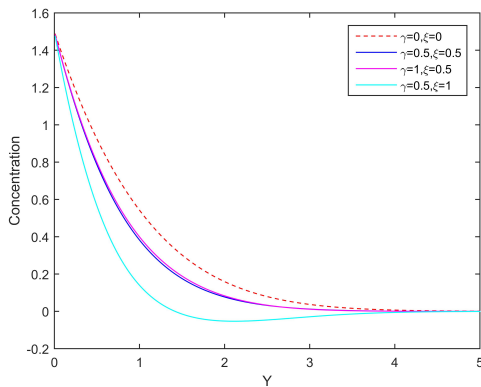


Figure 14. Effects of γ and ξ on Concentration Profile for $Gr = 5, Gc = 5, t = 1.5, M = 1, Da = 0.5$

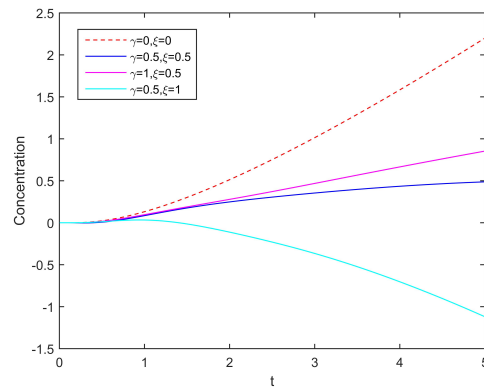


Figure 15. Effects of γ and ξ on Concentration Profile against time for $y = 1.5, Gr = 5, Gc = 5, M = 1, Da = 0.5$

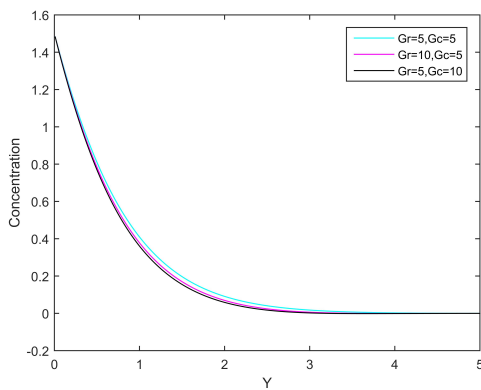


Figure 16. Effects of Gr and Gc on Concentration Profile for $\gamma = 1, \xi = 0.8, t = 1.5, M = 1, Da = 0.5$

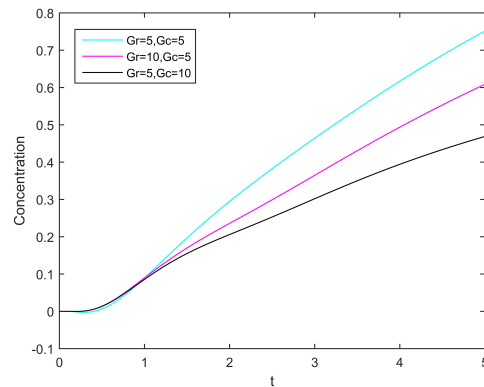


Figure 17. Effects of Gr and Gc on Concentration Profile against time for $y = 1.5, \gamma = 1, \xi = 0.8, M = 1, Da = 0.5$

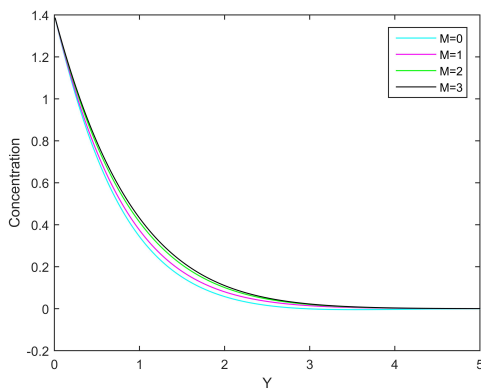


Figure 18. Effects of M on Concentration Profile for $\gamma = 1, \xi = 0.8, Gr = 5, Gc = 5, t = 1.5, Da = 0.5$

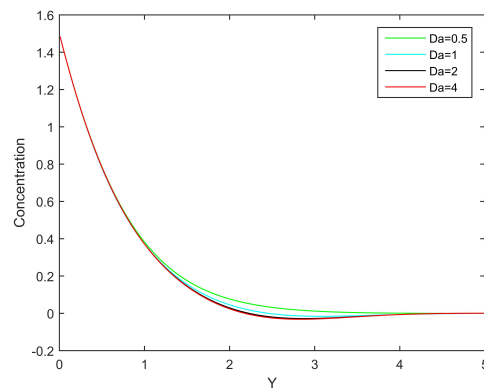


Figure 19. Effects of Da on Concentration Profile for $\gamma = 1, \xi = 0.8, Gr = 5, Gc = 5, t = 1.5, M = 1$

The effects of γ, ξ , thermal Grashof (Gr) and mass Grashof (Gc) numbers on skin-friction, Nusselt number and Sherwood number are presented in the figures 20 to 25. In classical case that is when $\gamma = 0$ and $\xi = 0$,

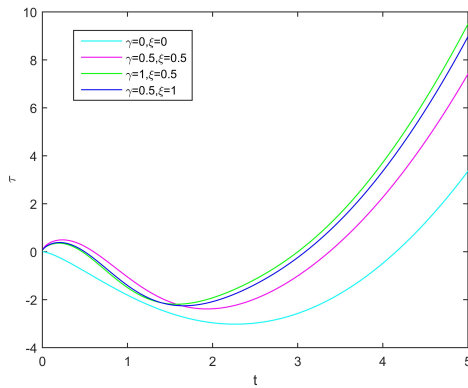


Figure 20. Effects of γ and ξ on skin-friction for $Gr = 5, Gc = 5, M = 1, Da = 0.5$

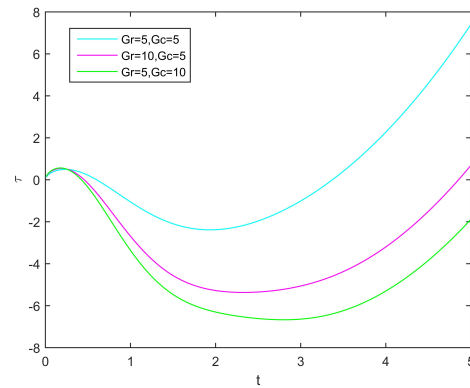


Figure 21. Effects of Gr and Gc on skin-friction for $\gamma = 1, \xi = 0.8, M = 1, Da = 0.5$

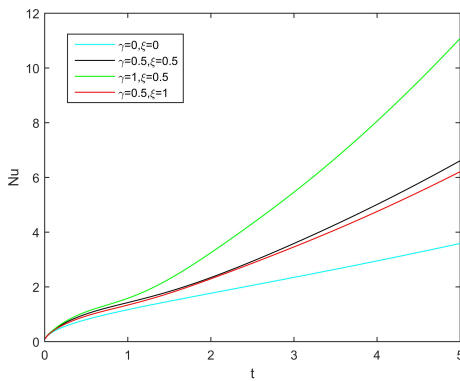


Figure 22. Effects of γ and ξ on Nusselt number for $Gr = 5, Gc = 5, M = 1, Da = 0.5$

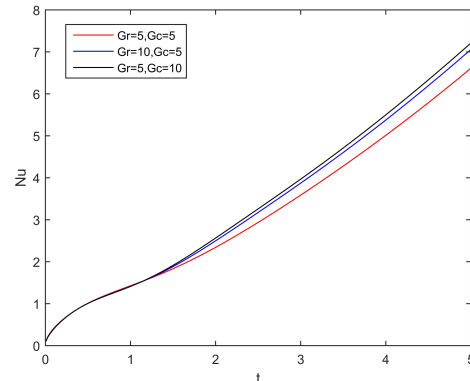


Figure 23. Effects of Gr and Gc on Nusselt number for $\gamma = 1, \xi = 0.8, M = 1, Da = 0.5$

skin-friction, Nusselt number and Sherwood number decrease as compared to the stratification case. It has been observed that while rising in the values of Gr and Gc , skin-friction falls down. In case of Nusselt and Sherwood numbers, when Gr and Gc increase, both Nusselt and Sherwood numbers increase.

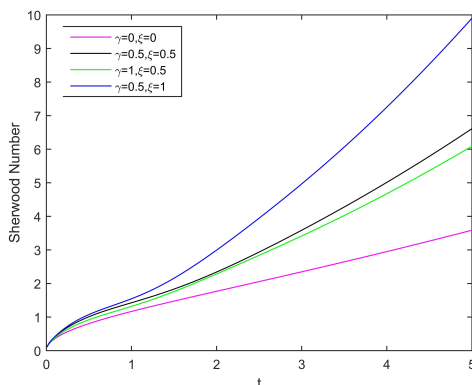


Figure 24. Effects of γ and ξ on Sherwood number for $Gr = 5, Gc = 5, M = 1, Da = 0.5$

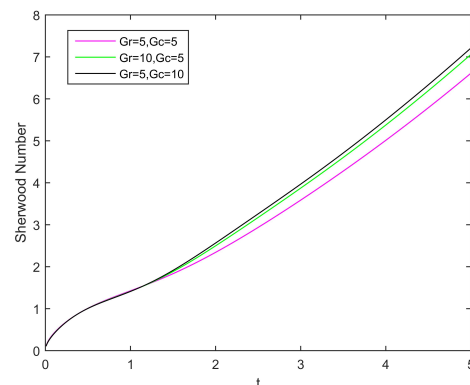


Figure 25. Effects of Gr and Gc on Sherwood number for $\gamma = 1, \xi = 0.8, M = 1, Da = 0.5$

4. CONCLUSION

We have explored the impact of thermal and mass stratification on unsteady MHD parabolic flow past an infinite vertical plate embedded in a porous medium with variable heat and mass diffusion. The present

study's findings have been juxtaposed with those of the classical scenario in which stratification is absent. The conclusion of our study that based on the results derived from the previous sections are as follows:

- When γ and ξ grow, velocity, temperature and concentration drop as both the stratification (thermal and mass) effect stabilises the fluid and becomes steady state. But in the classical situation, velocity, temperature and concentration are higher than in the thermally and mass stratified fluid.
- Velocity, temperature and concentration profiles grow as Gr and Gc increase but velocity decreases as M increases and both temperature and concentration rise as M grows.
- Velocity grows as Darcy number Da increases but temperature and concentration fall down as Da rises.
- Skin-friction, Nusselt number and Sherwood number decrease in isothermal case as compared to the stratification case.
- With rising the values of Gr and Gc , Nusselt number and Sherwood number also increase but skin-friction falls down.

ORCID

 Pappu Das, <https://orcid.org/0009-0007-8006-3659>;  Rudra Kanta Deka, <https://orcid.org/0009-0007-1573-4890>

REFERENCES

- [1] J.S. Park, and J.M. Hyun, "Transient behavior of vertical buoyancy layer in a stratified fluid," *Intl. J. Heat Mass Transfer*, **41**, 4393-4397 (1998). [https://doi.org/10.1016/S0017-9310\(98\)00175-6](https://doi.org/10.1016/S0017-9310(98)00175-6)
- [2] J.S. Park, "Transient buoyant flows of a stratified fluid in a vertical channel," *KSME. Intl. J.* **15**, 656-664 (2001). <https://doi.org/10.1007/BF03184382>
- [3] A. Shapiro, and E. Fedorovich, "Unsteady convectively driven flow along a vertical plate immersed in a stably stratified fluid," *J. Fluid Mech.* **498**, 333-352 (2004). <https://doi.org/10.1017/S0022112003006803>
- [4] E. Magyari, I. Pop, and B. Keller, "Unsteady free convection along an infinite vertical flat plate embedded in a stably stratified fluid-saturated porous medium," *Transport in Porous Media*, **62**, 233-249 (2006). <https://doi.org/10.1007/s11242-005-1292-6>
- [5] B.C. Neog, and R.K. Deka, "Unsteady natural convection flow past an accelerated vertical plate in a thermally stratified fluid," *Theoret. Appl. Mech.* **36**(4), 261-274 (2009). <https://doi.org/10.2298/TAM0904261D>
- [6] R.K. Deka, and A. Bhattacharya, "Magneto-Hydrodynamic (MHD) flow past an infinite vertical plate immersed in a stably stratified fluid," *International Journal of the Physical Sciences*, **6**(24), 5831-5836 (2011). <https://doi.org/10.5897/IJPS11.011>
- [7] S. Gurminder, P.R. Sharma, and A.J. Chamkha, "Effect of thermally stratified ambient fluid on MHD convective flow along a moving non isothermal vertical plate," *Intl. J. Phy. Sci.* **5**(3), 208-215 (2010). <https://doi.org/10.5897/IJPS.9000199>
- [8] R.C. Chaudhary, and A. Jain, "MHD heat and mass diffusion flow by natural convection past a surface embedded in a porous medium," *Theoret. Appl. Mech.* **36**(1), 1-27 (2009). <http://dx.doi.org/10.2298/TAM0901001C>
- [9] H. Kumar, and R.K. Deka, "Thermal and mass stratification effects on unsteady flow past an accelerated infinite vertical plate with variable temperature and exponential mass diffusion in porous medium," *East European Journal of Physics*, (4), 87-97 (2023). <https://doi.org/10.26565/2312-4334-2023-4-09>
- [10] R.S. Nath, R.K. Deka, and H. Kumar, "The Effect of Thermal Stratification on Unsteady Parabolic Flow past an Infinite Vertical Plate with Chemical Reaction," *East European Journal of Physics*, (4), 77-86 (2023). <https://doi.org/10.26565/2312-4334-2023-4-08>
- [11] A. Selvaraj, S.D. Jose, R. Muthucumaraswamy, and S. Karthikeyan, "MHD-parabolic flow past an accelerated isothermal vertical plate with heat and mass diffusion in the presence of rotation," *Materials Today: Proceedings*, **46**, 3546-3549 (2021). <https://doi.org/10.1016/j.matpr.2020.12.499>
- [12] R. Muthucumaraswamy, and P. Sivakumar, "Hydromagnetic effects on parabolic flow past an infinite vertical plate with variable mass diffusion in the presence of thermal radiation and chemical reaction," *ARPN Journal of Engineering and Applied Sciences*, **10**(12) (2015). <http://dx.doi.org/10.13140/RG.2.2.13011.84008>
- [13] R.B. Hetnarski, "An algorithm for generating some inverse laplace transforms of exponential form," *Zeitschrift fur angewandte Mathematik und Physik ZAMP*, **26**, 249-253 (1975). <https://doi.org/10.1007/BF01591514>
- [14] M. Abramowitz, I.A. Stegun, and R.H. Romer. "Handbook of mathematical functions with formulas, graphs, and mathematical tables," *American Journal of Physics*, **56**(10), 958 (1988). <https://doi.org/10.1119/1.15378>

**ВПЛИВ ТЕРМІЧНОЇ ТА МАСОВОЇ СТРАТИФІКАЦІЇ НА НЕСТАЦІОНАРНИЙ
МГД-ПАРАБОЛІЧНИЙ ПОТІК ПОВЗ НЕСКІНЧЕННУ ВЕРТИКАЛЬНУ ПЛАСТИНУ
ЗІ ЗМІННОЮ ТЕМПЕРАТУРОЮ ТА ДИФУЗИЄЮ МАСИ ЧЕРЕЗ
ПОРИСТЕ СЕРЕДОВИЩЕ**

Паппу Дас, Рудра Канта Дека

Факультет математики, Університет Гаухаті, Губахаті-781014, Ассам, Індія

У цьому дослідженні досліджується, як теплова та масова стратифікація впливає на нестационарний МГД-параболічний потік повз нескінченну вертикальну пластину через пористе середовище зі змінною дифузійною теплою та масою. Аналітичні рішення отримані для унітарних чисел Прандтля та Шмідта з використанням техніки перетворення Лапласа для моделювання фізичного процесу потоку. Дослідження бере до уваги те, як на поле течії впливає теплова та масова стратифікація. Після цього результати випадку стратифікації порівнюються зі сценарієм, у якому поле потоку не має стратифікації. Результати цього дослідження можуть допомогти нам зрозуміти більше про нестационарний МГД-параболічний потік і надати глибоку інформацію для стратифікованих систем.

Ключові слова: *МГД потік; вертикальна пластину; параболічний потік; електропровідна рідина; нестабільний потік; стратифікована рідина; пористе середовище*

NUMERICAL ANALYSIS OF ENTROPY GENERATION OF MHD CASSON FLUID FLOW THROUGH AN INCLINED PLATE WITH SORET EFFECT

 **Hiren Deka**,  **Parismita Phukan***, **Puja Haloi**

Department of Mathematics, Cotton University, Assam, India

**Corresponding Author e-mail: parismita12007@gmail.com*

Received March 12, 2024; revised April 19, 2024; accepted April, 22, 2024

In this present study, entropy generation for an unsteady MHD Casson fluid flow through an oscillating inclined plate is investigated. Here, along with reaction by chemical and thermal radiation incorporation of Soret effect is also analysed. The solution of the equation which governs the flow problem are obtained by finite difference method (FDM). The features of flow velocity, concentration and temperature are analyzed by designing graphs and their physical behaviour is reviewed in details to study the impact of different parameters on the fluid problem. The skin friction, the rate of heat and mass transfer of the fluid problem also has significant impact under the influence of the parameters. The results indicate that Soret effect and other parameters has considerable impact on an unsteady MHD Casson fluid and on the total entropy due to heat transfer and flow friction.

Keywords: *Entropy; Casson; MHD; Soret effect; Thermal radiation*

PACS: 44.05.+e, 44.40.+a, 47.11.-j

MSC2020: 76W05

1. INTRODUCTION

Conservation of energy to produce thermodynamically efficient heat transfer processes has been a topic of interest. The past few years we observed a growing interest in thermodynamics of heat transmission and heat exchange equipments. Heat transmission can be accompanied by entropy generation or thermodynamic irreversibility.

Entropy generation may be due variety of sources such as viscous effects and heat transfer down temperature gradients. It has its huge applications in heat engines, heat pumps, freezers, power plants, and air conditioners. A. Bejan showed how entropy generation rate can be reduced in simple components for heat exchange with an objective to how to reduce useful power. This study will lead the way in which a flow geometry may be selected to reduce generation of entropy. In the intervening years, research work on entropy generation has received considerable attention. Many researchers have contributed their work on entropy generation for a MHD flow. Bejan [1] analyzed the origin of entropy distribution and production for convective heat transmission. Bejan et al. [2] extended entropy generation through heat and fluid flow. Abu-Hijleh [3] numerically analysed the entropy generation for convective flow from a rotating cylinder. The analysis of entropy generation for various physical configurations has been able to draw attentions of researchers and were investigated by many researchers like Baytas[4], Mahmud and Islam [5], Oliveski et al. [6], Hooman et al. [7], Abdelhameed [8], Khan et al. [9], Mansour et al. [10], Sharma et al. [11]. Khan et al. [12] have deliberated the entropy generation of a flow through rotating cone with Dufour and Soret effect's impact. Shit et al. [13] examine the entropy generation for an unsteady flow of nanofluid. Afsana et al. [14] have analysed the entropy generation for a ferrofluid in a wavy enclosure. Qing et al. [15] analysed generation of entropy over a stretching/shrinking porous surface for flow of Casson Nanofluid. Aiboud and Saouli [16] analysed entropy over a stretched surface when a magnetic field is present for MHD viscous flow. Hussain et al. [17] analysed the entropy generation for a double diffusive convection in staggered cavity. Yazdi et al. [18] analysed the entropy generation of parallel open microchannels which is embedded with continuous moving permeable surface. Yazdi et al. [19] extended it for permeable micropatterned surface. Rashidi et al. [20] numerically investigated the generation of entropy over a porous rotating disk with influence of slip factor presented the MHD flow and entropy analysis of heat transmission in a square cavity occupied with Cu–Al₂O₃.

The present study of entropy generation for an unsteady MHD Casson fluid flow through an oscillating inclined plate is investigated along with reaction by chemical and thermal radiation and incorporation of Soret effect is also analysed great importance in various fields of energy storage systems and minimization of heat transfer. Heat transfer can be accompanied by entropy generation which has its various applications in different engineering process. Hence, from the literature and its wide applications has motivated the present analysis. The novel aspects of the present analysis are as follows:

- To examine total entropy generations of MHD flow through an inclined plane in addition with the features of flow velocity, temperature and concentration.
- The entropy generation for a free convection is associated with transfer of heat and flow friction of the fluid.
- Along with reaction by chemical and thermal radiation incorporation of Soret effect is also analysed.
- The non-dimensional governing equations are solved numerically by finite difference method in MATLAB.

2. STATEMENT

We consider an incompressible one-dimensional unsteady MHD free convection flow with mass and heat transfer of a Casson fluid flowing through an oscillating inclined plate. We consider a viscous fluid with the influence of thermal radiation and reaction by chemical. We consider a coordinate system, where the \bar{x} -axis represents the vertically upward direction and \bar{y} -axis is normal to the plate in the direction of the fluid flow. All the existing fluid properties except the influence of density in concentration and temperature are considered to be constant. The induced magnetic field in contrast to the applied magnetic field is considered to be negligible.

Keeping in view the assumptions made above and usual Boussinesq's approximation the equations which governs the flow are:

$$\frac{\partial u^*}{\partial \tau^*} = \nu \left(1 + \frac{1}{\alpha} \right) \frac{\partial^2 u^*}{\partial \eta^{*2}} + g\beta(T^* - T_{\infty}^*) \cos \gamma + g\beta^*(C^* - C_{\infty}^*) \cos \gamma - \frac{\sigma}{\rho} B_0^2 u^*, \quad (1)$$

$$\frac{\partial T^*}{\partial \tau^*} = \frac{k}{\rho C_p} \frac{\partial^2 T^*}{\partial \eta^{*2}} - \frac{1}{\rho C_p} \frac{\partial q_r^*}{\partial \eta^*}, \quad (2)$$

$$\frac{\partial C^*}{\partial \tau^*} = D_m \frac{\partial^2 C^*}{\partial \eta^{*2}} - kr'(C^* - C_{\infty}^*) + \frac{D_m K_T}{T_m} \left(\frac{\partial^2 T^*}{\partial \eta^{*2}} \right), \quad (3)$$

$$E_g = \frac{k}{T^*{}^2} \left[\left(\frac{\partial T^*}{\partial \eta^*} \right)^2 \right] + \frac{\mu}{T^*} \left[\left(\frac{\partial u^*}{\partial \eta^*} \right)^2 \right]. \quad (4)$$

The relevant initial and boundary conditions:

$$u^* = U, T^* = T_w^* + \epsilon e^{i\omega t} (T_w^* - T_{\infty}^*), C^* = C_w^* + \epsilon e^{i\omega t} (C_w^* - C_{\infty}^*) \text{ at } \eta^* = 0, \quad (5)$$

$$u^* \rightarrow 0, T^* \rightarrow 0, C^* \rightarrow 0 \text{ as } \eta^* \rightarrow \infty. \quad (6)$$

where component of velocity in x' direction is u^* , the kinematic viscosity is ν , the time is τ^* , the acceleration caused by gravity is g , the Casson parameter is α , the angle of inclination is γ , the thermal expansion coefficient is β , the coefficient of mass is β^* , the fluid temperature is T^* , the temperature away from plate is T_{∞}^* , the temperature near the plate is T_w^* , the fluid concentration is C^* , the fluid concentration when it is away from the plate is C_{∞}^* , the fluid concentration near the plate is C_w^* , the magnetic permeability of the fluid is σ , the density of the fluid is ρ , the coefficient of magnetic field is B_0 , the thermal conductivity is k , the specific heat at constant pressure is C_p , the thermal radiation flux is q_r^* , the chemical reaction rate constant kr' , the thermal diffusion ratio is K_T , the coefficient of mass diffusion is D_m , the mean fluid temperature is T_m , the scalar constant is ϵ , the dimensionless exponential index is ω .

The thermal radiation flux gradient q_r^* under Rosseland approximation is expressed as follows:

$$-\frac{\partial q_r^*}{\partial \eta^*} = 4a\sigma^* (T_{\infty}^* - T_4^*). \quad (7)$$

where σ^* is the Stefan-Boltzmann constant. The difference of temperature within the flow is considered to be into Taylor's series about the free stream temperature. Hence neglecting the higher order terms the result of the approximation is as follows:

$$T_4^* \cong 4T_{\infty}^{*3} T^* - 3T_{\infty}^{*4}$$

We now introduce the following parameters and non-dimensional quantities:

$$\bar{y} = \frac{\eta^* U}{\nu}, \bar{u} = \frac{u^*}{U}, \bar{t} = \frac{\tau^* U^2}{\nu}, \bar{\theta} = \frac{(T^* - T_{\infty}^*)}{T_w^* - T_{\infty}^*}, \bar{\phi} = \frac{(C^* - C_{\infty}^*)}{C_w^* - C_{\infty}^*}, Gr = \frac{g\beta\nu(T_w^* - T_{\infty}^*)}{U^3},$$

$$Gm = \frac{g\beta^*\nu(C_w^* - C_{\infty}^*)}{U^3}, Pr = \frac{\mu C_p}{k}, Sc = \frac{\nu}{D}, M = \frac{\sigma B_0^2 \nu}{\rho U^2}, R = \frac{16a\sigma^* \nu^2 T_{\infty}^{*3}}{U^2 \rho C_p}, S_T = \frac{E_g T_{\infty}^{*2} \nu^2}{k (T_w^* - T_{\infty}^*)^2 U^2},$$

$$\xi = \frac{\mu U^2 T_{\infty}^{*2}}{k (T_w^* - T_{\infty}^*)^2} Kr = \frac{\nu kr'}{U^2}, Sr = \frac{D_m K_T (T_w^* - T_{\infty}^*)}{T_m \nu (C_w^* - C_{\infty}^*)}.$$

Where Gm is the Grashof number for mass transfer, Gr is the Grashof number for heat transfer, Pr is the Prandtl number, Sc is the Schmidt number, Kr is the chemical reaction parameter, M is the Hartmann number and R is the radiation parameter and Sr is the Soret number.

Using the non-dimensional quantities, the equations (1) to (4) reduces to:

$$\frac{\partial \bar{u}}{\partial \bar{t}} = \left(1 + \frac{1}{\alpha}\right) \frac{\partial^2 \bar{u}}{\partial \bar{y}^2} + G_1 \bar{\theta} + G_2 \bar{\phi} - M \bar{u}, \tag{8}$$

$$\frac{\partial \bar{\theta}}{\partial \bar{t}} = \frac{1}{Pr} \frac{\partial^2 \bar{\theta}}{\partial \bar{y}^2} - R \bar{\theta}, \tag{9}$$

$$\frac{\partial \bar{\phi}}{\partial \bar{t}} = \frac{1}{Sc} \frac{\partial^2 \bar{\phi}}{\partial \bar{y}^2} - Kr \bar{\phi} + Sr \frac{\partial^2 \bar{\theta}}{\partial \bar{y}^2}, \tag{10}$$

$$S_T = \left(\frac{\partial \bar{\theta}}{\partial \bar{y}}\right)^2 + \xi \left(\frac{\partial \bar{u}}{\partial \bar{y}}\right)^2. \tag{11}$$

Here, $G_1 = Gr \cos \gamma, G_2 = Gm \cos \gamma$

The non-dimensional form of the corresponding boundary conditions is:

$$\begin{aligned} \bar{u} = 1, \bar{\theta} = 1 + \epsilon e^{i\omega t}, \bar{\phi} = 1 + \epsilon e^{i\omega t} \text{ at } \bar{y} = 0 \\ \bar{u} \rightarrow 0, \bar{\theta} \rightarrow 0, \bar{\phi} \rightarrow 0 \text{ as } \bar{y} \rightarrow \infty \end{aligned}$$

3. SOLUTIONS OF THE PROBLEM

In this section, the transformed equations (8) - (11) are coupled non-linear partial differential equations. So, the analytical or exact solutions seem to be not feasible. Finite Difference Method (FDM) is a method which is used to solve differential equations that are quite difficult or impossible to be solved analytically. It is comparatively precise, effective and has better stability characteristics.

The fundamental formula is:

$$\frac{\partial F}{\partial y'} = \lim_{\Delta y' \rightarrow 0} \frac{F(y') - F(y' - \Delta y')}{\Delta y'}$$

The equation above is used to discretise a PDE and then implement a numerical method to solve. The equivalent finite difference scheme for equations (8) to (11) is as follows:

$$\frac{\bar{u}_{i+1,j} - \bar{u}_{i,j}}{\Delta \bar{t}} = \frac{\left(1 + \frac{1}{\alpha}\right) \bar{u}_{i,j+1} - 2\bar{u}_{i,j} + \bar{u}_{i,j-1}}{(\Delta \bar{y})^2} + G_1 \bar{\theta}_{i,j} + G_2 \bar{\phi}_{i,j} - M \bar{u}_{i,j}, \tag{12}$$

$$\frac{\bar{\theta}_{i+1,j} - \bar{\theta}_{i,j}}{\Delta \bar{t}} = \frac{1}{Pr} \left(\frac{\bar{\theta}_{i,j+1} - 2\bar{\theta}_{i,j} + \bar{\theta}_{i,j-1}}{(\Delta \bar{y})^2} \right) - R \bar{\theta}_{i,j}, \tag{13}$$

$$\frac{\bar{\phi}_{i+1,j} - \bar{\phi}_{i,j}}{\Delta \bar{t}} = \frac{1}{Sc} \left(\frac{\bar{\phi}_{i,j+1} - 2\bar{\phi}_{i,j} + \bar{\phi}_{i,j-1}}{(\Delta \bar{y})^2} \right) - Kr \bar{\phi}_{i,j} + Sr \left(\frac{\bar{\theta}_{i,j+1} - 2\bar{\theta}_{i,j} + \bar{\theta}_{i,j-1}}{(\Delta \bar{y})^2} \right), \tag{14}$$

$$S_T = \left(\frac{\bar{\theta}_{i+1,j} - \bar{\theta}_{i,j}}{\Delta \bar{y}}\right)^2 + \xi \left(\frac{\bar{u}_{i+1,j} - \bar{u}_{i,j}}{\Delta \bar{y}}\right)^2. \tag{15}$$

4. RESULT AND DISCUSSION

The problem of an unsteady MHD Casson fluid flow past an inclined moving plate in the influence of reaction by chemical, thermal radiation and Soret-effect has been investigated. The mathematical formulation that governs the fluid flow problem is given in equations (1) - (4). Solving these equations, numerical solution has been obtained for the total entropy generation, fluid velocity, concentration, temperature, skin friction, coefficient of the rate of mass and heat transfer in terms of Sherwood number and Nusselt number. Ignoring the imaginary part, numerical results have been displayed in figures and tables. Numerical results obtained using Finite Difference method (FDM) on the governing partial differential equations which analysis the unsteady MHD Casson fluid flow through an oscillating inclined plate with the influence of reaction by chemical, thermal radiation and Soret effect are displayed in graphs and tables. For our computational analysis, we employed $Gr=5, Gm=5, Pr=.7, R=1, M=5, Sc=.22, Sr=1, Kr=1, T=1.25, \epsilon = .05, \omega = 10$. unless otherwise stated.

Figure (1)-(4) is portrayed to study the most significant characteristics of the present analysis that is the total entropy generation due to the incorporation of chemical reaction, radiation parameter, Casson parameter and Soret effect. Here, the total entropy for free convection is associated with heat transfer and flow friction. Figure (1) illustrates the chemical reaction influence on total entropy. As the chemical reaction parameter rise the total entropy behaves inversely. Along with it the total entropy decreases with the rise in Hartmann number. Figure (2) illustrates that the increase in the impact of radiation parameter the generation of entropy lowers. Figure (3) shows that the generation of entropy expressed as a function of Hartmann number rise proportionately with the rise in Casson parameter. Figure (4) illustrates that the total entropy lowers with the rise in Soret effect.

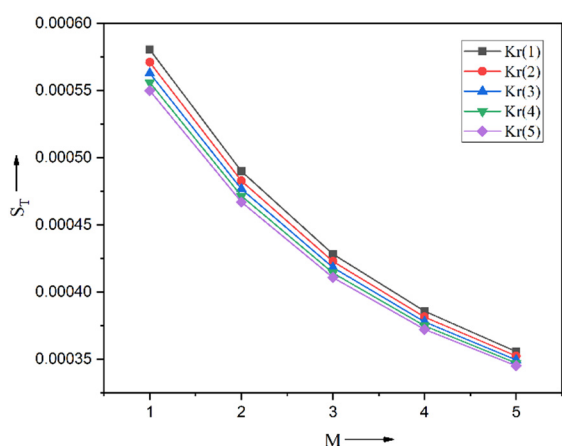


Figure 1. Total entropy with change in chemical reaction

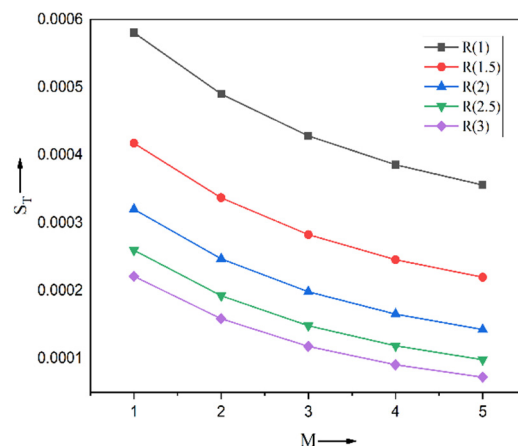


Figure 2. Total entropy with change in radiation parameter

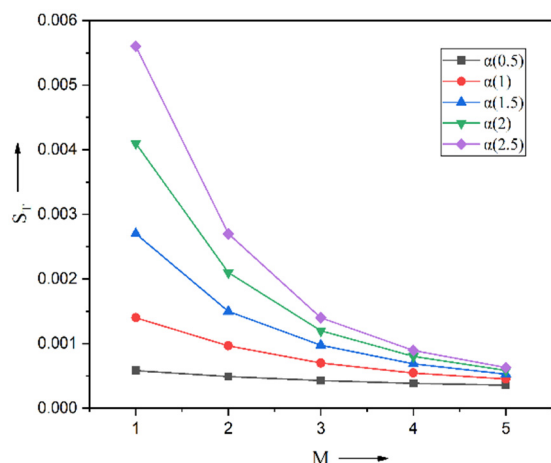


Figure 3. Total entropy with change in Casson parameter

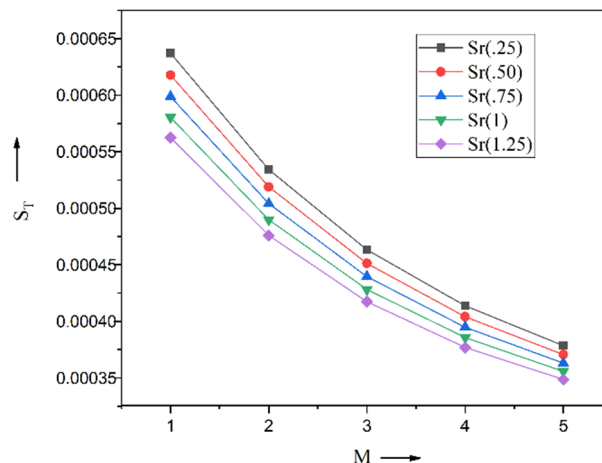


Figure 4. Total entropy with change in Soret effect

Figures (5)-(18) portray the influence of all apposite parameters on the fluid velocity, concentration and temperature. Effect of flow parameters on the skin friction, Nusselt number and Sherwood number are also illustrated in tabular form. Figures (5) and (6) demonstrates the variation of temperature against y with the impact of radiation parameter (R) and Prandtl number (Pr) on temperature profile.

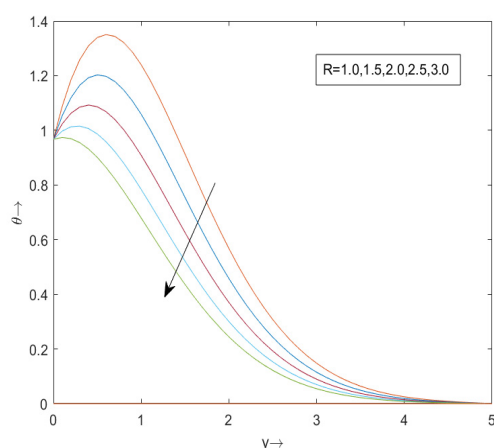


Figure 5. Variation of radiation parameter on temperature

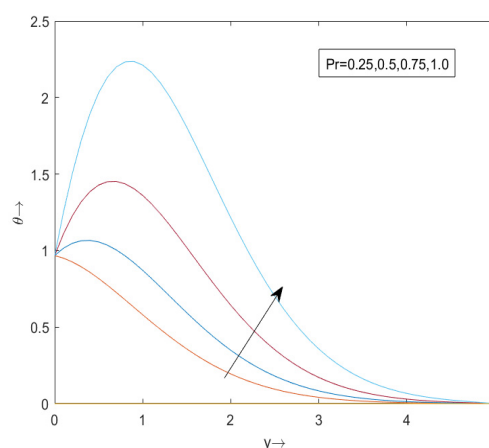


Figure 6. Variation of Prandtl number on temperature

The degree of temperature of fluid falls with the rise in radiation parameter and rises with the rise in Prandtl number. Figures (7)-(13) exhibit the effect of different parameters on velocity profile. It is seen from the Figure (7) that velocity profile decreases with the rise in Chemical reaction parameter Kr and from the Figure (8) one can find that the velocity increases proportionately with the Prandtl number. Hartmann number M is the ratio of electromagnetic forces to inertia forces. The Schmidt number Sc differentiates the relative thickness of velocity and the concentration boundary layers.

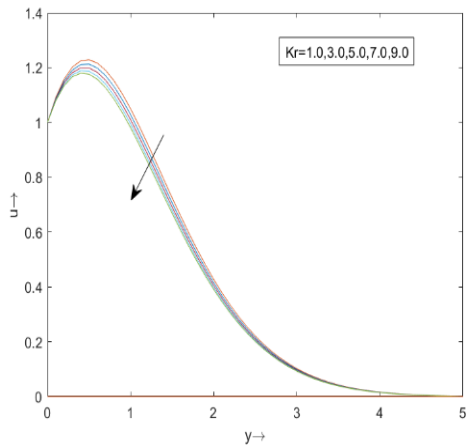


Figure 7. Variation of Chemical reaction parameter on velocity

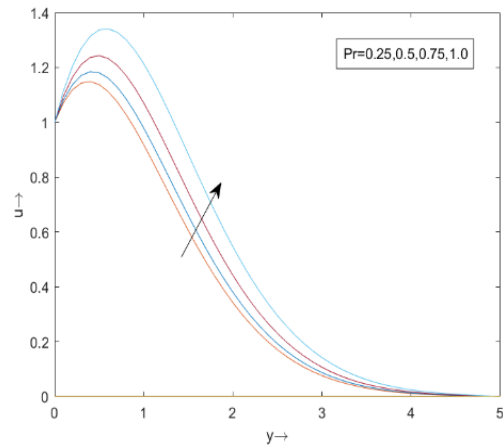


Figure 8. Variation of Prandtl number on velocity

Figure (9) and (10) portray that velocity profile decelerated with the increase in Hartmann number and Schmidt number.

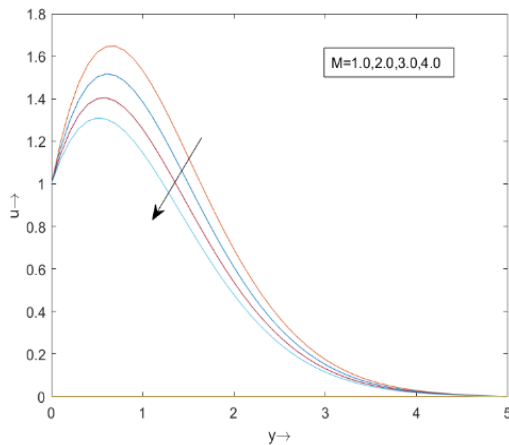


Figure 9. - Variation of Hartmann number on velocity

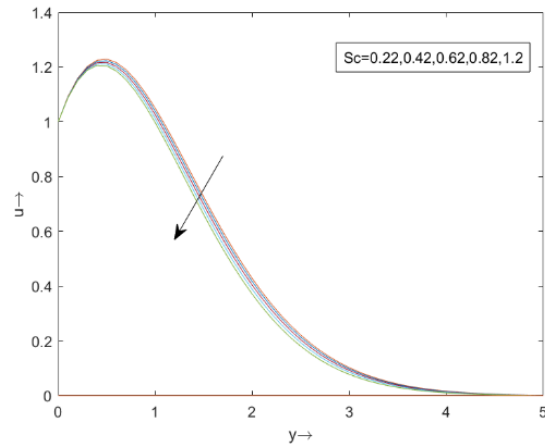


Figure 10. Variation of Schmidt number on velocity

From Figure (11) it is observed that, the velocity profile rise with the rise in casson parameter. The thermo-diffusion or Soret effect Sr may take place due to the presence of temperature gradient. It is evident from the Figure-(12) that, velocity falls with the rise in Soret number and the Figure (13) shows that as the radiation parameter increases, the velocity profile decreases. Figures (14)-(18) demonstrate the change in concentration profile with the influence of different parameters. It is observed that in the figure-(14) the concentration decreases as the Schmidt number increases. Figure (15) and (16) shows that concentration decreases with the increase in the chemical reaction parameter and the Soret effect. Figure (17) shows that concentration profile increases proportionately with radiation parameter. Figure (18) depicts that concentration profile decreases with the increase in Prandtl number.

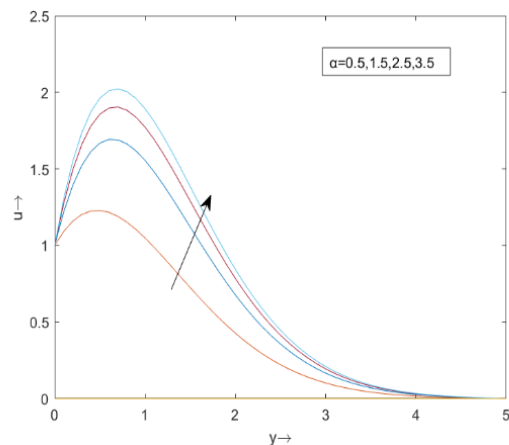


Figure 11. -Variation of Casson parameter on velocity

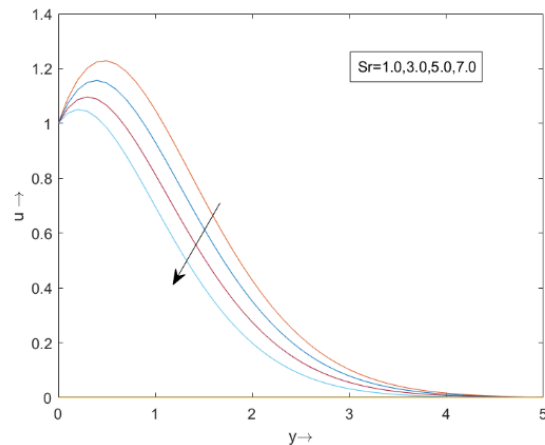


Figure 12. Variation of Soret number on velocity

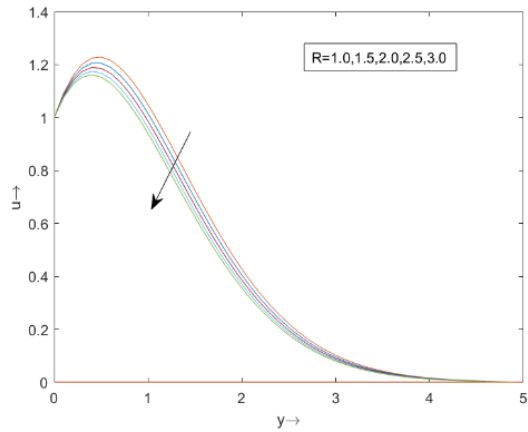


Figure 13. Variation of Radiation parameter on velocity

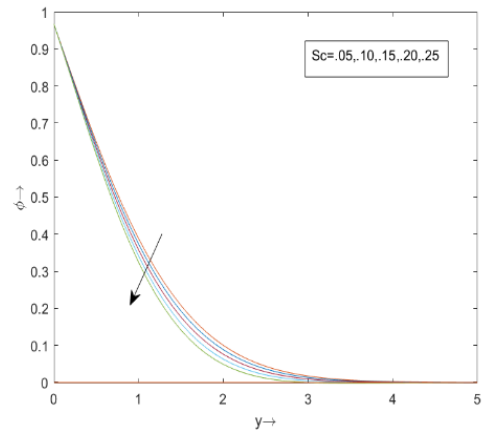


Figure 14. Variation of Schmidt number on concentration

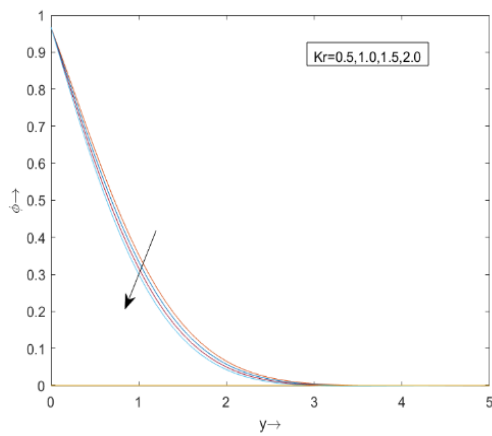


Figure 15. Variation of Chemical reaction parameter on concentration

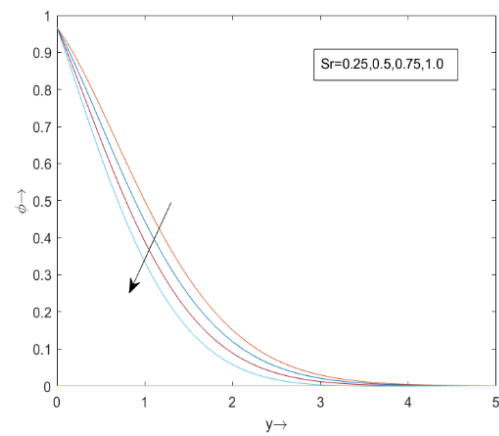


Figure 16. Variation of Soret effect on concentration

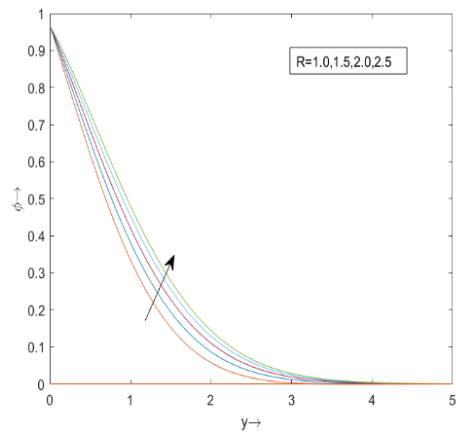


Figure 17. Variation of radiation parameter on concentration

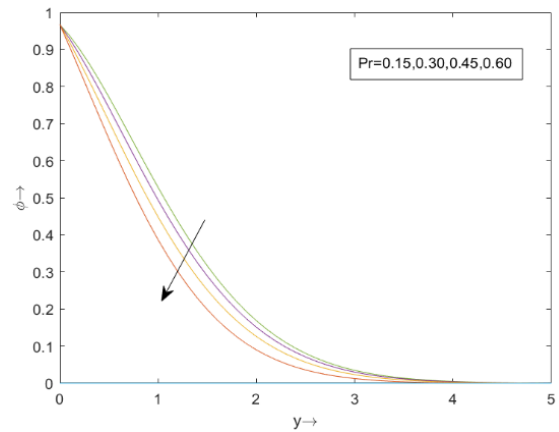


Figure 18. Variation of Prandtl number on concentration

Table 1. Nusselt Number

Pr	R	Nusselt Number
0.25	1.0	-0.1733
0.50	1.0	0.4975
0.75	1.0	1.4629
1.00	1.0	2.9249
0.70	1.0	1.2382
0.70	1.5	0.8860
0.70	2.0	0.5783
0.70	2.5	0.3077
0.70	3.0	0.0684

Table 2. Sherhood Number

Pr	R	Sc	kr	Sr	Sherhood Number
0.25	1.0	0.22	1.0	1.0	-0.3623
0.50	1.0	0.22	1.0	1.0	-0.5297
0.75	1.0	0.22	1.0	1.0	-0.7701
1.00	1.0	0.22	1.0	1.0	-1.1326
0.70	1.0	0.22	1.0	1.0	-0.7143
0.70	1.5	0.22	1.0	1.0	-0.6266
0.70	2.0	0.22	1.0	1.0	-0.5499
0.70	2.5	0.22	1.0	1.0	-0.4824
0.70	1.0	0.22	1.0	1.0	-0.7143
0.70	1.0	0.42	1.0	1.0	-0.7722
0.70	1.0	0.62	1.0	1.0	-0.8428
0.70	1.0	0.82	1.0	1.0	-0.9263
0.70	1.0	0.22	1.0	1.0	-0.7143
0.70	1.0	0.22	3.0	1.0	-0.9096
0.70	1.0	0.22	5.0	1.0	-1.0819
0.70	1.0	0.22	7.0	1.0	-1.2354
0.70	1.0	0.22	1.0	2.0	-1.1885
0.70	1.0	0.22	1.0	4.0	-2.1371
0.70	1.0	0.22	1.0	6.0	-3.0856
0.70	1.0	0.22	1.0	8.0	-4.9827

Table 3. Skin friction

Pr	R	Sc	kr	Sr	M	α	Skin friction
0.25	1.0	0.22	1.0	1.0	5.0	0.5	0.6972
0.50	1.0	0.22	1.0	1.0	5.0	0.5	0.7922
0.75	1.0	0.22	1.0	1.0	5.0	0.5	0.9268
1.00	1.0	0.22	1.0	1.0	5.0	0.5	1.1235
0.70	1.0	0.22	1.0	1.0	5.0	0.5	0.8958
0.70	1.5	0.22	1.0	1.0	5.0	0.5	0.8468
0.70	2.0	0.22	1.0	1.0	5.0	0.5	0.8036
0.70	2.5	0.22	1.0	1.0	5.0	0.5	0.7654
0.70	1.0	0.22	1.0	1.0	5.0	0.5	0.8958
0.70	1.0	0.42	1.0	1.0	5.0	0.5	0.8866
0.70	1.0	0.62	1.0	1.0	5.0	0.5	0.8769
0.70	1.0	0.82	1.0	1.0	5.0	0.5	0.8670
0.70	1.0	0.22	1.0	1.0	5.0	0.5	0.8958
0.70	1.0	0.22	3.0	1.0	5.0	0.5	0.8589
0.70	1.0	0.22	5.0	1.0	5.0	0.5	0.8265
0.70	1.0	0.22	7.0	1.0	5.0	0.5	0.7981
0.70	1.0	0.22	1.0	2.0	5.0	0.5	0.8069
0.70	1.0	0.22	1.0	4.0	5.0	0.5	0.6292
0.70	1.0	0.22	1.0	6.0	5.0	0.5	0.4514
0.70	1.0	0.22	1.0	8.0	5.0	0.5	0.2737
0.70	1.0	0.22	1.0	1.0	1.0	0.5	1.9257
0.70	1.0	0.22	1.0	1.0	2.0	0.5	1.6283
0.70	1.0	0.22	1.0	1.0	3.0	0.5	1.3601
0.70	1.0	0.22	1.0	1.0	4.0	0.5	1.1171
0.70	1.0	0.22	1.0	1.0	5.0	0.5	0.8958
0.70	1.0	0.22	1.0	1.0	5.0	1.5	2.1472
0.70	1.0	0.22	1.0	1.0	5.0	2.5	2.6835
0.70	1.0	0.22	1.0	1.0	5.0	3.5	2.9814

5. CONCLUSIONS

Following are the conclusion of the present investigation:

- The total entropy lowers with the rise in chemical reaction parameter, radiation parameter and Soret effect.
- Entropy generation rise proportionately with the rise in Casson parameter.
- The degree of temperature falls with the increasing radiation parameter and rise with the increasing Prandtl number.
- The velocity of fluid flow is decelerated with increasing reaction by chemical, Hartmann number, Schmidt number, Soret effect and radiation parameter and is accelerated proportionately with the Prandtl number and Casson parameter

- The level of concentration of the fluid rises with the rise in radiation parameter and falls with the rise in Schmidt number, reaction by chemical, Soret effect and Prandtl number.
- Skin friction coefficient increases proportionately with Prandtl number and casson parameter.
- Skin friction is decreasing with the increasing Hartmann number, radiation parameter, Schmidt number, reaction by chemical and Soret effect.
- The rate of heat transfer rise with the increasing Prandtl number, whereas it is reduced with the increasing radiation parameter.
- The rate of mass transfer rise with the increasing radiation parameter, whereas it falls with the increasing Prandtl number, Soret effect, Schmidt number and reaction by chemical.

Nomenclature

ν = kinematic viscosity	K_T = thermal diffusion ratio
α = casson parameter	T_m = mean fluid temperature
γ = angle of inclination	q'_r = radiative heat flux
ξ = ratio of viscous to thermal entropy	u = dimensionless velocity
β = thermal expansion coefficient	θ = nondimensional temperature
β^* = mass expansion coefficient	ϕ = nondimensional concentration
g = acceleration due to gravity	Gr = Grashof number for heat transfer
C' = species concentration	Gm = Grashof number for mass transfer
C'_∞ = fluid concentration far away from the wall	Pr = Prandtl number
T' = temperature of the fluid	Sc = Schmidt number
T'_∞ = fluid temperature far away from the wall	M = Hartmann number
σ = electrical conductivity	R = radiation parameter
ρ = fluid density	Kr = chemical reaction parameter
B_0 = magnetic field	Sr = Soret number
C_p = specific heat at constant pressure	τ = skin friction
D_m = mass diffusivity	Nu = Nusselt number
Kr' = chemical reaction rate constant	Sh = Sherwood number

ORCID

©Hiren Deka, <https://orcid.org/0009-0002-1512-5984>; ©Parimita Phukan, <https://orcid.org/0000-0002-2116-5571>

REFERENCES

- [1] A. Bejan, "A study of entropy generation in fundamental convective heat transfer," *Journal of Heat Transfer*, **101**(4), 718–725 (1979). <https://doi.org/10.1115/1.3451063>
- [2] A. Bejan, and J. Kestin, "Entropy generation through heat and fluid flow," *Journal of Applied Mechanics*, **50**(2), 475 (1983). <https://doi.org/10.1115/1.3167072>
- [3] B.A. Abu-Hijleh, and W.N. Heilen, "Entropy generation due to laminar natural convection over a heated rotating cylinder," *International Journal of Heat and Mass Transfer*, **42**(22), 4225–4233 (1999). [https://doi.org/10.1016/S0017-9310\(99\)00078-2](https://doi.org/10.1016/S0017-9310(99)00078-2)
- [4] S.A. Bayta, "Entropy generation for natural convection in an inclined porous cavity," *International Journal of Heat and Mass Transfer*, **43**(12), 2089–2099 (2000). [https://doi.org/10.1016/S0017-9310\(99\)00291-4](https://doi.org/10.1016/S0017-9310(99)00291-4)
- [5] S. Mahmud, and A.S. Islam, "Laminar free convection and entropy generation inside an inclined wavy enclosure," *International Journal of Thermal Sciences*, **42**(11), 1003–1012 (2003). [https://doi.org/10.1016/S1290-0729\(03\)00076-0](https://doi.org/10.1016/S1290-0729(03)00076-0)
- [6] R.D.C. Oliviski, M.H. Macagnan, and J.B. Copetti, "Entropy generation and natural convection in rectangular cavities," *Applied Thermal Engineering*, **29**(8-9), 1417–1425 (2009). <https://doi.org/10.1016/j.applthermaleng.2008.07.012>
- [7] K. Hooman, and A. Haji-Sheikh, "Analysis of heat transfer and entropy generation for a thermally developing brinkman–brinkman forced convection problem in a rectangular duct with isoflux walls," *International Journal of Heat and Mass Transfer*, **50**(21-22), 4180–4194 (2007). <https://doi.org/10.1016/j.ijheatmasstransfer.2007.02.036>
- [8] T.N. Abdelhameed, "Entropy generation analysis for MHD flow of water past an accelerated plate," *Scientific Reports*, **11**(1), 11964 (2021). <https://doi.org/10.1038/s41598-021-89744-w>
- [9] Z. Khan, O. Makinde, R. Ahmad, and W. Khan, "Numerical study of unsteady MHD flow and entropy generation in a rotating permeable channel with slip and Hall effects," *Communications in Theoretical Physics*, **70**(5), 641 (2018). <https://doi.org/10.1088/0253-6102/70/5/641>
- [10] M. Mansour, S. Siddiqa, R.S.R. Gorla, and A. Rashad, "Effects of heat source and sink on entropy generation and MHD natural convection of Al_2O_3 -Cu/water hybrid nanofluid filled with square porous cavity," *Thermal Science and Engineering Progress*, **6**, 57–71 (2018). <https://doi.org/10.1016/j.tsep.2017.10.014>
- [11] B. Sharma, R. Gandhi, N.K. Mishra, and Q.M. Al-Mdallal, "Entropy generation minimization of higher-order endothermic/exothermic chemical reaction with activation energy on MHD mixed convective flow over a stretching surface," *Scientific Reports*, **12**(1), 17688 (2022). <https://doi.org/10.1038/s41598-022-22521-5>
- [12] S.A. Khan, T. Hayat, M.I. Khan, and A. Alsaeidi, "Salient features of Dufour and Soret effect in radiative MHD flow of viscous fluid by a rotating cone with entropy generation," *International Journal of Hydrogen Energy*, **45**(28), 14552–14564 (2020). <https://doi.org/10.1016/j.ijhydene.2020.03.123>
- [13] G. Shit, R. Haldar, and S. Mandal, "Entropy generation on MHD flow and convective heat transfer in a porous medium of exponentially stretching surface saturated by nanofluids," *Advanced Powder Technology*, **28**(6), 1519–1530 (2017). <https://doi.org/10.1016/j.apt.2017.03.023>

- [14] S. Afsana, M.M. Molla, P. Nag, L.K. Saha, and S. Siddiq, "MHD natural convection and entropy generation of non-Newtonian ferrofluid in a wavy enclosure," *International Journal of Mechanical Sciences*, **198**, 106350 (2021). <https://doi.org/10.1016/j.ijmecsci.2021.106350>
- [15] J. Qing, M.M. Bhatti, M.A. Abbas, M.M. Rashidi, and M.E.-S. Ali, "Entropy generation on MHD Casson nanofluid flow over a porous stretching/shrinking surface," *Entropy*, **18**(4), 123 (2016). <https://doi.org/10.3390/e18040123>
- [16] S. Aiboud, and S. Saouli, "Entropy analysis for viscoelastic magnetohydrodynamic flow over a stretching surface," *International Journal of Non-Linear Mechanics*, **45**(5), 482–489 (2010). <https://doi.org/10.1016/j.ijnonlinmec.2010.01.007>
- [17] S. Hussain, S. Shoeibi, and T. Armaghani, "Impact of magnetic field and entropy generation of Casson fluid on double diffusive natural convection in staggered cavity," *International Communications in Heat and Mass Transfer*, **127**, 105520 (2021). <https://doi.org/10.1016/j.icheatmasstransfer.2021.105520>
- [18] M.H. Yazdi, S. Abdullah, I. Hashim, and K. Sopian, "Entropy generation analysis of open parallel microchannels embedded within a permeable continuous moving surface: application to magnetohydrodynamics (MHD)," *Entropy*, **14**(1), 1–23 (2011). <https://doi.org/10.3390/e14010001>
- [19] M.H. Yazdi, S. Abdullah, I. Hashim, and K. Sopian, "Reducing entropy generation in MHD fluid flow over open parallel microchannels embedded in a micropatterned permeable surface," *Entropy*, **15**(11), 4822–4843 (2013). <https://doi.org/10.3390/e15114822v>
- [20] M. Rashidi, N. Kavyani, and S. Abelman, "Investigation of entropy generation in MHD and slip flow over a rotating porous disk with variable properties," *International Journal of Heat and Mass Transfer*, **70**, 892–917 (2014). <https://doi.org/10.1016/j.ijheatmasstransfer.2013.11.058>

ЧИСЛОВИЙ АНАЛІЗ ГЕНЕРАЦІЇ ЕНТРОПІЇ МГД ПОТОКОМ РІДИНИ КАССОНА ЧЕРЕЗ ПОХИЛУ ПЛАСТИНУ З ЕФЕКТОМ СОРЕ

Хірен Дека, Парісміта Пхукан, Пуджа Халой

Факультет математики, Університет Коттон, Ассам, Індія

У цьому дослідженні досліджується генерація ентропії для нестационарного МГД потоку рідини Кассона через коливальну похилу пластину. Тут, поряд з реакцією хімічним і тепловим випромінюванням, також аналізується включення ефекту Сорє. Розв'язок рівняння, яке керує проблемою потоку, отримано методом кінцевих різниць (FDM). Характеристики швидкості потоку, концентрації та температури аналізуються шляхом побудови графіків, а їх фізична поведінка детально розглядається для вивчення впливу різних параметрів на проблему рідини. Тертя шкіри, швидкість тепло- та масообміну рідини також мають значний вплив під впливом параметрів. Результати показують, що ефект Сорє та інші параметри мають значний вплив на нестационарну МГД кассонову рідину та на загальну ентропію через теплообмін і тертя потоку.

Ключові слова: ентропія; Кассон; МГД; ефект Сорє; теплове випромінювання

THERMO-DIFFUSION AND DIFFUSION-THERMO EFFECTS ON MHD CONVECTIVE FLOW PAST AN IMPULSIVELY STARTED VERTICAL PLATE EMBEDDED IN POROUS MEDIUM

©Kangkan Choudhury*, Sweety Sharma, Shahir Ahmed

Department of Mathematics, University of Science and Technology Meghalaya, India

*Corresponding Author e-mail: kangkan22@gmail.com

Received March 27, 2024; revised April 15, 2024; April 30, 2024

This study introduces an analytical solution for the unsteady MHD free convection and mass transfer flow past a vertical plate embedded in porous medium, taking into account the Soret and Dufour effects. Initially, the perturbation method is employed to decouple the equations resulting from the coupling of the Soret and Dufour effects. Subsequently, the Laplace Transform Technique is applied to solve the governing equations. The expressions for velocity, temperature, concentration, skin-friction, Nusselt, and Sherwood numbers are derived. The effects of the main parameters are discussed, revealing that an increase in the Soret number leads to a decrease in temperature while increasing velocity and concentration. Similarly, the Dufour parameter causes an increase in temperature and velocity, while concentration decreases. However, the effect of the Dufour and Soret parameters on velocity does not show a significant difference.

Keywords: MHD; Soret effect; Dufour effect; Perturbation; Laplace Transform

PACS: 44.25.+f

1. INTRODUCTION

Environmental and mass transfer are very important in many mechanical systems used directly in processes, solar collectors, nuclear reactor heating, etc. [1-10]. Many studies have been conducted on temperature-induced and concentration-induced flow behavior [11-18]. Convection is more important when concentration and temperature interact simultaneously. In 1879, Charles Soret [19] conducted an experiment in which he discovered that the temperature of a salt mixture in a tube was different and not the same at its two ends. The salt concentration near the edge of the cryogenic tube is higher than that near the high temperature end. This led him to conclude that the decrease in minerals was caused by changes in temperature. This is called the Sorét effect or thermophoresis. However, when heat transfer occurs due to a concentration gradient, the phenomenon is called the Dufour effect. Both of these effects are significant in flow systems where density variations exist, such as during isotope separation, chemical processing, etc. [20-26]. Kafoussias and Williams [27] observed that when heat and mass transfer occur simultaneously in a moving fluid, there will always be a complex relationship between the flow and the driving force. This result was obtained after studying the influence of Soret and Dufour on the constant heat and mass transfer near the boundary layer with mixed forced free convection. Their conclusion was that concentration gradients can also create energy flow. Using HAM, the authors [28] solved the system of equations governing steady 2D flow through a long moving porous wall containing conductive fluid in a permeable medium. The authors in [29] presented an analytical study of the Soret and Dufour effects of a second-quality fluid flow along an elongated cylinder taking into account the influence of thermal radiation. It is expected that when the Soret and Dufour parameters change simultaneously, the heat and mass transfer rates will have an inverse relationship with each other.

MHD is a branch of physics that studies the behavior of fluids in magnetic fields. MHD liquids flowing through pipelines are of great significance in many scientific and technical fields such as bioengineering, petroleum industry, drainage and irrigation. The application of MHD principle is widely used in fusion reactors, MHD pump design, MHD generators, MHD speedometers, etc. MHD principles are also used in medicine and biology. Alfven [30], Cowling [31], Shercliff [32], Crammer and Pai [33] are other notable authors whose contributions have led to the development of MHD to its present form. Jha and Gambo [34] used an analytical approach to study inelastic flow and mass transfer on fixed plates by Soret and Dufour. The author first uses the perturbation method to simplify the system of equations, and then uses the Laplace transform technique to solve the system of equations.

The main objective of the present investigation is to present comprehensive analytical solutions for unsteady MHD-free convection and mass transfer on a vertical plate impulsively moved and embedded in a porous medium in the presence of aspect of the Soret and Dufour effects. The coupled equations of the temperature and concentration fields are decoupled using perturbation techniques and then solved by applying the Laplace transform technique. The present work generalizes the work done by [34] by introducing a magnetic field and considering the porosity of the medium. The results presented here are compared with the existing literature in which the magnetic and porosity parameters are not available. The solution of Jha and Gambo [34] is given as a special case in the absence of magnetic and porosity parameters.

2. MATHEMATICAL ANALYSIS

The MHD unsteady natural convection flow beyond the pulse-initiated vertical plate embedded in the porous medium is considered. The y -axis is taken along the normal line of the plate and the x - axis is parallel to it. Initially at

$t' \leq 0$, the liquid and the plate are considered to be at rest with the same constant temperature (T'_∞) and concentration (C'_∞). At $t' > 0$, the plate starts moving with a vertical velocity U_0 and the fluid, temperature, and concentration at the plate are maintained at T'_W and C'_W , respectively. All physical quantities depend on t' and y' only because the plate occupying the plane $y' = 0$ is considered to be of infinite length.

The equations governing the flow under such assumptions and Boussinesq approximation in the presence of magnetic field are:

$$\frac{\partial u'}{\partial t'} = \nu \frac{\partial^2 u'}{\partial y'^2} + g\beta(T' - T'_\infty) + g\bar{\beta}(C' - C'_\infty) - \frac{\sigma B_0^2 u'}{\rho} - \frac{\nu u'}{K'}, \tag{1}$$

$$\frac{\partial T'}{\partial t'} = \alpha \frac{\partial^2 T'}{\partial y'^2} + D^* \frac{\partial^2 C'}{\partial y'^2}, \tag{2}$$

$$\frac{\partial C'}{\partial t'} = D_M \frac{\partial^2 C'}{\partial y'^2} + S^* \frac{\partial^2 T'}{\partial y'^2}. \tag{3}$$

Subject to

$$t' \leq 0: u' = 0, T' = T'_\infty, C' = C'_\infty \text{ for } y' \geq 0, \tag{4}$$

$$t' > 0: \begin{cases} u' = U_0, T' = T'_W, C' = C'_W \text{ at } y' = 0 \\ u' \rightarrow 0, T' \rightarrow T'_\infty, C' \rightarrow C'_\infty \text{ as } y' \rightarrow \infty \end{cases} \tag{5}$$

While the following non-dimensional quantities are introduced

$$u = \frac{u'}{U_0}, y = \frac{y' U_0}{\nu}, t = \frac{t' U_0^2}{\nu}, \theta = \frac{T' - T'_\infty}{T'_W - T'_\infty}, \phi = \frac{C' - C'_\infty}{C'_W - C'_\infty},$$

$$G_T = \frac{\nu g \beta (T'_W - T'_\infty)}{U_0^3}, G_M = \frac{\nu g \bar{\beta} (C'_W - C'_\infty)}{U_0^3}, \text{Pr} = \frac{\nu}{\alpha}, S_c = \frac{\nu}{D_M},$$

$$M = \frac{\sigma B_0^2 \nu}{\rho U_0^2}, K_p = \frac{K' U_0^2}{\nu^2}, D_u = \frac{D^* (C'_W - C'_\infty)}{(T'_W - T'_\infty)}, S_r = \frac{D^* (T'_W - T'_\infty)}{(C'_W - C'_\infty)}, \xi = M + \frac{1}{K_p}.$$

Where Pr is the Prandtl number, S_c the Schmidt number, G_T the Grashof number, G_M the modified Grashof number, M the magnetic parameter, K_p the permeability parameter, S_r the Soret parameter and D_u is the Dufour parameter in Eqs (1-3), we get

$$\frac{\partial u}{\partial t} = \frac{\partial^2 u}{\partial y^2} + G_T \theta + G_M \phi - \xi u, \tag{6}$$

$$\frac{\partial \theta}{\partial t} = \frac{1}{\text{Pr}} \frac{\partial^2 \theta}{\partial y^2} + \frac{D_u}{\text{Pr}} \frac{\partial^2 \phi}{\partial y^2}, \tag{7}$$

$$\frac{\partial \phi}{\partial t} = \frac{1}{S_c} \frac{\partial^2 \phi}{\partial y^2} + \frac{S_r}{S_c} \frac{\partial^2 \theta}{\partial y^2}. \tag{8}$$

Subject to the following initial and boundary conditions

$$t \leq 0: u = 0, \theta = 0, \phi = 0 \text{ for } y \geq 0, \tag{9}$$

$$t > 0: \begin{cases} u = 1, \theta = 1, \phi = 1 \text{ at } y = 0 \\ u \rightarrow 0, \theta \rightarrow 0, \phi \rightarrow 0 \text{ as } y \rightarrow \infty \end{cases} \tag{10}$$

3. ANALYTICAL SOLUTIONS

In order to solve the coupled equations (6 - 8) analytically, we use a non-zero parameter ε (sufficiently small) in the following form, so that the equations are decoupled:

$$u = u_0 + \varepsilon u_1 + O(\varepsilon^2), \tag{11}$$

$$\theta = \theta_0 + \varepsilon\theta_1 + O(\varepsilon^2), \quad (12)$$

$$\phi = \phi_0 + \varepsilon\phi_1 + O(\varepsilon^2). \quad (13)$$

Here $D_u = k\varepsilon$, $S_r = \lambda\varepsilon$

and k , λ are constants of $O(1)$. Then substituting (11 - 13) into (6 - 10) gives:

3.1 Order ε^0

$$\frac{\partial u_0}{\partial t} = \frac{\partial^2 u_0}{\partial y^2} + G_T \theta + G_M \phi - \xi u_0, \quad (14)$$

$$\frac{\partial \theta_0}{\partial t} = \frac{1}{\text{Pr}} \frac{\partial^2 \theta_0}{\partial y^2}, \quad (15)$$

$$\frac{\partial \phi_0}{\partial t} = \frac{1}{S_c} \frac{\partial^2 \phi_0}{\partial y^2}, \quad (16)$$

$$u_0(y, t) = 1, \theta_0(y, t) = 1, \phi_0(y, t) = 1 \text{ at } y = 0, \quad (17)$$

$$u_0(y, t) = 0, \theta_0(y, t) = 0, \phi_0(y, t) = 0 \text{ as } y \rightarrow \infty. \quad (18)$$

3.2. Order ε^1

$$\frac{\partial u_1}{\partial t} = \frac{\partial^2 u_1}{\partial y^2} + G_T \theta + G_M \phi - \xi u_1, \quad (19)$$

$$\frac{\partial \theta_1}{\partial t} = \frac{1}{\text{Pr}} \frac{\partial^2 \theta_1}{\partial y^2} + \frac{k}{\text{Pr}} \frac{\partial^2 \phi_0}{\partial y^2}, \quad (20)$$

$$\frac{\partial \phi_1}{\partial t} = \frac{1}{S_c} \frac{\partial^2 \phi_1}{\partial y^2} + \frac{\lambda}{\text{Pr}} \frac{\partial^2 \theta_0}{\partial y^2}, \quad (21)$$

$$u_1(y, t) = 0, \theta_1(y, t) = 0, \phi_1(y, t) = 0 \text{ at } y = 0, \quad (22)$$

$$u_1(y, t) = 0, \theta_1(y, t) = 0, \phi_1(y, t) = 0 \text{ as } y \rightarrow \infty. \quad (23)$$

Using Laplace Transform Technique with relevant boundary conditions, the solutions are obtained as

$$\theta(y, t) = P_2 \operatorname{erfc} \left(\frac{y}{2} \sqrt{\frac{\text{Pr}}{t}} \right) - P_1 \operatorname{erfc} \left(\frac{y}{2} \sqrt{\frac{S_c}{t}} \right), \quad (24)$$

$$\phi(y, t) = P_4 \operatorname{erfc} \left(\frac{y}{2} \sqrt{\frac{S_c}{t}} \right) - P_3 \operatorname{erfc} \left(\frac{y}{2} \sqrt{\frac{\text{Pr}}{t}} \right), \quad (25)$$

$$u(y, t) = \left(1 - \frac{Z_1}{a_1} - \frac{Z_2}{a_2} \right) f_1 + \frac{Z_1}{a_1} \operatorname{erfc} \left(\frac{y}{2} \sqrt{\frac{\text{Pr}}{t}} \right) + \frac{Z_2}{a_2} \operatorname{erfc} \left(\frac{y}{2} \sqrt{\frac{S_c}{t}} \right) + \frac{Z_1}{a_1} e^{a_1 t} (f_2 - f_3) + \frac{Z_2}{a_2} e^{a_2 t} (f_4 - f_5), \quad (26)$$

where

$$P_1 = \frac{D_u S_c}{S_c - \text{Pr}}, P_2 = 1 + P_1, P_3 = \frac{\text{Pr} S_r}{\text{Pr} - S_c}, P_4 = 1 + P_3, a_1 = \frac{\xi}{\text{Pr} - 1}, a_2 = \frac{\xi}{S_c - 1}$$

$$Z_1 = \frac{G_T (\text{Pr} - S_c) - S_r \text{Pr} G_M - D_u S_c G_T}{(\text{Pr} - 1)(\text{Pr} - S_c)}, Z_2 = \frac{G_M (S_c - \text{Pr}) - S_r \text{Pr} G_M - D_u S_c G_T}{(S_c - 1)(S_c - \text{Pr})}$$

$$f_1 = f(1, \xi, y, t), f_2 = f(1, \xi + a_1, y, t), f_3 = f(\text{Pr}, a_1, y, t)$$

$$f_4 = f(1, \xi + a_2, y, t), f_5 = f(S_c, a_2, y, t)$$

$$f(x, z, y, t) = \frac{1}{2} \left[e^{y\sqrt{z}} \operatorname{erfc} \left(\frac{y}{2} \sqrt{\frac{x}{t} + \sqrt{zt}} \right) + e^{-y\sqrt{z}} \operatorname{erfc} \left(\frac{y}{2} \sqrt{\frac{x}{t} - \sqrt{zt}} \right) \right]$$

The non-dimensional form of Nusselt number, Sherwood number, and skin friction coefficient in heat and mass transfer process as

$$Nu = - \left[\frac{\partial \theta}{\partial y} \right]_{y=0} = -P_1 \sqrt{\frac{S_c}{\pi t}} + P_2 \sqrt{\frac{\text{Pr}}{\pi t}} \tag{27}$$

$$Sh = - \left[\frac{\partial \phi}{\partial y} \right]_{y=0} = -P_3 \sqrt{\frac{\text{Pr}}{\pi t}} + P_4 \sqrt{\frac{S_c}{\pi t}} \tag{28}$$

$$C_f = - \left[\frac{\partial u}{\partial y} \right]_{y=0} = \left(1 - \frac{Z_1}{a_1} - \frac{Z_2}{a_2} \right) \left(\sqrt{\xi} \operatorname{erfc}(\sqrt{\xi t}) + \frac{1}{\sqrt{\pi t}} \right) + \frac{Z_1}{a_1} \sqrt{\frac{\text{Pr}}{\pi t}} + \frac{Z_2}{a_2} \sqrt{\frac{S_c}{\pi t}} - \frac{Z_1}{a_1} e^{a_1 t} g_1 - \frac{Z_2}{a_2} e^{a_2 t} g_2. \tag{29}$$

Where

$$g_1 = g(a_1, \xi + a_1, t), g_2 = g(a_2, \xi + a_2, t), g(x, z, t) = \sqrt{x} \operatorname{erfc}(\sqrt{xt}) - \sqrt{z} \operatorname{erfc}(\sqrt{zt})$$

4. RESULTS AND DISCUSSIONS

The mathematical model describes the free convection flow associated with heat and mass transfer across a vertical plate that initiates pulses in addition to thermal diffusion and thermal-diffusion effects. Numerical calculations were performed to provide an overall understanding of the problem and the results are presented in Figures 1 to 9 and Table 1.

To have a clear overview of the problem, the calculations Numbers for the velocity field, dimensionless temperature and concentration fields, surface friction, heat and mass transfer rates have been taken and they are represented graphically for the thermal Grashof number G_T , the modified Grashof number G_M , Schmidt number S_c , Prandtl number P_r , magnetic parameter M , Soret parameter S_r , Dufour parameter and permeability parameter. The Prandtl P_r number is chosen to be 0.71, representing air at a temperature of 290 K and a pressure of 1 atm. In this study, air is considered as the primary fluid (solvent) and certain fluids are considered as secondary substances (solute) such as helium (He), water vapor (H_2O), ammonia (NH_3), etc. is diffused in the air. The Schmidt number Sc is assumed to be 0.78 typical for ammonia (NH_3), while the values of the other parameters are chosen arbitrarily.

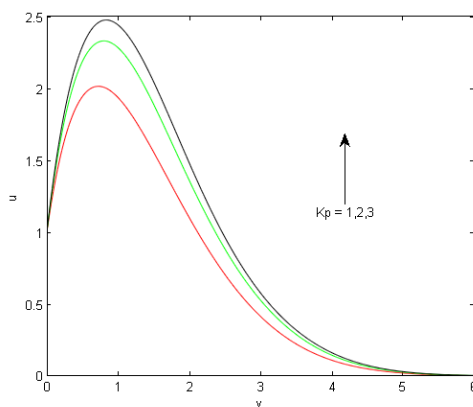


Figure 1. Velocity profile with respect to permeability parameter for $k_p = 1; S_c = 0.78; P_r = 0.71; G_T = 5; G_M = 5; M = 1; t = 1; D_u = 0.15; S_r = 0.15$

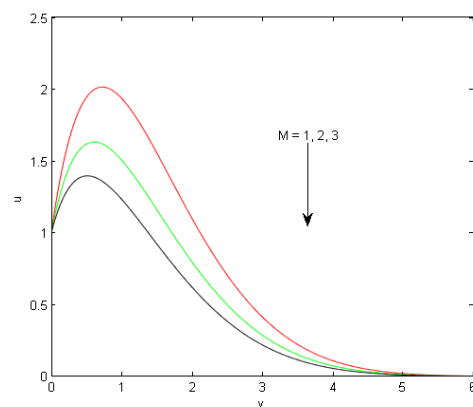


Figure 2. Velocity profile with respect to magnetic parameter for $k_p = 1; S_c = 0.78; P_r = 0.71; G_T = 5; G_M = 5; M = 1; t = 1; D_u = 0.15; S_r = 0.15$

Figure 1 depicts the influence of permeability parameter K_p on the velocity fields. It is found that the velocity increases with increase of permeability parameter K_p for the cooling surface. Physically, when the holes of the porous

medium become large, the resistance of the medium may be neglected and as a consequence the fluid velocity gets increased.

Figure 2 show that velocity decreases comprehensively for increasing Hartmann number. In other words, the fluid flow is decelerated due to imposition of the transverse magnetic field. This observation is consistent with the physical fact that a magnetic body force viz. Lorentz force develops due to interaction of the fluid velocity and the magnetic field which serves as a resistive force to the fluid flow and as a consequence the flow gets decelerated.

The variation in the velocity distribution of the flow field with respect to y for four specific values of Soret parameter (S_r) is shown in Figure 3. It is evident in the figure that the velocity profile diminutions near the plate due to the Soret effect, but at far away from the plate, Soret effect can be used to boost the fluid velocity.

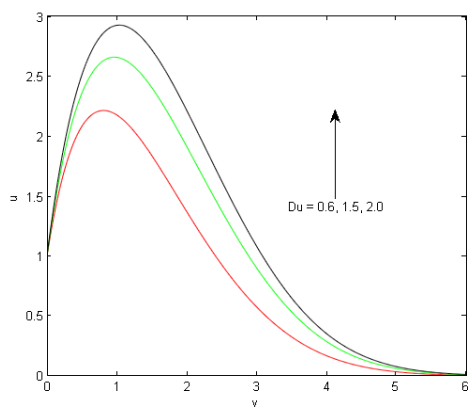


Figure 3. Velocity profile with respect to Dufour parameter for $k_p = 1; S_c = 0.78; P_r = 0.71; G_T = 5; G_M = 5; M = 1; t = 1; D_u = 0.15; S_r = 0.15$

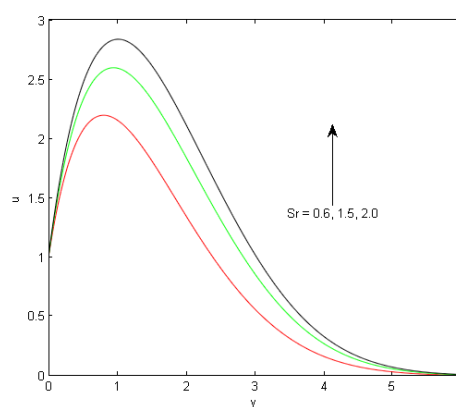


Figure 4. Velocity profile with respect to Soret parameter for $k_p = 1; S_c = 0.78; P_r = 0.71; G_T = 5; G_M = 5; M = 1; t = 1; D_u = 0.15; S_r = 0.15$

The consequences of diffusion-thermo on the velocity field are displayed in Figure 4. The Dufour number D_u signifies the contribution of the concentration gradients to the thermal energy flux in the flow. As D_u increases, a rise in fluid velocity can be seen in Figure 4.

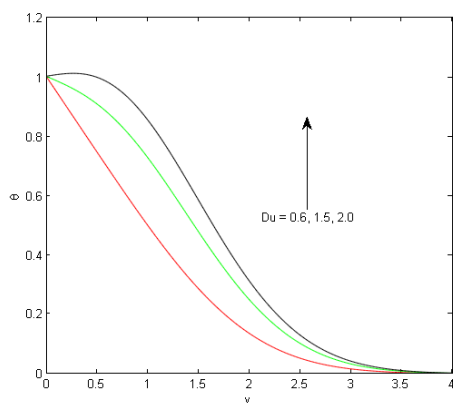


Figure 5. Temperature profile with respect to Dufour parameter for $k_p = 1; S_c = 0.78; P_r = 0.71; G_T = 5; G_M = 5; M = 1; t = 1; D_u = 0.15; S_r = 0.15$

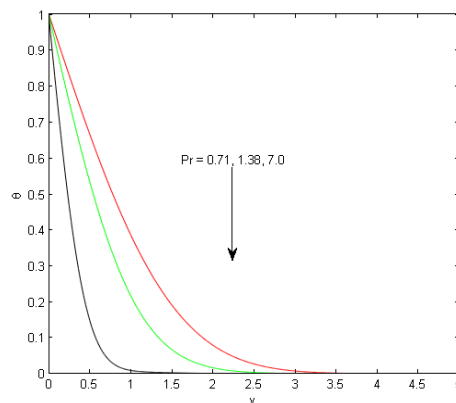


Figure 6. Temperature profile with respect to Prandtl number for $k_p = 1; S_c = 0.78; P_r = 0.71; G_T = 5; G_M = 5; M = 1; t = 1; D_u = 0.15; S_r = 0.15$

Figure 5 illuminates the effect of Prandtl number P_r on fluid temperature. Prandtl number defines the ratio of momentum diffusivity to thermal diffusivity. As P_r increases thermal diffusivity decreases resulting in a drop in fluid temperature. And hence the fluid temperature decreases. Dufour effect on the temperature profile is demonstrated in Figure 6. It is evident that the temperature of the fluid increased with the increasing values of Dufour parameter. Figure 7 indicates the temperature distribution with respect to time. As time progress, temperature of the fluid increases.

In Figure 8, the effect of Schmidt number S_c on concentration field has been depicted. An increase in Schmidt number S_c means a fall in mass diffusivity and hence indicates a fall in the concentration level. Figure 9 presented thermal diffusion effect on concentration profile. It is observed that fluid concentration increased with the increasing values of the Soret parameter S_r . Physically, the presence of thermal diffusion increases the concentration level of the fluid.

From Table 1, as G_T, G_M, K_p increase, skin friction increases. In addition to this, it is seen from Table 1 that the skin friction gets reduced for increasing magnetic parameter M . This indicates that the imposition of a transverse magnetic field inhibits viscous drag due to its application on thin films with high aspect ratio. Henceforth, the coefficient of momentum at the planar surface becomes larger for increasing M . Also, as S_r and D_u increase, viscous drag at the plate decreases.

In Table 2, we have compared our work with previously published work done by [34]. In absence of magnetic parameter and porosity parameter, the variation of skin friction in terms of Soret and Dufour effects are examined. It is found that the findings of the current study are consistent with the prior outcomes.

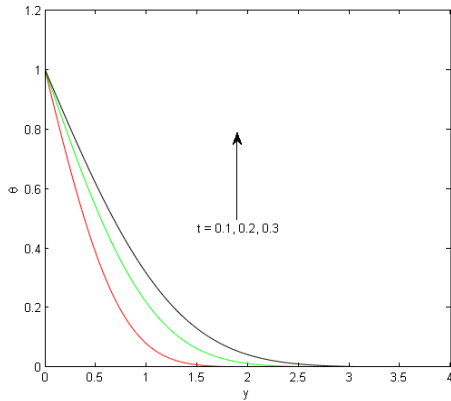


Figure 7. Temperature profile with respect to time for $k_p = 1$; $S_c = 0.78$; $P_r = 0.71$; $G_T = 5$; $G_M = 5$; $M = 1$; $t = 1$; $D_u = 0.15$; $S_r = 0.15$

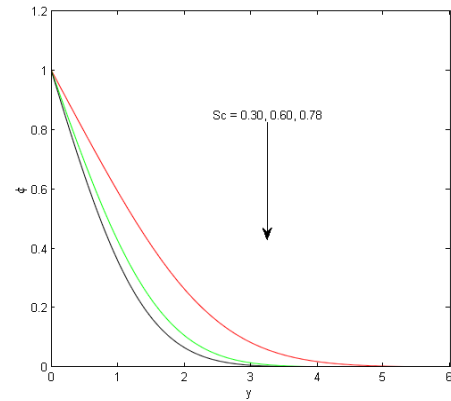


Figure 8. Concentration profile with respect to Schmidt number for $k_p = 1$; $S_c = 0.78$; $P_r = 0.71$; $G_T = 5$; $G_M = 5$; $M = 1$; $t = 1$; $D_u = 0.15$; $S_r = 0.15$

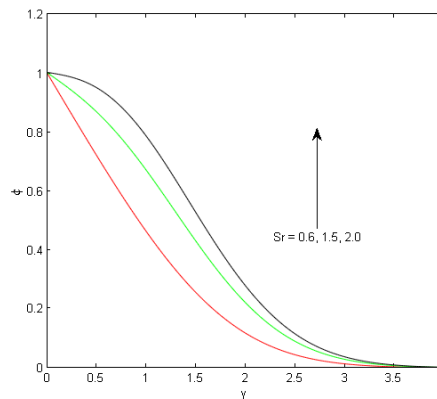


Figure 9. Concentration profile with respect to Soret parameter for $k_p = 1$; $S_c = 0.78$; $P_r = 0.71$; $G_T = 5$; $G_M = 5$; $M = 1$; $t = 1$; $D_u = 0.15$; $S_r = 0.15$

Table 1. Skin friction for the variations of different parameters (M, k_p, S_r, D_u, S_c) for $k_p = 1$; $S_c = 0.78$; $P_r = 0.71$; $G_T = 5$; $G_M = 5$; $M = 1$; $t = 1$; $D_u = 0.15$; $S_r = 0.15$

M	k_p	D_u	S_r	S_c	τ
2	1	0.15	0.15	0.78	0.8807
3	1	0.15	0.15	0.78	0.8673
4	1	0.15	0.15	0.78	0.8527
3	1	0.15	0.15	0.78	0.8673
3	2	0.15	0.15	0.78	0.8749
3	3	0.15	0.15	0.78	0.8772
3	1	0	0.15	0.78	1.0057
3	1	0.15	0.15	0.78	0.8673
3	1	0.3	0.15	0.78	0.7788
3	1	0.15	0	0.78	0.9879
3	1	0.15	0.15	0.78	0.8673
3	1	0.15	0.3	0.78	0.7858
3	1	0.15	0.15	0.30	1.1474
3	1	0.15	0.15	0.60	0.9861
3	1	0.15	0.15	0.78	0.8673

Table 2: Comparison of the coefficient of skin friction with the previously published work in absence of magnetic parameter (M) and permeability parameter (k_p).

S_r	D_u	Work done by [34]	τ (Present work)
0.0	0.15	2.762960	2.7615
0.15	0.15	2.815850	2.8043
0.3	0.15	2.869490	2.8451
0.15	0.0	2.756830	2.7458
0.15	0.15	2.815850	2.8082
0.15	0.3	2.875640	2.8725

5. CONCLUSIONS

In the present investigation, we have studied theoretically the effect of unsteady MHD heat and mass transfer natural fluid flow past an impulsively started vertical plate embedded in porous medium. The present investigation leads to the following conclusions:

- i. Fluid velocity decreases with the increasing values of the magnetic field parameter in the boundary layer region and thus magnetic field can be effectively used in controlling the fluid motion.
- ii. Fluid motion enhances under the effect of Grashof number (G_T) and modified Grashof number (G_M) while the fluid velocity reduced with the increase in Prandtl number and Schmidt number.
- iii. Fluid velocity increases with the increasing values of permeability parameter.
- iv. Fluid velocity increases as Soret (S_r) and Dufour (D_u) number increase.
- v. Temperature of the fluid decreases under the influence of Prandtl number.
- vi. Coefficient of skin-friction of plate is decreased due to the application of the strength of the magnetic field.
- vii. Viscous drag at the plate is increased with the increasing values of permeability parameter.
- viii. Skin friction is decreased with the increasing values of Soret (S_r) and Dufour (D_u) number.

ORCID

©Kangkan Choudhury, <https://orcid.org/0000-0003-2809-8428>

REFERENCES

- [1] N. Marneni, S. Tippa, and R. Pendyala, "Ramp temperature and Dufour effects on transient MHD natural convection flow past an infinite vertical plate in a porous medium," *Eur. Phys. J. Plus.* **130**, 251 (2015). <https://doi.org/10.1140/epjp/i2015-15251-9>
- [2] R. Derakhshan, A. Shojaeia, K. Hosseinzadeh, M. Nimafar, and D.D. Ganji, "Hydrothermal analysis of magneto hydrodynamic nanofluid flow between two parallel by AGM," *Case Stud. Therm. Eng.* **14**, 100439 (2019). <https://doi.org/10.1016/j.csite.2019.100439>
- [3] M.R. Zangoee, Kh. Hosseinzadeh, D.D. Ganji, "Hydrothermal analysis of MHD nanofluid (TiO₂-GO) flow between two radiative stretchable rotating disks using AGM," *Case Stud. Therm. Eng.* **14**, 100460 (2019). <https://doi.org/10.1016/j.csite.2019.100460>
- [4] M. Gholinia, Kh. Hosseinzadeh, H. Mehrzadi, D.D. Ganji, and A.A. Ranjbar, "Investigation of MHD Eyring-Powell fluid flow over a rotating disk under effect of homogeneous-heterogeneous reactions," *Case Stud. Therm. Eng.* **13**, 100356 (2019). <https://doi.org/10.1016/j.csite.2018.11.007>
- [5] M. Gholinia, M. Armin, A.A. Ranjbar, and D.D. Ganji, "Numerical thermal study on CNTs/C₂H₆O₂-H₂O hybrid base nanofluid upon a porous stretching cylinder under impact of magnetic source," *Case Stud. Therm. Eng.* **14**, 100490 (2019). <https://doi.org/10.1016/j.csite.2019.100490>
- [6] M. Gholinia, S. Gholinia, Kh. Hosseinzadeh, and D.D. Ganji, "Investigation on ethylene glycol Nano fluid flow over a vertical permeable circular cylinder under effect of magnetic field," *Results Phys.* **9**, 1525-1533 (2018). <https://doi.org/10.1016/j.rinp.2018.04.070>
- [7] S.M. Mousazadeh, M.M. Shahmardan, T. Tavangar, Kh. Hosseinzadeh, and D.D. Ganji, "Numerical investigation on convective heat transfer over two heated wall-mounted cubes in tandem and staggered arrangement," *Theor. Appl. Mech. Lett.* **8**, 171-183 (2018). <https://doi.org/10.1016/j.taml.2018.03.005>
- [8] S.S. Ghadikolaei, Kh. Hosseinzade, M. Yassari, H. Sadeghi, and D.D. Ganji, "Analytical and numerical solution of non-Newtonian second-grade fluid flow on a stretching sheet," *Therm. Sci. Eng. Prog.* **5**, 309-316 (2018). <https://doi.org/10.1016/j.tsep.2017.12.010>
- [9] S.S. Ardahaie, A.J. Amiri, A. Amouei, K. Hosseinzadeh, and D.D. Ganji, "Investigating the effect of adding nanoparticles to the blood flow in presence of magnetic field in a porous blood arterial," *Inform. Med. Unlocked*, **10**, 71-81 (2018). <https://doi.org/10.1016/j.imu.2017.10.007>
- [10] J. Rahimi, D.D. Ganji, M. Khaki, and Kh. Hosseinzadeh, "Solution of the boundary layer flow of an Eyring-Powell non-Newtonian fluid over a linear stretching sheet by collocation method," *Alex. Eng. J.* **56**, 621-627 (2017). <https://doi.org/10.1016/j.aej.2016.11.006>
- [11] S.S. Ghadikolaei, K. Hosseinzadeh, and D.D. Ganji, "Investigation on Magneto Eyring-Powell nanofluid flow over inclined stretching cylinder with nonlinear thermal radiation and Joule heating effect," *World J. Eng.* **16**, 51-63 (2019). <https://doi.org/10.1108/WJE-06-2018-0204>
- [12] S.S. Ghadikolaei, Kh. Hosseinzade, and D.D. Ganji, "Investigation on ethylene glycol-water mixture fluid suspend by hybrid nanoparticles (TiO₂-CuO) over rotating cone with considering nanoparticles shape factor," *J. Mol. Liq.* **272**, 226-236 (2018). <https://doi.org/10.1016/j.molliq.2018.09.084>

- [13] S.S. Ghadikolaie, Kh. Hosseinzadeh, and D.D. Ganji, "Numerical study on magnetohydrodynamic CNTs-water nanofluids as a micropolar dusty fluid influenced by non-linear thermal radiation and joule heating effect," *Powder Technol.* **340**, 389–399 (2018). <https://doi.org/10.1016/j.powtec.2018.09.023>
- [14] S.S. Ghadikolaie, K. Hosseinzadeh, M. Hatami, and D.D. Ganji, "MHD boundary layer analysis for micropolar dusty fluid containing Hybrid nanoparticles (Cu-Al₂O₃) over a porous medium," *J. Mol. Liq.* **268**, 813–823 (2018). <https://doi.org/10.1016/j.molliq.2018.07.105>
- [15] S.S. Ghadikolaie, Kh. Hosseinzadeh, and D.D. Ganji, "MHD radiative boundary layer analysis of micropolar dusty fluid with graphene oxide (Go)-engine oil nanoparticles in a porous medium over a stretching sheet with joule heating effect," *Powder Technol.* **338**, 425–437 (2018). <https://doi.org/10.1016/j.powtec.2018.07.045>
- [16] S.S. Ghadikolaie, K. Hosseinzadeh, M. Hatami, D.D. Ganji, and M. Armin, "Investigation for squeezing flow of ethylene glycol (C₂H₆O₂) carbon nanotubes (CNTs) in rotating stretching channel with nonlinear thermal radiation," *J. Mol. Liq.* **263**, 10–21 (2018). <https://doi.org/10.1016/j.molliq.2018.04.141>
- [17] S.S. Ghadikolaie, Kh. Hosseinzadeh, and D.D. Ganji, "Investigation on three-dimensional squeezing flow of mixture base fluid (ethyleneglycol–water) suspended by hybrid nanoparticle (Fe₃O₄–Ag) dependent on shape factor," *J. Mol. Liq.* **262**, 376–388 (2018). <https://doi.org/10.1016/j.molliq.2018.04.094>
- [18] S.S. Ghadikolaie, K. Hosseinzadeh, M. Hatami, and D.D. Ganji, "Fe₃O₄-(CH₂OH)₂ nanofluid analysis in a porous medium under MHD radiative boundary layer and dusty fluid," *J. Mol. Liq.* **258**, 172–185 (2018). <https://doi.org/10.1016/j.molliq.2018.02.106>
- [19] J.K. Platten, "The Soret effect: a review of recent experimental results," *J. Appl. Mech.* **73**(1), 5–15 (2006). <https://doi.org/10.1115/1.1992517>
- [20] M.A. Rahman, and M.Z. Saghir, "Thermodiffusion or Soret effect: historical review," *Int. J. Heat Mass. Transf.* **73**, 693–705 (2014). <https://doi.org/10.1016/j.ijheatmasstransfer.2014.02.057>
- [21] M. Bourich, M. Hasnaoui, M. Mamou, et al., "Soret effect inducing subcritical and Hopf bifurcations in a shallow enclosure filled with a clear binary fluid or a saturated porous medium: a comparative study," *Phys Fluids*, **16**, 551–568 (2004). <https://doi.org/10.1063/1.1636727>
- [22] M.S. Malashetty, "Anisotropic thermoconvective effects on the onset of double diffusive convection in a porous medium," *Int. J. Heat Mass. Transf.* **36**, 2397–2401 (1993). [https://doi.org/10.1016/S0017-9310\(05\)80123-1](https://doi.org/10.1016/S0017-9310(05)80123-1)
- [23] R.G. Mortimer, and H. Eyring, "Elementary transition state theory of the Soret and Dufour effects," *Proc. Natl. Acad. Sci. USA*, **77**, 1728–1731 (1980). <https://www.ncbi.nlm.nih.gov/pmc/articles/PMC348577/pdf/pnas00667-0043.pdf>
- [24] G.V.R. Reddy, "Soret and Dufour Effects on MHD free convective flow past a vertical porous plate in the presence of heat generation," *Int. J. Appl. Mech. Eng.* **21**, 649–665 (2016). <https://doi.org/10.1515/ijame-2016-0039>
- [25] K.J. Basant, and O.A. Abiodun, "Free convective flow of heat generating/absorbing fluid between vertical porous plates with periodic heat input," *Int. Commun. Heat Mass.* **36**, 624–631 (2009). <https://doi.org/10.1016/j.icheatmasstransfer.2009.03.003>
- [26] Kh. Hosseinzadeh, M. Alizadeh, and D.D. Ganji, "Hydrothermal analysis on MHD squeezing nanofluid flow in parallel plates by analytical method," *Int. J. Mech. Mater. Eng.* **13**, 4 (2018). <https://doi.org/10.1186/s40712-018-0089-7>
- [27] N.G. Kafoussias, and E.W. Williams, "Thermal-diffusion and diffusion-thermo effects on mixed free-forced convective and mass transfer boundary layer flow with temperature dependent viscosity," *Int. J. Eng. Sci.* **33**, 1369–1384 (1995). [https://doi.org/10.1016/0020-7225\(94\)00132-4](https://doi.org/10.1016/0020-7225(94)00132-4)
- [28] A.J. Omowaye, A.I. Fagbade, and A.O. Ajayi, "Dufour and soret effects on steady MHD convective flow of a fluid in a porous medium with temperature dependent viscosity: homotopy analysis approach," *J. Niger. Math.* **34**, 343–360 (2015). <https://doi.org/10.1016/j.jnnms.2015.08.001>
- [29] A. Shojaei, A.J. Amiri, S.S. Ardahaie, K. Hosseinzadeh, and D.D. Ganji, "Hydrothermal analysis of non-Newtonian second grade fluid flow on radiative stretching cylinder with Soret and Dufour effects," *Case Stud. Therm. Eng.* **13**, 100384 (2019). <https://doi.org/10.1016/j.csite.2018.100384>
- [30] H. Alfvén, Discovery of Alfvén Waves, *Nature*, **150**, 405–406 (1942). <https://doi.org/10.1038/150405d0>
- [31] T.G. Cowling, *Magnetohydrodynamics*, (Wiley Inter Science, New York, 1957).
- [32] J.A. Shercliff, *A Textbook of Magnetohydrodynamics*, (Pergamon Press, London, 1965).
- [33] K.R. Cramer, and S.I. Pai, *Magneto Fluid Dynamics for Engineers and Applied Physicists*, (Mc Graw Hill Book Co., New York, 1973).
- [34] B.K. Jha, and Y.Y. Gambo, "Unsteady free convection and mass transfer flow past an impulsively started vertical plate with Soret and Dufour effects: an analytical approach," *SN Applied Sciences*, **1**, 1234 (2019). <https://doi.org/10.1007/s42452-019-1246-1>

ТЕРМОДИФУЗІЙНИЙ ТА ДИФУЗІЙНО-ТЕРМОЕФЕКТИ НА МГД КОНВЕКТИВНИЙ ПОТІК ПОВЗ ІМПУЛЬСЬКО ЗАПУЩЕНОЮ ВЕРТИКАЛЬНОЮ ПЛАСТИНОЮ, ЗАЛОЧЕНОЮ В ПОРИСТЕ СЕРЕДОВИЩЕ

Канган Чоудхурі, Світі Шарма, Шахір Ахмед

Факультет математики, Університет науки і технологій Мегхала, Індія

У цьому дослідженні представлено аналітичне рішення для нестационарної вільної МГД-конвекції та потоку масообміну повз вертикальну пластину, вбудовану в пористе середовище, з урахуванням ефектів Соре та Дюфура. Спочатку метод збурень використовується для роз'єднання рівнянь, що є результатом зв'язку ефектів Соре та Дюфура. Для розв'язання керівних рівнянь використовується метод перетворення Лапласа. Отримано вирази для швидкості, температури, концентрації, шкірного тертя, чисел Нуссельта та Шервуда. Обговорюються ефекти основних параметрів, показуючи, що збільшення числа Соре призводить до зниження температури при збільшенні швидкості та концентрації. Подібним чином параметр Дюфура викликає підвищення температури та швидкості, тоді як концентрація зменшується. Однак вплив параметрів Дюфура та Соре на швидкість не демонструє істотної різниці.

Ключові слова: МГД; ефект Соре; ефект Дюфура; збурення; перетворення Лапласа